

NORTHWESTERN UNIVERSITY

Inhibition of amyloid beta oligomer formation, binding, and downstream tau phosphorylation:
three potential therapeutic approaches for Alzheimer's disease

A DISSERTATION

SUBMITTED TO THE GRADUATE SCHOOL
IN PARTIAL FULFILLMENT OF THE REQUIREMENTS

for the degree

DOCTOR OF PHILOSOPHY

Field of Chemistry

By

Elizabeth A. Johnson

EVANSTON, ILLINOIS

March 2023

© Copyright by Elizabeth Johnson, 2023

All Rights Reserved

Abstract

Amyloid beta oligomers (A β O) are a key instigator of neurodegeneration in Alzheimer's disease (AD). The work presented in this thesis includes three disease-modifying approaches to disrupt pathological A β O-related mechanisms in AD: (1) inhibiting A β O buildup, (2) blocking A β O-induced tau phosphorylation, and (3) neutralizing A β O. These three approaches were tested in primary hippocampal neuron cultures to which A β monomer or A β O were applied.

First, the small molecule NU-9, which was previously developed to provide protection in models of amyotrophic lateral sclerosis proteopathy, was shown in this work to additionally prevent buildup of neuron-binding A β O. The mechanism of NU-9, which acted on a cellular target, was determined to be lysosome- and cathepsin B-dependent. Further, the buildup of neuron-binding A β O in this model occurred by a dynamin- and cathepsin L-dependent intracellular trafficking mechanism. These results provide new insight into the mechanisms of pathological A β O buildup in neurons and uncover a novel avenue for protection against A β O accumulation with potential application to multiple neurodegenerative proteopathies.

Second, the effect of specific inhibition of the neuronal isoform of nitric oxide synthase (nNOS) was tested. The results obtained in this work demonstrate the role of nNOS activation in A β O-induced tau phosphorylation, A β O formation, and modulation of spine morphology. These results support the conclusion that multiple forms of AD neurodegeneration may be nNOS-dependent and can be disrupted by specific inhibition of nNOS.

Third, monospecific mono, di, and trivalent Nuscl megamolecules were used to bind and neutralize A β O, preventing A β O from binding to neurons. Differential A β O binding and neutralization corresponded to megamolecule valency. These findings support the use of Nuscl-based megamolecules to robustly neutralize A β O in AD.

In this work, three promising avenues of potential therapeutic relevance to AD were investigated, and the results provided insight into the mechanisms of A β O buildup and A β O-instigated pathology.

Acknowledgments

I would like to profoundly thank my mentors, Rick Silverman and Bill Klein. Rick, thank you for your insightful guidance, for your patient support, for encouraging me to follow my scientific curiosity even in unexpected directions, and for inspiring me to become the best person and scientist that I can be. Bill, thank you for encouraging me to pursue the big questions, for challenging me to think deeply about the meaning behind each finding, for teaching me how to become a more organized scientist, and for inspiring me to become a better writer.

To my chemistry mentor, Ha Do, thank you for kindly teaching me so many synthetic chemistry techniques, for encouraging me to be assertive, and for so many fun and lively conversations in the lab. To my biology mentor, Kirsten Viola, thank you for generously and patiently taking the time to teach me, for lending your wisdom whenever I had questions, and for encouraging me to rest when I needed to. Your vast wealth of knowledge and kindness to share it are a bedrock for the lab. And, to Erika Cline, thank you for teaching me how to be a meticulous biochemist.

To former graduate student Galen Miley, thank you for being a role model and for encouraging me. To Weijian Huang and Yifan Xu, thank you for your willingness to help with so many cell cultures, for lending your insight and ideas to improving the cell culture, and for being great friends. Thanks also to the many fellow graduate students, Huining Li, Evelyn Ho, Hongjie Xia, Sam Bartley, for uplifting conversations and support.

To Pam Beck, thank you for your thoughtful encouragement and profound kindness. It made a big difference in those moments where I needed it most.

Finally, thank you to my parents for their unconditional support and encouragement and to my brother Daniel for inspiring me to chase after my goals. And thank you to Rishav, not only for reading constant new drafts, but also for filling my days with joy and for always knowing how to make me smile.

Table of Contents

ABSTRACT	3
ACKNOWLEDGEMENTS	5
TABLE OF CONTENTS	7
LIST OF FIGURES	15
CHAPTER 1: INTRODUCTION	18
1.1 Alzheimer’s disease	19
<i>1.1.1 Epidemiology</i>	19
<i>1.1.2 Symptoms and disease course</i>	19
<i>1.1.3 Genetic and environmental causes</i>	20
<i>1.1.4 Plaques and tangles</i>	22
<i>1.1.5 Other pathology</i>	22
<i>1.1.6 Current treatment</i>	23
1.2 Amyloid beta (Aβ)	24
<i>1.2.1 Aβ formation</i>	24
<i>1.2.2 Aβ changes in AD</i>	24
1.3 AβO formation and structure	25
<i>1.3.1 Formation</i>	25
<i>1.3.2 Structure</i>	26
<i>1.3.3 Function</i>	29
1.4 Presence of AβO in AD	29
<i>1.4.1 AβO distinguish AD patients from controls</i>	29
<i>1.4.2 AβO levels are highly correlated with disease</i>	30

1.4.3 <i>AβOs are sufficient to cause AD pathology</i> - - - - -	31
1.4.4 <i>AβOs are necessary for memory loss in AD</i> - - - - -	32
1.5 <i>AβO-neuron interactions</i> - - - - -	33
1.5.1 <i>Some AβOs can form pores in membranes</i> - - - - -	33
1.5.2 <i>AβOs specifically bind to synaptic targets</i> - - - - -	34
1.5.3 <i>N-Methyl-D-aspartate receptor (NMDAR)</i> - - - - -	34
1.5.4 <i>Metabotropic glutamate receptor 5 (mGluR5)</i> - - - - -	35
1.5.5 <i>Prion protein (PrP^c)</i> - - - - -	35
1.5.6 <i>Sodium/potassium ATPase α3 subunit (NKAA3)</i> - - - - -	36
1.5.7 <i>Insulin receptor (IR)</i> - - - - -	36
1.5.8 <i>Frizzled receptor (Fz)</i> - - - - -	37
1.5.9 <i>p75 neurotrophin receptor (p75NTR)</i> - - - - -	37
1.5.10 <i>Alpha-amino-3-hydroxy-5-methyl-4-isoxazolepropionic acid receptor (AMPA)</i> - -	38
1.5.11 <i>α7 nicotinic acetylcholine receptor (α7nAChR)</i> - - - - -	38
1.5.12 <i>Receptor summary</i> - - - - -	38
1.5.13 <i>Intracellular AβOs</i> - - - - -	39
1.6 <i>AβO-directed therapeutic strategies</i> - - - - -	40
1.7 <i>Three strategies to disrupt AβOs</i> - - - - -	42
1.7.1 <i>Disrupt formation and accumulation of AβOs</i> - - - - -	42
1.7.2 <i>Block AβO induced pTau and downstream effects</i> - - - - -	42
1.7.3 <i>Neutralize AβO binding</i> - - - - -	43
1.7.4 <i>Summary</i> - - - - -	44

CHAPTER 2: INHIBITION OF AMYLOID BETA OLIGOMER ACCUMULATION BY	
NU-9: A NOVEL THERAPEUTIC APPROACH FOR ALZHEIMER'S DISEASE - - - -	45
2.1 Introduction - - - - -	46
2.1.1 <i>AβOs comprise a key instigator of AD pathology</i> - - - - -	46
2.1.2 <i>Prevention of AβO buildup could halt disease progression in AD</i> - - - - -	47
2.1.3 <i>Accumulation of oligomeric species and larger aggregates is a characteristic feature and potential therapeutic target in multiple neurodegenerative disorders</i> - - - - -	47
2.1.4 <i>The small molecule NU-9 conferred protection in models of ALS</i> - - - - -	48
2.1.5 <i>Could NU-9 protect against accumulation of AβOs?</i> - - - - -	48
2.2 Results - - - - -	49
2.2.1 <i>Small molecule compound NU-9 reduces neuronal binding of AβOs formed from Aβ monomer administered to cultured neurons</i> - - - - -	49
2.2.2 <i>NU-9 reduces AβO accumulation on neurons by a cell-based mechanism</i> - - - - -	51
2.2.3 <i>Proteasome inhibition does not alter the effect of NU-9 on AβO accumulation</i> - - - - -	54
2.2.4 <i>Lysosome inhibition prevents the effect of NU-9 on AβO accumulation</i> - - - - -	54
2.2.5 <i>The effect of NU-9 is mimicked by cathepsin L inhibition, but NU-9 does not inhibit cathepsin L</i> - - - - -	56
2.2.6 <i>Cathepsin B is necessary for the effect of NU-9, but NU-9 does not directly activate cathepsin B</i> - - - - -	59
2.2.7 <i>NU-9 rescued memory performance in preliminary experiments</i> - - - - -	62
2.3 Discussion - - - - -	64
2.3.1 <i>Summary</i> - - - - -	64
2.3.2 <i>NU-9 previously protected upper motor neurons against ALS proteopathies</i> - - - - -	64

2.3.3 <i>AβO</i> s cause neurodegeneration in AD	65
2.3.4 NU-9 prevents the buildup of neuron-binding <i>AβO</i> s	65
2.3.5 NU-9 may restore trafficking of <i>Aβ</i> to active lysosomes to prevent buildup of neuron-binding <i>AβO</i> s	67
2.3.6 Alternative possible mechanisms for NU-9	68
2.3.7 Neuron-binding <i>AβO</i> buildup from exogenous <i>Aβ</i> is dynamin-dependent	69
2.3.8 Cellular <i>AβO</i> formation is cathepsin-L dependent	70
2.3.9 Future directions	71
2.3.10 Potential therapeutic application of NU-9	72
2.3.11 Conclusion	73
2.4 Materials	73
2.5 Methods	74
2.5.1 <i>Aβ</i> film preparation	74
2.5.2 Amyloid beta oligomer preparation	75
2.5.3 Hippocampal neuron cell culture	75
2.5.4 Hippocampal neuron cell treatment	76
2.5.5 Immunofluorescence	76
2.5.6 Analysis of <i>AβO</i> binding assay	77
2.5.7 Cell-free incubation of <i>Aβ</i>	78
2.5.8 Dot blot biochemical assay of <i>Aβ</i>	78
2.5.9 Lysosome characterization using LysoTracker	79
2.5.10 Cathepsin B purified activity assay	79
2.5.11 Cathepsin L purified activity assay	80

<i>2.5.12 Intracellular cathepsin activity assays</i> - - - - -	81
<i>2.5.13 Novel object and novel placement recognition assay</i> - - - - -	81

CHAPTER 3: DISRUPTION OF AMYLOID BETA OLIGOMER ACCUMULATION

AND TAU PHOSPHORYLATION BY NNOS INHIBITION - - - - - **83**

3.1 Introduction: Alzheimer's disease and nNOS - - - - - **84**

3.1.1 A β O_s trigger tau phosphorylation and neurodegeneration - - - - - 84

3.1.2 Connection between nNOS and A β O binding - - - - - 85

3.1.3 Physiologic and pathologic roles of nNOS - - - - - 86

3.1.4 Evidence for the overactivation of nNOS in AD- - - - - 87

3.1.5 Potential targets of nNOS in AD - - - - - 88

3.1.6 nNOS inhibitors - - - - - 89

3.1.7 Development of nNOS inhibitors - - - - - 90

3.1.8 Low bioavailability of nNOS inhibitors - - - - - 90

3.1.9 Prodrug approach to nNOS inhibitors - - - - - 91

3.1.10 Non-prodrug optimization of nNOS inhibitors - - - - - 92

3.1.11 Research objective - - - - - 92

3.2 Results - - - - - **93**

3.2.1 Synthesis of carbamate prodrugs for nNOS inhibitors - - - - - 93

3.2.2 Passive permeability of nNOS inhibitor carbamate prodrugs was reduced - - - - - 94

3.2.3 Permeability predictions for prodrugs of HD-1-86 - - - - - 94

3.2.4 Neuronal production of nitric oxide radicals can be prevented by NOS inhibition- - - 97

3.2.5 Cellular expression of nNOS was variable across cell culture - - - - - 99

3.2.6 Inhibition of nNOS blocked A β O-induced tau phosphorylation at Thr205 and

<i>pSer396</i> -----	100
3.2.7 <i>nNOS inhibition increases synaptic puncta from baseline</i> -----	102
3.2.8 <i>nNOS inhibition reduces Aβ-derived AβO buildup</i> -----	103
3.3 Methods -----	104
3.3.1 <i>Summary of results</i> -----	104
3.3.2 <i>Mechanisms of interest</i> -----	105
3.3.3 <i>nNOS-dependence of tau phosphorylation at Thr205 – a potential role for Cdk5</i> --	106
3.3.4 <i>nNOS-dependence of tau phosphorylation at Ser396 – a potential role for GSK-3β</i>	107
3.3.5 <i>Potential Fyn kinase contribution to nNOS signaling</i> -----	108
3.3.6 <i>Potential role of nNOS in tau acetylation</i> -----	109
3.3.7 <i>Dexas1 activation and tau nitration as potential effects of nNOS</i> -----	110
3.3.8 <i>nNOS increases the number of synapses</i> -----	112
3.3.9 <i>nNOS inhibition can prevent AβO buildup from monomer</i> -----	112
3.3.10 <i>Potential therapeutic applications of nNOS inhibitors</i> -----	113
3.4 Methods -----	113
3.4.1 <i>Synthesis</i> -----	113
3.4.2 <i>PAMPA-BBB assay</i> -----	115
3.4.3 <i>Neuron culture in phenol red-free media for NO assays</i> -----	117
3.4.4 <i>DAF-FM DA assay for NO production in neurons</i> -----	117
3.4.5 <i>Neuron culture on coverslips for immunofluorescence of fixed cells</i> -----	118
3.4.6 <i>Cell treatment and immunofluorescent detection of pTau levels</i> -----	118
3.4.7 <i>AβO-induced pTau formation – method optimization/troubleshooting</i> -----	120
3.4.8 <i>Synaptic spine measurement with phalloidin</i> -----	121

3.4.9 <i>AβO binding assay</i> - - - - -	122
3.4.10 <i>Microscopy</i> - - - - -	123
CHAPTER 4: BLOCKAGE OF AMYLOID BETA OLIGOMER BINDING USING NUSC1 MEGAMOLECULES - - - - -	124
4.1 Introduction - - - - -	125
4.1.1 <i>Neutralization of AβOs provides neuroprotection</i> - - - - -	125
4.1.2 <i>Application of scFv technology to antibody therapy</i> - - - - -	126
4.1.3 <i>Nusc1 is an AβO-specific scFv antibody fragment</i> - - - - -	126
4.1.4 <i>Megamolecule technology for antibody fragments</i> - - - - -	127
4.1.5 <i>Application of megamolecules to Nusc1</i> - - - - -	129
4.2 Results - - - - -	130
4.2.1 <i>Megamolecules bind to cell-bound AβOs in neuron culture</i> - - - - -	130
4.2.2 <i>Neutralization with higher concentrations of megamolecules block AβO binding for monomer and dimer</i> - - - - -	134
4.2.3 <i>Differential neutralization by Nusc1 across concentrations</i> - - - - -	135
4.2.4 <i>Differential neutralization by Nusc1 megamolecules across concentrations</i> - - - - -	136
4.3 Discussion - - - - -	139
4.3.1 <i>Summary of results</i> - - - - -	139
4.3.2 <i>Nusc1 monomer effectively detects and neutralizes AβOs</i> - - - - -	139
4.3.3 <i>Nusc1 dimer exhibits multi-fold enhancement of AβO neutralization</i> - - - - -	140
4.3.4 <i>Nusc1 trimer scaffold interacts non-specifically with substrates</i> - - - - -	141
4.3.5 <i>Future work</i> - - - - -	141
4.3.6 <i>Significance</i> - - - - -	142

4.4 Methods - - - - -	143
4.4.1 <i>Megamolecule synthesis</i> - - - - -	143
4.4.2 <i>Hippocampal neuronal cell culture</i> - - - - -	143
4.4.3 <i>Synthesis of crosslinked AβOs (xLAβOs)</i> - - - - -	144
4.4.4 <i>Megamolecule immunofluorescence</i> - - - - -	144
4.4.5 <i>AβO neutralization assays</i> - - - - -	146
REFERENCES - - - - -	149
APPENDICES - - - - -	174

List of Tables, Illustrations, Figures, and Graphs

Table 1.1 Milestones establishing A β O clinical significance - - - - -	33
Figure 2.1 Small molecule compound NU-9 reduces neuronal binding of A β O _s formed from A β monomer administered to cell culture - - - - -	50
Figure 2.2 NU-9 reduces A β O accumulation on neurons by a cell-based mechanism - - - - -	53
Figure 2.3 Lysosome inhibition prevents the effect of NU-9 on A β O accumulation - - - - -	55
Figure 2.4 The effect of NU-9 is mimicked by cathepsin L inhibition, but NU-9 does not inhibit cathepsin L - - - - -	57
Figure 2.5 Control – inhibition of cathepsin L enzyme by cathepsin L inhibitor Z-FY-CHO - -	58
Figure 2.6 Cathepsin B inhibition blocks the effect of NU-9, but NU-9 does not directly activate cathepsin B - - - - -	60
Figure 2.7 Control – inhibition of cathepsin B by CA-074 - - - - -	61
Figure 2.8 NU-9 rescued memory performance in preliminary experiments - - - - -	63
Figure 2.9 Proposed mechanism: NU-9 restores trafficking of A β species to active lysosomes -68	68
Figure 3.1 Mechanism of NMDAR and nNOS-dependent excitotoxicity - - - - -	85
Figure 3.2 Mechanism of physiological NMDAR/nNOS signaling - - - - -	87
Figure 3.3 Potential mechanisms of nNOS-mediated neurodegeneration- - - - -	89
Figure 3.4 Synthesis of (1) methyl, (2) ethyl, (3) benzyl, and (4) dual methyl carbamate derivatives of HD-1-86 - - - - -	93
Table 3.1 PAMPA-BBB results for compounds 1-3 - - - - -	94
Table 3.2 CNS MPO scores for compounds 1-6 - - - - -	95
Figure 3.5 Central nervous system multi-parameter optimization (CNS-MPO) score correlates with measured permeability (P _e) - - - - -	96
Figure 3.6 Proposed Schiff base (5) and dihydropyridine (6) derivatives of HD-I-86 - - - - -	96
Figure 3.7 Glutamate induces NO production - - - - -	97
Figure 3.8 NOS inhibition prevents glutamate NO production - - - - -	98
Figure 3.9 Nitric oxide production in neurons - - - - -	99

Figure 3.10 nNOS expression is varied throughout neuron culture	-100
Figure 3.11 nNOS inhibition blocks pTau (Thr205)	101
Figure 3.12 nNOS inhibition blocks pTau (Ser396)	-102
Figure 3.13 nNOS inhibition increased synaptic puncta	103
Figure 3.14 nNOS reduces A β -derived A β O buildup	-104
Figure 3.15 Activation of tau kinases	107
Figure 3.16 Potential Fyn contribution to nNOS signaling	109
Figure 3.17 Tau acetylation	-110
Figure 3.18 CAPON and Dexras1 activation	111
Figure 3.19 nNOS antibody titration	-119
Figure 3.20 AT8 optimization	121
Figure 4.1 Megamolecule synthesis overview	-128
Figure 4.2 Monomer, dimer, and trimer megamolecules of Nuscl	130
Figure 4.3 Nuscl megamolecules detect cell-bound A β O (images)	-131
Figure 4.4 Nuscl megamolecules detect cell-bound A β O (quantification)	132
Figure 4.5 Both specific and nonspecific binding of Nuscl megamolecules increase with n-mer size (images)	-133
Figure 4.6 Both specific and nonspecific binding of Nuscl megamolecules increases with n-mer size (quantification)	-133
Figure 4.7 High concentration Nuscl monomer and dimer prevent A β O binding; Nuscl trimer prevents A β O binding but scaffold reduces binding as well	134
Figure 4.8 Neutralization by the original Nuscl scFv was effective at the highest concentration, less effective with dilutions (images)	135
Figure 4.8 Neutralization by the original Nuscl scFv was effective at the highest concentration, less effective with dilutions (quantification)	-136
Figure 4.10 Nuscl monomer reduced A β O binding in a dose-dependent manner	137
Figure 4.11 Nuscl dimer reduced A β O binding across the measured range	-137

Figure 4.12 Trimer cutinase scaffold reduced A β O binding ----- 138

Figure 4.13 Nuscl megamolecule immunofluorescence conditions ----- 145

CHAPTER 1:
INTRODUCTION

CHAPTER 1: INTRODUCTION

1.1 Alzheimer's disease

1.1.1 Epidemiology

More than 50 million people worldwide suffer from dementia¹, of which Alzheimer's disease (AD) accounts for approximately 60-70%². In the United States alone, about 6.5 million individuals have Alzheimer's dementia, which affects about 1 in 9 people age 65 and older². AD is projected to cost the United States \$321 billion in 2022, and it is currently the 7th most common cause of death. Deaths from AD have increased 145% since 2000, and currently 1 in 3 seniors dies with Alzheimer's or another form of dementia. Alzheimer's dementia places a substantial personal burden not just on individuals suffering from it³ but also their loved ones, who provided a combined 16 billion hours of unpaid care in the United States alone in 2021^{2,4,5}.

1.1.2 Symptoms and disease course

Pathological changes in the brain that eventually cause AD likely appear decades prior to the onset of symptoms. Studies from individuals with familial dementia in a cohort in Colombia⁶ and the Dominantly Inherited Alzheimer's Network⁷ suggest that over 20 years before the onset of clinical symptoms, aberrations in biomarkers can be measured, including levels of amyloid beta (A β) peptide in plasma and cerebrospinal fluid (CSF) (-25 estimated years to symptom onset (EYO); the number of years thought to have occurred prior to symptom onset)^{11, 12}. Additionally, in CSF, phosphorylation of tau at Thr217 (-21 EYO)⁸, and increases of neurofilament light, an indicator of neuronal damage (-22 EYO)⁹, have been detected. After this time, phosphorylation

of tau at additional epitopes is observed in CSF (-19 EYO for Thr181, -13 EYO for Thr205)⁸, along with the deposition of A β peptides in brain plaques (-15 to -21 EYO)^{8,10-12}.

Alzheimer's dementia is also preceded by a prodromal phase called mild cognitive impairment (MCI) in which modest changes in memory are detectable, but individuals are able to maintain most activities of daily living¹³⁻¹⁶ (~4y duration¹⁷). The onset of dementia is defined by loss in cognitive function that interferes with the activities of daily life and leads to a loss of independence^{18,19}. In Alzheimer's disease in particular, dementia often involves loss of memory, difficulties with language and communication, difficulties with problem solving and other cognitive skills, disorientation and confusion, and behavioral changes². One individual with dementia described the experience by saying "Sometimes it feels like thinking in syrup—it is possible, but it takes a long time, it's sticky and it's difficult."³ Individuals with Alzheimer's also frequently described fears of losing their sense of self, and of burdening their loved ones. Approximately 3-6 years after the diagnosis of dementia, the disease progresses to the point of difficulty ambulating and swallowing, leading to death^{2,17,20}.

1.1.3 Genetic and environmental causes

The strongest risk factor for AD is age. About 5.0% of people 65-74, 13.1% of people 75-84, and 33.2% of people >85 years old have AD²¹. Data from twin studies indicate that Alzheimer's disease is 60-80% heritable²². Several rare, dominant mutations can cause Alzheimer's disease; all of these mutations result in elevated production of more aggregation-prone isoforms of A β ²³⁻²⁶. Additionally, duplication of the amyloid precursor protein (APP) gene, either by duplication of the entire chromosome 21 in Down's syndrome²⁷ or by microduplication of the APP gene specifically²⁸, causes early development of AD. Conversely,

the APP A637T mutation, which reduces A β production, also reduces the chance of AD development²⁹.

A genetic risk factor which affects a much greater number of people is the ϵ 4 allele of apolipoprotein E (ApoE4). Having one copy of the allele increases AD risk 3-4x, while having two copies increases risk 8-12x³⁰⁻³³. More recent genome-wide association studies have identified numerous other risk genes, most of which are associated with APP metabolism, cholesterol homeostasis, endocytic trafficking, and inflammation/immune responses^{34,35}. The combination of these genes can be used to predict development of AD with 80% accuracy³⁶.

The remainder of AD risk is environmental. Maintenance of cardiovascular health, physical activity, and healthy diet are associated with lower risks of dementia overall^{2,37}. Additionally, education,^{38,39} socio-economic status, and social interactions⁴⁰ may also be protective factors. Conversely, repeated history of traumatic brain injury increases the risk of dementia⁴¹⁻⁴³.

Given that a substantial portion of Alzheimer's disease risk is genetically inherited, the effectiveness of lifestyle interventions to prevent disease, while important, may be limited. As such, the development of therapeutics to slow and stop the progression of AD is critical. In this regard, the vast scope of genetic information obtained regarding AD can provide insight into the cellular pathways of AD development and is a rich resource to help inform the development of such therapeutics.

1.1.4 Plaques and tangles

The prototypical histopathologic features of AD are the deposition of extracellular plaques comprised of insoluble fibrils of A β peptide and the buildup of intracellular tangles of hyperphosphorylated tau protein^{44,45}. Current evidence of disease progression indicates that the buildup of tau tangles is preceded by the development of A β pathology⁴⁶⁻⁴⁹. Development of both A β plaques and tau tangles tends to follow a stereotyped path, appearing in basal neocortex, spreading throughout the hippocampus, and finally spreading to other areas of the cortex⁵⁰. The burden of deposited amyloid plaques does not correlate well with the severity of cognitive loss, indicating that insoluble A β is not the primary driver of neurodegeneration⁵¹. Rather, plaques build up steadily and tend to plateau with the onset of dementia⁵². Meanwhile, tau tangles generally increase with age⁵⁰.

Current hypotheses regarding the major instigators of neurodegeneration in AD highlight a role for smaller, soluble A β and tau species, rather than the large plaques and tangles^{53,54}. These larger aggregates may, in fact, represent sinks for the smaller, more neurotoxic species⁵⁵. Alternatively, the structure of A β plaques, comprising a dense core and a diffuse surrounding region, with a halo of surrounding smaller A β oligomers and neuronal death suggests that plaques may leak smaller neurotoxic species⁵⁶.

1.1.5 Other pathology

Additional features of AD histopathology are often observed in regions adjacent to A β plaques. This localization of these features is hypothesized to be instigated by diffusion of A β oligomers leaking out from the plaques⁵⁶. One such feature is the inflammatory activation of astrocytes and microglia^{57,58}. Also observed in proximity to A β plaques in the AD brain are lipid

peroxidation, protein carbonyls, and tyrosine nitration, along with other indicators of oxidative stress⁵⁹. This oxidative damage likely contributes to two key features of energy dyshomeostasis in AD: the impairment of glucose metabolism and insulin resistance⁵⁹. The observation of insulin resistance in AD has led to the proposal that AD represents a form of brain-specific diabetes⁶⁰. Vascular pathology is also observed in AD, including stiffness of arteries and degeneration of the blood-brain barrier^{61,62}. Finally, a close pathological correlate to dementia severity in AD is the loss of neuronal synapses^{51,63}. Eventually, this damage results in diffuse loss of overall brain volume⁶⁴.

1.1.6 Current treatment

Currently, five FDA-approved therapeutics exist for the treatment of AD. Rivastigmine, galantamine, and donepezil provide symptomatic relief by inhibiting the degradation of the excitatory neurotransmitter acetylcholine, but do not modify disease course⁶⁵. Memantine, an N-methyl-D-aspartate receptor (NMDAR) inhibitor, also provides symptomatic relief, but its mechanism is incompletely understood. It can mitigate some of the excitotoxicity that occurs in AD by preventing hyperactivation of the NMDAR⁶⁶. Recently, in 2021, the antibody therapeutic aducanumab was also approved by the FDA. This antibody partially targets oligomers of A β and provided some improvements in cognitive function. This promising result hints at the importance of A β oligomers in AD. However, there is still a significant unmet need for therapeutic agents that robustly protect against memory loss in AD.

1.2 Amyloid beta (A β)

1.2.1 A β formation

A β peptide, which makes up the characteristic plaques in AD, is produced by consecutive cleavage of APP by different secretases⁶⁷⁻⁶⁹. First, β -secretase cleaves the transmembrane portion of APP to produce the β C-terminal fragment of APP (β -CTF) and APPs β . Alternatively, an α -secretase, usually a disintegrin and metalloproteinase-domain-containing protein 10 (ADAM10) can cleave the transmembrane portion to release α -CTF and APPs α . Finally, cleavage by γ -secretase produces the APP intracellular domain (AICD) and either A β (from β -CTF) or p3 (from α -CTF). Then APPs α is proposed to serve neuroprotective functions, while AICD, in addition to A β , has been proposed to play a role in neurodegeneration^{68,70,71}. Production of A β in neurons is mostly intracellular in acidic endosomes or in the Golgi after which A β may be trafficked to synaptic vesicles. Some A β can also be produced at the cell membrane for extracellular release⁷²⁻⁷⁵.

1.2.2 A β changes in AD

Soluble A β is elevated in brain tissue from AD patients. Particularly, the 42-amino acid peptide (A β ₄₂) and a small amount of A β ₄₃ are enriched in AD brains^{76,77}. The overproduction of aggregation-prone A β proteoforms is implicated as a genetic cause of AD^{23,26,28,78}. For example, mutations in APP can directly increase aggregation potential of A β ⁷⁹ and can also enhance the production of longer isoforms such as A β ₄₂, which have elevated tendencies for self-aggregation due to their greater hydrophobic character⁸⁰. Mutations in the presenilin (PSEN) 1 and 2 genes alter the processivity of the γ -secretase enzyme, of which either presenilin enzyme forms the catalytic core^{81,82}, resulting in the production of longer A β isoforms.

In late-onset disease, A β production may be upregulated due to its potential physiological roles as a response to infection^{83,84} and to strengthen otherwise failing synapses⁸⁵, which might occur due to aging or environmental factors. A third factor implicated in disease development due to either mutations, aging, or sleep deprivation is a failure to remove basal levels of A β due to faulty proteolysis and clearance^{86,87}. Accordingly, the enrichment of A β_{42} in the brain in AD patients corresponds with a reduction in CSF A β_{42} , suggesting reduced clearance of these species from the brain to CSF in AD^{88,89}.

The concentration of soluble A β in the CSF is a strong inverse correlate of synapse loss⁹⁰, which unsurprisingly has been the best predictor of dementia severity. Furthermore, soluble A β levels in brain were not elevated in brains from cognitively normal individuals but which nevertheless contained plaques. This evidence supporting the role of aggregation-prone, soluble A β in disease progression eventually led to the discovery of a crucial pathologic species, A β oligomers (A β Os)⁹¹.

1.3 A β O formation and structure

1.3.1 Formation

Prior to forming plaques, A β forms smaller, soluble clusters known as A β Os⁹². Buildup of A β Os follows the cleavage of amyloid precursor protein at Golgi or endosomal membranes, which produces an intracellular pool of A β , or at the cell membrane, which produces an extracellular pool of A β ^{93,94}. In experimental settings, even at picomolar concentrations, A β Os can form spontaneously from monomer^{95,96}. *In vitro*, A β Os spontaneously form a variety of species, ranging in size from dimers, trimers, and tetramers to larger annular and spherical species.^{54,97,98} The formation of different oligomer structures can be affected by concentration,

pH, salt composition, mechanical disturbances, time, and temperature, as well as the particular A β proteoform involved^{99,100}.

It has been hypothesized that *in vivo* the earliest formation of A β O_s occurs intracellularly^{92,101,102}, catalyzed by concentration of A β into the acidic environment of endo-lysosomal compartments¹⁰³⁻¹⁰⁷. This could occur directly following formation of the intracellular pool of A β in endosome or could result from endocytosis of extracellular A β . Receptor-mediated endocytosis of A β can be mediated by the low-density lipoprotein receptor-related protein 1¹⁰⁸ or by binding to the receptor for advanced glycation end products (RAGE)^{109,110}. A β O formation could also be promoted by GM1 ganglioside, either at the cell membrane or within endo-lysosomal vesicles¹¹¹. In mouse models and in humans, A β O_s accumulate in trafficking vesicles, especially in late endosome or multivesicular bodies^{112,113}.

After intracellular formation, A β O_s can mediate intra-neuronal damage¹¹³⁻¹¹⁵. Intracellularly, A β O_s can inhibit proteasome activity¹¹⁶, impair mitochondrial function^{115,117,118}, and damage lysosomes^{115,119}. Further, intracellular A β O_s can spread directly from cell to cell¹²⁰. Exosomal release or direct puncture of membranes also allows A β O_s to be released extracellularly^{121,122}, where they can exert damage upon binding to neuronal receptors, or upon internalization by receptor-mediated endocytosis.

1.3.2 Structure

Oligomer structure has proved difficult to investigate, given the meta-stable, aggregation-prone nature of A β . Nonetheless, valuable information has been obtained from studies using size-exclusion chromatography, atomic force microscopy, 2-dimensional nuclear magnetic resonance spectroscopy, and cryo-electron microscopy, among other techniques.

In general, oligomers have been classified into two groups: those that are “on-pathway” to form fibrils, and others that are “off-pathway” and remain relatively stable in an oligomeric conformation. Although these definitions are presented as binary in much of the literature, it is expected that all these species exist along thermodynamic gradients in which different conditions might stabilize a particular A β O or reverse its course from the “on-pathway” to “off-pathway.” Regardless, these studies provide significant insight into the diverse range of A β O structures that might form in AD.

The “on-pathway” oligomers range from smaller, disk-shaped pentamers (1-2 nm) and decamers (3-4 nm) of loosely aggregated strands¹²³ to larger spherical amyloid intermediates (13-35 nm) with parallel β -sheet structure¹²⁴ and eventually form fibrillar oligomers (13-28 nm length) that comprise 19-mers with a parallel β -sheet structure within a superhelix¹²⁵. Eventually, these develop the characteristic structure of A β fibrils: parallel, in-register β -sheets¹²⁶. While some “on-pathway” A β oligomers exhibit greater cytotoxicity than fibrils, they are relatively unstable at human body temperature, and are, therefore, likely to be relatively short-lived within disease pathology. As such, the “off-pathway” oligomers are, therefore, predicted to instigate more lasting damage within AD.

“Off-pathway” A β O importantly are not ordered in the parallel, in-register β -sheets of fibrils and “on-pathway” oligomers. Instead, they encompass a variety of globular, annular, and protofibril structures. For example, globular A β O (1-10 nm, 150 kDa, 30-35mer) made on micelles of dilute detergent at 25 °C contained both parallel and antiparallel β -sheet structure¹²⁷⁻¹²⁹. At slightly higher temperature (37 °C), smaller “globulomers” (4-5 nm, 60 kDa, 12mer) were obtained¹³⁰; these also comprised a mixed β -sheet structure due to the presence of a β -hairpin¹³¹.

Sandberg et al. stabilized the β -hairpin by introducing a di-cysteine mutation, a modification that stabilized “off-pathway” oligomers (6 nm, ~100 kDa, 20-22mer), producing an antiparallel β -sheet structure that could form protofibrils¹³². Doi et al. confirmed that wild-type A β in the absence of detergent at 37 °C also yields protofibrils (100 nm length), which are arranged in non-parallel β -sheets¹³³. Further, Kaye et al. produced annular protofibrils (8-25 nm outer diameter) by incubation of globular A β O with liposomes¹³⁴⁻¹³⁶.

Lambert et al. used incubation in F12 media to produce globular A β O of variable size depending on the exact concentration and temperature (1-6 nm species, 10–700 kDa, ~2-155mer)^{91,137,138}. In PBS, Nirmalraj et al. also produced globular A β O (7-9 nm) whose formation and stability was monitored over 120 h by atomic force microscopy¹³⁹. Using increased agitation, Noguchi et al. produced amylospheroids (10-15 nm, 158–669 kDa, ~35-150mer) with parallel, out-of-register β -sheet structure^{140,141}. Although Noguchi et al. reported these species were “off-pathway”, after about 7 days at reduced salt concentration, they converted to a larger spherical intermediate (35 nm), which quickly rearranged to form fibrils¹⁴². This observation highlights the fact that A β O are unlikely to be perfectly stable “off-pathway”, but that the biological environment in which they reside is an important factor to establish which A β O are stable *in vivo* and present in the AD brain. Kass et al. studied the most common A β O in human AD samples and mouse models and identified a fraction of soluble A β O \geq 400 kDa as the most common form¹⁴³.

Additionally, synthetic biological strategies have enabled A β O imaging with higher-resolution techniques; it will be important to validate the relevance of these structures in disease. Kreutzer et al. stabilized dimers in a β -hairpin structure using a macrocycle, enabling X-ray

crystallography, which was used to demonstrate the formation of triangular trimers, which assembled to dodecamers, and finally to a higher-order annular A β O¹⁴⁴. Using wild-type A β in a lipid-mimicking solution, Ciudad et al. also formed an annular A β O at 37 °C, which was comprised of tetramers and octamers with antiparallel β -sheets, and formed pores in a membrane¹⁴⁵. Wu et al. also prepared annular A β O_s by fusing A β to α -hemolysin; this stabilized annular heptamers and provided a reference to enable higher-resolution cryo-electron microscopy imaging¹⁴⁶. This detailed structure again demonstrated the key features of β -sheets containing β -hairpins, formed into an annular structure. In this way, creative strategies for the characterization of A β O_s and technological advancements in imaging technology are predicted to provide additional insights into the structure of these species in the future.

1.3.3 Function

A β O_s have also been demonstrated to serve physiological functions. For example, at picomolar levels, A β O_s can strengthen synapses to boost long-term potentiation^{85,147-150}. Additionally, Bartley et al. observed transient expression of A β O_s during embryonic development of the chicken retina, suggesting a potential developmental function for A β O_s¹⁵¹. Finally, antimicrobial functions of A β O_s have also been observed⁸³. However, overproduction of A β O_s in disease leads to dysfunction and neurodegeneration.

1.4 Presence of A β O_s in AD

1.4.1 A β O_s distinguish AD patients from controls

Studies using brain tissue and CSF samples from AD patients have been important to determine the correlation of A β O_s with disease. To that end, several conformation-specific

antibodies have been designed and used to identify A β O in AD patient samples. Specific antibodies developed against amylospheroids, rpASD1 and mASD3, showed a significant elevation of these species in brain tissue from AD patients, which was correlated with severity of disease¹⁴⁰. Globular A β O-specific antibodies, NU1 and NU4, also distinguished AD brain from control brain¹⁵². Likewise, globulomer-specific antibodies, 8F8 and 5598, distinguished AD brains from a healthy control, and were not found in MCI brains¹³⁰. Additionally, a moderately selective, protofibril-specific antibody (mAb158) distinguished AD brains from a healthy control¹⁵³. These experiments have demonstrated an overall elevation of various A β O structures in AD.

1.4.2 A β O levels are highly correlated with disease

A β O levels are highly correlated with AD. As previously discussed, A β O are elevated in the frontal cortex of individuals with AD compared to controls^{143,154}. Further, an elevated ratio of A β O levels to plaque density distinguished individuals with AD dementia from those with A β plaques but no dementia, indicating that A β O are a specific indicator of memory loss^{155,156}. A β O composed of dimers were also specific to AD dementia; they were not found in other types of dementia¹⁵⁷. Elevated synaptic A β O levels also distinguished AD patients from controls, and buildup of synaptic A β O preceded tau phosphorylation during disease progression¹⁵⁶. Importantly, A β O levels in frontal cortex from AD patients were correlated with the loss of synapses and the level of cognitive impairment^{140,158}.

In addition to brain, A β O in CSF, plasma, and even nasal discharge are elevated in AD and accumulate as the disease progresses. In CSF, Georganopolou et al. detected elevated levels of A β O in samples from AD patients compared to controls¹⁵⁹. Plasma A β O levels were also

elevated in individuals with AD compared to controls and correlated well with AD biomarkers such as CSF pTau and total tau, decreases in plasma A β ₄₂, and amyloid PET in brain^{160,161}. Plasma A β O_s also correlate with lower cognitive performance among individuals with AD¹⁶² and even among individuals in the very early stage of AD with MCI¹⁶³. Further, when nasal discharge was profiled longitudinally in patients with mild to moderate AD, levels of A β O_s increased over time in individuals with declining cognitive performance and were correlated with cognitive dysfunction¹⁶⁴. Taken together, this evidence robustly demonstrates that A β O_s are specifically elevated in AD, build up early and increasingly throughout disease progression, and correlate with memory loss.

1.4.3 A β O_s are sufficient to cause AD pathology

Genetic and animal evidence indicate that A β O_s are sufficient to induce AD. In individuals with the Osaka mutation of AD (E693 Δ in APP, E22 Δ in A β), which causes minimal A β plaques but substantial A β O buildup, neurodegeneration and memory loss occur¹⁶⁵⁻¹⁶⁹. Although postmortem tissue is not available from humans with the E693 Δ mutation, E693 Δ animal models develop other features of AD subsequent to A β O buildup, including tau hyperphosphorylation, activation of astrocytes and microglia, synapse degeneration, and memory loss¹⁷⁰. Similarly, the Arctic mutation of AD (E693G in APP, E22G in A β) promotes the formation of A β O protofibrils¹⁷¹. Minimal plaques form in individuals with this mutation, but this alteration in A β O formation is sufficient to cause pathologic increases in CSF pTau, formation of tau tangles, abnormalities in glucose metabolism, and memory impairment^{172,173}.

In healthy animals, injection of A β O_s is sufficient to induce AD pathology. In mice and rats expressing the human APP gene, A β O injection triggers activation of astrocytes and

microglia, tau phosphorylation, and degeneration of neurites¹⁷⁴⁻¹⁷⁷, as well as deficits in long-term memory¹⁷⁸, working memory¹⁷⁹, and spatial memory¹⁸⁰. In non-human primates, A β O injection also triggered manifestation of AD pathology. Intracerebroventricular injection of A β O caused synapse loss and tau hyperphosphorylation in cynomolgus monkeys (*Macaca fascicularis*)¹⁸¹; in rhesus macaques (*Macaca mulatta*) A β O injection caused spine loss in dorsolateral prefrontal cortex and neuroinflammation¹⁸². More direct intracerebral injection of A β O to cynomolgus monkeys resulted in formation of A β plaques and tau tangles, activation of microglia and astrocytes, and synapse loss¹⁸³. Recently, Wakeman et al. showed that intrathecal injection of A β O in African green monkeys (*Chlorocebus sabaeus*) also stimulated tau phosphorylation and caused reduction in hippocampal brain volume¹⁸⁴. These studies provide strong evidence that A β O are sufficient to cause AD pathology.

1.4.4 A β O are necessary for memory loss in AD

Conversely, prevention of A β O buildup by antibody treatment or enhancement of clearance protects against memory loss. Intranasal delivery of the A β O-specific antibody, NU4, lowered cerebral A β levels and improved spatial learning in an AD mouse model¹⁷⁵. Similarly, the pan-oligomer specific antibody W20 also rescued cognitive impairment in AD model mice¹⁷⁶. Additionally, RD2, a compound developed to enhance clearance of A β O, restored memory in AD model mice¹⁸⁵.

Evidence from several Phase 3 clinical trials of antibody therapeutics in humans also supports this conclusion. Although antibodies that removed monomeric and fibrillar A β did not provide significant therapeutic effect¹⁸⁶⁻¹⁸⁸, two antibodies with promising Phase 3 trial results, aducanumab and lecanemab, bound to a subset of species that includes A β O somewhat more

selectively¹⁸⁹⁻¹⁹². These species also showed modest efficacy to protect memory. These provide the first human evidence that A β O are necessary instigators of AD memory loss. Key evidence supporting the clinical importance of A β O are presented in Table 1.1.

Table 1.1. Milestones establishing A β O clinical significance

Milestones establishing AβO clinical significance
Introduction of the A β O hypothesis ⁹¹ .
A β O impair synaptic plasticity, inhibiting long-term potentiation ^{91,193,194} and promoting long-term depression ¹⁹⁵ .
A β O instigate key features of AD pathology (synapse loss, tau hyperphosphorylation, glial activation, and selective nerve cell death) ¹⁹⁶⁻¹⁹⁹ .
A β O cause memory dysfunction in animals ^{138,200,201} .
A β O buildup is AD-dependent (in human brain and CSF ^{154,202} and in animal AD models ^{96,203}).
Brain-derived and synthetic A β O are structurally homologous ¹⁵⁴ and bind selectively to synapses ²⁰⁴ .
A β O-targeting antibodies, in animal AD models, rescue memory function ²⁰¹ .
Clinical trials have been initiated to assess A β O-targeting therapeutics in humans ²⁰⁵ .

1.5 A β O-neuron interactions

1.5.1 Some A β O can form pores in membranes

One postulated form of nonspecific, A β O-induced damage is based on the ability of annular A β O to form pores in membranes^{206 207}. This has been proposed to enable calcium influx into neurons and associated toxicity^{208,209}. Additionally, the ability of A β O to damage membranes by compromising membrane integrity without pore formation has also been described²¹⁰. In these ways, A β O can induce nonspecific, ion-associated damage to cells.

1.5.2 A β O_s specifically bind to synaptic targets

However, several features of A β O interaction with cells suggest specific binding to synaptic targets. First, A β O_s specifically damage certain cell types in disease^{211,212} and *in vitro*^{154,199}, including certain subpopulations of excitatory neurons. Further, A β O_s exhibit specific, saturable, and high-affinity binding to a subset of cell types, where they colocalize with receptors at excitatory synapses^{154,204,213}. Disruption of A β O binding by knockout or knockdown of receptors prevented A β O binding and protected neuronal health^{214,215}. Additionally, nerve terminals with bound A β O_s also developed pTau¹⁵⁶. This evidence suggests that A β O_s induce damage by acting as toxic ligands at specific receptor targets.

1.5.3 N-Methyl-D-aspartate receptor (NMDAR)

One key receptor engaged by A β O_s is the NMDAR²¹⁶, a glutamate receptor involved in long-term potentiation²¹⁷. Physiological activation of the NMDAR by glutamate triggers opening of its calcium channel and subsequent calcium influx into the cell. Synaptic NMDARs containing NR2A subunits close more rapidly, while extra-synaptic NMDARs containing NR2B subunits remain active for longer²⁰⁶. A β O_s bind to NR2B-containing NMDARs and activate them, causing a disruption of calcium homeostasis that leads to downstream formation of reactive oxygen species and loss of synaptic spines^{216 218-221}. Accordingly, the NMDAR inhibitor memantine is partially protective against A β O-induced neuronal damage, as were NR2B-selective inhibitors²²². A β O binding to cells requires the presence of the NMDAR, as knockdown²¹⁴ or blockade by an anti-NMDAR antibody²¹⁶ prevented A β O binding to cells. However, NMDAR expression is not sufficient to enable A β O binding²¹⁴, supporting the

conclusion that a receptor complex may be involved in A β O binding to neurons. Dysregulation of this group of receptors by A β O might then cause dysfunction via multiple signaling cascades.

1.5.4 Metabotropic glutamate receptor 5 (mGluR5)

Evidence from Renner et al. supports the hypothesis that A β O engage a complex of receptors²¹³. A co-immunoprecipitation identified both mGluR5 and NMDARs bound to A β O. A β O bind to neurons and form clusters of increasing size over time, with concurrent reduction in lateral diffusion. Over the same time period, the metabotropic glutamate receptor 5 (mGluR5) is also increasingly aberrantly clustered and co-accumulates at synapses with A β O. Disrupting the A β O-mGluR5 interaction by mGluR5 knockout or use of an anti-mGluR5 antibody significantly reduced A β O binding to cells, indicating that it enhances A β O binding affinity to the complex. The presence of mGluR5 was also necessary for an A β O-induced increase in intracellular calcium and synapse deterioration, which was prevented by an mGluR5 antagonist^{213,222}. mGluR5 was also found to mediate A β O-induced Fyn kinase activation, in a prion protein dependent manner, suggesting a role for the prion protein in the A β O receptor complex as well²²³.

1.5.5 Prion protein (PrP^c)

A β O bind with nanomolar affinity to the cellular prion protein (PrP^c)²²⁴, which is best known for its role in prion diseases, but which also contributes physiologically to memory and sleep homeostasis²²⁵. A β O bind to the PrP^c with nanomolar affinity, activating Fyn kinase, which then phosphorylates the NMDAR NR2B subunit, causing a transient increase in NMDARs at the cell surface prior to loss of synapses²²⁶. In this way, A β O interaction with PrP^c causes a disruption in synaptic plasticity²²⁴. Additionally, aberrant signaling of several receptors

is associated with PrP^c-mediated, A β O-induced dysfunction²²⁷⁻²²⁹. As such, the PrP^c has been hypothesized to act as a scaffolding protein that coordinates protein complexes of A β O-associated receptors to mediate neurodegeneration^{230,231}. PrP^c-mediated A β O toxicity also requires lipid rafts, which likely enable the formation of such protein complexes at the cell membrane²³².

1.5.6 Sodium/potassium ATPase α 3 subunit (NKAA3)

A β O_s also bind to the sodium/potassium ATPase α 3 (NKAA3) subunit and inhibit function, leading to calcium dyshomeostasis, tau abnormalities, and neurodegeneration²³³. Komura et al. observed that A β O_s developed intraneuronally in excitatory neurons were released and caused neurotoxicity of nearby NKAA3-expressing cells²³⁴. Recent literature suggests additional pathogenic effects of A β and A β O interactions with NKAA3^{235,236}. This receptor has also been proposed as a “docking station” at which bound A β O_s could recruit other receptors²³⁷.

1.5.7 Insulin receptor (IR)

The complex of receptors that A β O_s bind can also include the insulin receptor (IR). A β O_s bind to the IR and prevent insulin-induced IR autophosphorylation, thereby inhibiting LTP²³⁸. Further, binding of A β O_s causes rapid, significant internalization of neuronal surface insulin receptors specifically on dendrites bound by A β O_s^{239,240}. These results implicate A β O_s as a possible cause of the insulin resistance found in AD. IR autophosphorylation was restored by the application of NMDAR inhibitors²³⁹. Additionally, application of extracellular insulin was protective to neurons by preventing A β O binding, indicating a protective role for insulin^{240,241}. Accordingly, application of liraglutide, a therapeutic agent that enhances insulin release,

protected against A β O-induced tau hyperphosphorylation and synapse pathology in non-human primates²⁴².

1.5.8 Frizzled receptor (Fz)

A β O_s also bind to the cysteine-rich domain of the frizzled receptor (Fz), a receptor that typically stimulates signaling via the canonical Wingless/Int-1 (Wnt) signaling pathway²²⁴. A β O binding inhibits the canonical Wnt signaling pathway²⁴³⁻²⁴⁵. This causes tau phosphorylation and formation of tau tangles, possibly because Wnt signaling inhibits GSK-3 β , a tau kinase²⁴³. The canonical Wnt signaling pathway, in turn, is neuroprotective against A β O-induced mitochondrial damage, so Fz inhibition by A β O_s likely contributes to a cycle of neurodegenerative effects.

1.5.9 p75 neurotrophin receptor (p75NTR)

Another binding target of A β proteoforms is the p75 neurotrophin receptor (p75NTR)²⁴⁶. A β binding can activate the p75NTR, causing neuronal cell death^{111,247-249}. However, Costantini et al. observed that, while cell death caused by A β fibrils was p75NTR-dependent²⁴⁸, cytotoxicity induced by A β O was p75NTR-independent²³⁶. They and Zhang et al. concluded that p75NTR activation, in fact, provided protection against A β O-induced cytotoxicity^{235, 236}. Conversely, using different A β O preparations, A β O_s were observed to trigger p75NTR-dependent neuronal cell death¹¹¹, as well as tau phosphorylation and synapse degeneration²⁵⁰. Patnaik et al. also found that A β O_s activated the p75NTR, resulting in signaling via the Ras homolog family member A and rho-associated, coiled-coil-containing protein kinase signaling cascade, which stabilizes actin and thereby triggers synaptic spine distension²⁴⁹. Because Patnaik et al. used sub-lethal, nanomolar concentrations of A β O_s rather than the higher concentrations used in prior experiments, this effect may be most representative of the role of the p75NTR in AD.

1.5.10 *Alpha-amino-3-hydroxy-5-methyl-4-isoxazolepropionic acid receptor (AMPA)*

A β O binding to neurons colocalizes with alpha-amino-3-hydroxy-5-methyl-4-isoxazolepropionic acid receptors (AMPA) at synaptic spines, particularly those containing a GluR2 subunit²⁵¹. Co-immunoprecipitation experiments revealed a preferential interaction of A β O with GluR2-containing complexes. Binding of A β O to AMPA results in rapid calcineurin-dependent internalization, likely as an effect of NMDA-dependent or mGluR-dependent long-term depression. Removal or inhibition of AMPA reduces A β O binding, and AMPA inhibitors prevented the internalization of AMPA and synaptic spine loss. Zhao et al. also demonstrated that A β O inhibit GluR1 signaling, indicating multiple forms of AMPA dysfunction in AD^{220,252}.

1.5.11 *α 7 nicotinic acetylcholine receptor (α 7nAChR)*

A β proteoforms also bind to the α 7 nicotinic acetylcholine receptor (α 7nAChR) with high affinity, resulting in internalization of the A β species with the α 7nAChR²⁵³. In neuroblastoma cells, binding of A β species to α 7nAChR killed neuroblastoma cells, an effect that was rescued by α 7nAChR agonists²⁵⁴. In AD model mice, increased expression of α 7nAChR led to increased tau pathology²⁵⁵. However, the α 7nAChR may also serve a protective role to suppress A β O formation²⁵⁶.

1.5.12 *Receptor summary*

In summary, extracellular A β O can cause damage to neurons by engaging with a cluster of receptors including the NMDA, mGluR5, PrP^c, and IR. The NMDA, mGluR5, PrP^c, p75NTR, and AMPA GluR1 are all aberrantly activated by A β O binding, leading to calcium

dyshomeostasis and synapse degeneration. Meanwhile, A β O binding inhibits the IR and Fz, leading to energy dyshomeostasis and tau phosphorylation, while activation of these pathways is neuroprotective. Finally, A β and A β O_s are internalized upon binding the IR, AMPAR, or α 7nAChR. Intracellular A β O_s further instigate neurodegeneration.

1.5.13 Intracellular A β O_s

In addition to extracellular A β O_s, neurodegeneration in AD is also instigated by intracellular A β O_s. As previously mentioned, most A β O_s likely form intracellularly^{101,257}. APP internalization from the cell membrane, followed by intracellular cleavage, produces intracellular A β , which then oligomerizes to produce A β O_s. In addition, A β O_s formed intracellularly can be externalized, and extracellular A β O_s can be endocytosed upon association with IR, AMPAR, α 7nAChR, or other receptors^{258,259}. Yu et al. identified dynamin-dependent endocytosis and intraneuronal accumulation as a key feature of A β O-induced neurotoxicity²⁶⁰.

Regardless of the mechanism, accumulation of intraneuronal A β is an early event in disease¹⁰², observed both in AD animal models^{247, 248} and AD patients^{101,261}. Intracellular A β accumulates in endosomes, endoplasmic reticulum, trans-Golgi network, and multi-vesicular bodies and is often trafficked to lysosomes¹⁰². After escape from trafficking compartments, A β also accumulates in mitochondria, and cytosol. The presence of intracellular A β and A β O_s in AD are associated with formation of reactive oxygen species, lipid peroxidation, lysosome degradation, synapse dysfunction, tau phosphorylation, neuronal loss, and cognitive loss^{102,260}

1.6 A β O-directed therapeutic strategies

Currently available AD treatments can only provide symptomatic treatment to slightly bolster neurotransmission or to clear larger A β aggregates^{263,264}. Given that A β O is an early, key instigator of neurodegeneration in AD, promoting tau phosphorylation, synapse loss, and energy dyshomeostasis, and a significant body of evidence indicates that they are necessary and sufficient to cause memory impairment, several therapeutic strategies have been proposed to target A β O. These have included directly blocking A β O formation^{265,266}, bolstering A β /A β O degradation²⁶⁷⁻²⁶⁹, and neutralizing A β O with targeted antibodies^{205,270}.

In 2022, 63% of agents in Phase 3 clinical trials were disease-modifying therapeutic agents²⁷¹. Among disease-modifying therapeutic agents, small molecules and biologics targeted at A β comprised 29%, indicating significant interest in targeting A β . Additionally, aducanumab, approved by the FDA in 2021, is an antibody with modest selectivity for A β O and modestly protected memory^{190,272}.

In Phase 3 clinical trials, several therapeutic agents designed to neutralize A β O or prevent their binding to targets are being tested. These include the antibodies remternetug (LY3372993), donanemab, gantenerumab, and lecanemab, as well as the vaccine formulation UB-311, which are all currently undergoing Phase 3 clinical trials. Remternetug and donanemab both target the pyroglutamate form of A β , a proteoform for which A β O formation is enhanced^{273,274}. Ganenterumab was designed to bind fibrils, but may also partially neutralize A β O²⁷⁵. Lecanemab is an antibody with moderate selectivity for A β protofibrils; in recently-reported Phase 3 clinical trial results, lecanemab moderately protected memory¹⁹². UB-311 is a synthetic A β vaccine that induces the production of antibodies against various forms of A β ,

including A β O_s²⁷⁶. In Phase 2, two small molecule candidates that would be anticipated to release A β O_s from receptor targets are also being tested: intranasal insulin²⁴⁰ and CT1812²⁷⁷. The most specific A β O-neutralizing agents are currently being tested in Phase 1: the A β O-selective antibody ACU193 and the A β O-based vaccine ALZ-101. Results from these trials will help to clarify the effect of neutralizing A β O_s, which may provide robust protection from further A β O-induced neurodegeneration.

Additional therapeutic agents designed to block A β O formation are also currently being tested in clinical trials. Currently in Phase 3 trials to block A β oligomerization are valiltramiprosate (ALZ-801) and ALZT-OP1 (combination cromolyn sodium, intal, and ibuprofen). Valiltramiprosate is a prodrug of homotaurine, which physically disrupts A β O formation¹⁸⁸. Phase 2 results for this agent were promising, and the Phase 3 trial is ongoing²⁷⁸. Cromolyn is an FDA-approved asthma medication that also prevented A β O formation in AD mouse models²⁷⁹. In Phase 1 and Phase 2 trials, epigallocatechin gallate (EGCG)²⁸⁰, PBT2²⁸¹, and contraloid²⁸², which all help to prevent A β oligomerization, along with varoglutamstat²⁸³, which prevents formation of pyroglutamate A β , are also being tested. These potential therapeutics would also be expected to prevent A β O-induced damage and might be especially therapeutic if initiated in early or even preclinical stages of AD.

The development of numerous A β O-targeting therapeutics provides exciting clinical promise. Additionally, these are predicted to provide valuable information about clinical effects of A β O neutralization and the inhibition of A β oligomerization. Similar A β O-targeting strategies, building upon these and enabling additional insight into the pathological formation and effectors of A β O_s, will be explored in the present work.

1.7 Three strategies to disrupt A β O_s

1.7.1. *Disrupt formation and accumulation of A β O_s*

In this work, using primary cultures of hippocampal neurons, three strategies for disruption of A β O-induced neurodegeneration were examined. The first was disruption of one of the earliest points in the AD pathway: the formation and buildup of A β O_s. For these experiments, the small molecule compound NU-9, which protected against aggregates observed in amyotrophic lateral sclerosis, was tested in neurons for its potential to disrupt buildup of A β O_s from A β monomer. Unlike many of the small molecules currently in clinical trials, NU-9 does not physically interact with A β monomer to disrupt A β O binding directly, but instead acts via a cellular mechanism. As such, evidence revealing the mechanism of NU-9 provides insight into cellular mechanisms that may be leveraged to disrupt A β O formation. Its lysosome-dependent mechanism, involving differential roles for cathepsin B and cathepsin L, was elaborated in this work. These findings will be valuable toward understanding the shared mechanisms of unstructured protein accumulation in various neurodegenerative diseases and begin to provide insight into therapeutic interventions that might protect against multiple diseases.

1.7.2. *Block A β O induced pTau and downstream effects*

A second strategy tested in this work was to determine the effect of an inhibitor of A β O-mediated tau phosphorylation. The currently-used AD therapeutic memantine acts by a related mechanism, by blocking A β O-induced calcium influx through the NMDAR²⁸⁴. However, A β O-induced calcium dysregulation can be mediated by a variety of receptors, and significant evidence supports a potential role for neuronal nitric oxide synthase (nNOS) in mediating

downstream A β O-induced tau phosphorylation and other features of AD pathology; thus far the exact role of the neuronal isoform of NOS has not been established in these pathways²⁸⁵⁻²⁹⁰. In this work, a specific inhibitor of nNOS was applied for the first time to a model of A β O-induced tau phosphorylation. Inhibition of nNOS was observed to prevent A β O-induced tau phosphorylation. Additionally, nNOS inhibition disrupted A β O buildup from A β monomer and increased synaptic puncta density. These results support the use of nNOS inhibition as a potential therapeutic strategy to mitigate A β O-related neurodegeneration.

1.7.3. Neutralize A β O binding

The third strategy proposed is the neutralization of A β O using megamolecules of the specific, A β O-binding single-chain variable fragment (scFv) antibody Nusc1. Given that antibodies with partial specificity for A β O provided partial memory protection¹⁸⁹⁻¹⁹², use of a specific A β O-targeting antibody is predicted to provide even more effective protection. Additionally, the megamolecule platform enables precise combination of several scFvs, while maintaining a similar or smaller size as typical antibodies²⁹¹⁻²⁹³. In this work, Nusc1 megamolecules, including Nusc1 monomer, dimer, and trimer, were verified to bind to A β O in cell culture. At the concentrations tested, the Nusc1 dimer detected A β O with the highest specificity, and Nusc1 dimer demonstrated a robust ability to neutralize A β O. This work provided a proof of concept for the use of Nusc1 in megamolecules to bind and neutralize A β O. These megamolecules could be expanded to include targeting moieties for CNS entry or a multi-modal therapeutic approach²⁷¹.

1.7.4 Summary

This body of work has explored potential therapeutic avenues that intervene at three discrete points in the sequence of A β O-induced toxicity. These findings help to further elucidate the complex pathologic mechanisms by which A β O_s exert their toxic effects in AD and have the potential to abrogate these effects in early, mid, and late stages of disease.

CHAPTER 2:
INHIBITION OF AMYLOID BETA OLIGOMER ACCUMULATION BY NU-9:
A NOVEL THERAPEUTIC APPROACH FOR ALZHEIMER'S DISEASE

CHAPTER 2: INHIBITION OF AMYLOID BETA OLIGOMER ACCUMULATION BY NU-9: A NOVEL THERAPEUTIC APPROACH FOR ALZHEIMER'S DISEASE

2.1 Introduction

2.1.1 *AβOs comprise a key instigator of AD pathology*

Alzheimer's disease (AD) is the most common cause of dementia and the 7th most common cause of death in the United States². AD pathology in the brain is characterized by the deposition of extracellular amyloid beta (Aβ) plaques and intracellular tangles of hyperphosphorylated tau^{44,45}. Human evidence of disease progression indicates that buildup of tau tangles is preceded by the development of Aβ pathology^{46,47}. Prior to the formation of plaques, Aβ forms smaller, soluble clusters known as amyloid beta oligomers (AβOs)⁹². AβOs, which range in size from dimers, trimers, and tetramers to larger annular and spherical species, including a number of post-translational modifications^{54,97,98,100}, comprise a key instigator of AD pathology. AβOs are elevated in the brains of individuals with AD^{140,154,155,157-159,163,164,294,295} and AD animal models^{296,297}, where they build up increasingly throughout disease progression. In individuals with the Osaka mutation of AD (E693Δ), minimal Aβ plaques form, yet neurodegeneration and memory loss are nonetheless instigated by AβO buildup¹⁶⁵⁻¹⁶⁹. Injection of AβOs to healthy animals induces tau phosphorylation, activation of astrocytes and microglia, synapse degeneration, and memory loss^{179,181-184}. Conversely, prevention of AβO buildup by antibody treatment or anti-aggregation therapy protects against memory loss in AD mouse models^{298,299}.

2.1.2 Prevention of A β O buildup could halt disease progression in AD

Excess buildup of A β O in AD can be caused by the overproduction of aggregation-prone A β proteoforms, which is implicated as a genetic cause of AD^{23,26,28,78}. Additionally, A β O production may be upregulated due to its potential physiological roles as a response to infection^{83,84} and to strengthen otherwise failing synapses⁸⁵, which might occur due to aging or environmental factors. A third factor implicated in disease development due to either mutations, aging, or sleep deprivation, is a failure to remove basal levels of A β O due to faulty proteolysis and clearance^{86,87}. Accordingly, proposed therapeutic strategies to protect against A β O have included directly blocking A β O formation^{265,266}, bolstering A β /A β O degradation²⁶⁷⁻²⁶⁹, and neutralizing A β O with targeted antibodies^{205,270}. Currently available AD treatments can only provide symptomatic treatment to slightly bolster neurotransmission, or to clear larger A β aggregates^{263,264}. Given that A β O are known to instigate pathology and that their removal is protective, new A β O-targeting strategies would be expected to provide more robust protection. Blocking A β O buildup could halt disease progression and promote a healthy environment for synaptic rewiring.

2.1.3 Accumulation of oligomeric species and larger aggregates is a characteristic feature and potential therapeutic target in multiple neurodegenerative disorders

The accumulation of intrinsically disordered or misfolded proteins into oligomeric species and larger aggregates is not unique to AD. It is a characteristic feature, as well as a potential therapeutic target, in multiple other neurodegenerative disorders, including Parkinson's disease, Huntington's disease, and amyotrophic lateral sclerosis (ALS)^{300,301}. In ALS, for example, aggregates of superoxide dismutase 1 (SOD1) and TAR DNA-binding protein 43

(TDP-43) are associated with death of upper and lower motor neurons, depending on the disease subtype, leading to muscle weakness and wasting³⁰²⁻³⁰⁵.

2.1.4 The small molecule NU-9 conferred protection in models of ALS

The small organic molecule (S)-5-(1-(3,5-bis(trifluoromethyl)phenoxy)ethyl)cyclohexane-1,3-dione (NU-9) was developed to prevent aggregation of mutant G93A SOD1 and conferred protection in a cell model of ALS³⁰⁶. Similarly, in the hSOD1 G93A and hTDP-43 A315T rodent models of ALS, NU-9 reduced levels of mutant protein, conferred protection to upper motor neurons, and preserved limb function³⁰⁷. NU-9 thereby demonstrated an ability to protect neurons from dysfunction in two separate ALS translational models in which two different misfolded protein species aggregate. However, its ability to prevent accumulation of unstructured proteins in other neurodegenerative diseases has not been evaluated. In addition, the mechanism of action by which it prevents this buildup has not been elucidated.

2.1.5 Could NU-9 protect against accumulation of A β O $_s$?

In this study, we evaluated whether NU-9 could protect against accumulation of A β O $_s$ implicated in AD and investigated key effectors of this protection. In neurons exposed to A β , we identified the ability of NU-9 to prevent accumulation of neuron-binding A β O $_s$. We characterized the mechanism of NU-9, which acted on a cellular target and was lysosome- and cathepsin B-dependent. Further, we determined that the buildup of cell-binding A β O $_s$ in cells treated with A β monomer relied upon a cathepsin L- and dynamin-dependent trafficking mechanism. Our work to identify key effectors that could mediate protection against different types of misfolded protein aggregation or oligomerization will help to reveal the cellular machinery involved in pathogenesis of A β O $_s$ accumulation, illuminate the shared mechanisms by

which unstructured proteins build up across separate neurodegenerative diseases, and provide novel insight into interventions that might be effective against multiple diseases.

2.2 Results

2.2.1 Small molecule compound NU-9 reduces neuronal binding of A β O_s formed from A β monomer administered to cultured neurons

As a model for the accumulation of neuron-binding A β O_s in a hippocampal cell environment, we applied aggregation-prone A β 42 monomer (500 nM, 30 min) to mature E18 rat hippocampal neurons (18-25 *div*). Neuron-bound A β O_s were then detected by immunofluorescent labeling with the A β O-specific antibody NU2 and a dendrite-specific antibody against microtubule-associated protein 2 (MAP2)¹⁵². A β O_s formed and bound along dendrites in cells treated with A β 42 monomer within 30 s ($p = 0.0008$, Figure 2.1A). This rapid formation of oligomers is in line with previous observations^{96,308}. A β O_s continued to increase in number, size, and intensity over the measured time course. A second significant increase in bound A β O_s was observed between 10 and 30 min ($p = 0.027$). Therefore, the 30 min time point was chosen for future incubations with A β monomer, as a majority of A β O_s had accumulated by this timepoint.

To determine whether NU-9 confers protection against accumulation of A β O_s, we pretreated mature hippocampal neurons for 30 min with 3 μ M NU-9 or DMSO vehicle, a concentration which previously protected 90% of cortical neurons from proteasome inhibitor-induced neurotoxicity³⁰⁹. Then, monomeric A β 42 was applied to hippocampal neurons and consequent A β O buildup was quantified. Pretreatment with NU-9 significantly suppressed A β O accumulation on dendrites compared to the control (61%, $p < 0.0001$, Figure 2.1B). Across 10

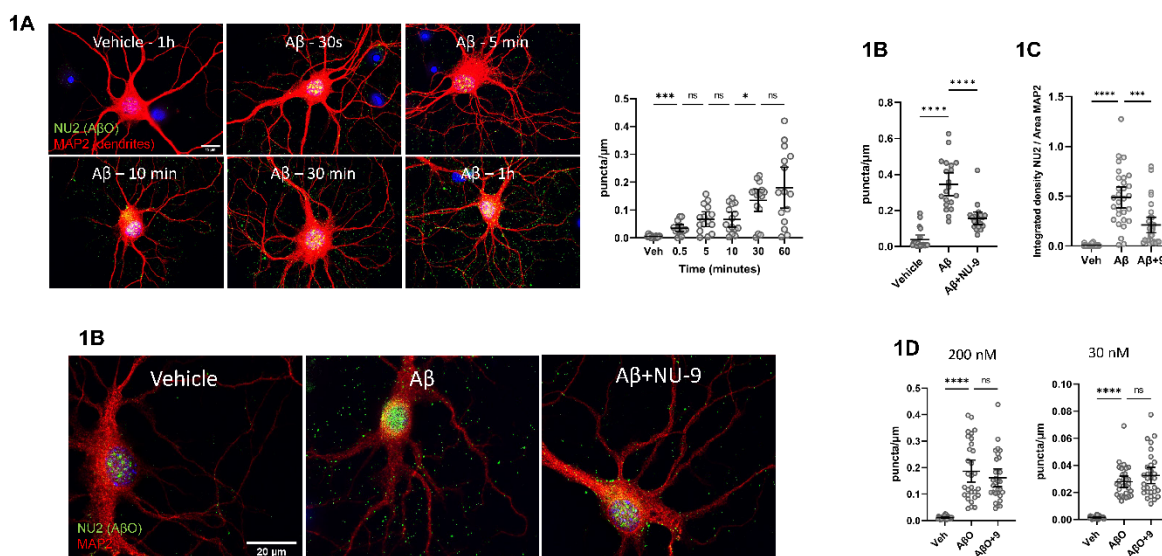


Figure 2.1 Small molecule compound NU-9 reduces neuronal binding of A β O_s formed from A β monomer administered to cell culture. *1A.* A β monomers added to cultured hippocampal neurons rapidly form A β O_s that bind to dendrites. Anhydrous A β monomer solution in DMSO was applied to mature hippocampal neurons, 23 div, in conditioned media, at 500 nM, for 30 sec-1 h. After treatment, coverslips were washed and neuron-bound A β O_s were detected by co-labeling with NU2 and MAP2. (Left) Representative images of A β O_s (green, NU2) bound to dendrites (red, MAP2) of mature hippocampal neurons over 30 s to 1 h. (Right) Quantification of the number of puncta per micron along dendrites was conducted using ImageJ for 15 images in each condition from two coverslips imaged. This overall trend was observed in a separate culture. *1B.* Neuroprotective small molecule NU-9 suppresses A β O accumulation on dendrites. (Below) Representative images of A β O_s (green, NU2) bound to dendrites (red, MAP2) of mature hippocampal neurons following addition of 500 nM A β 42 with or without 30-minute pretreatment with 3 μ M NU-9. (Above) Quantification of A β O puncta per μ m along the dendrites, which was conducted using ImageJ, n = 20 images/condition. Data were analyzed by ANOVA followed by post-hoc Dunnett's T3 multiple comparisons test. (**** denotes p < 0.0001). This trend was replicated in 10 bio-replicates. *1C.* NU-9 reduces intracellular A β O accumulation. Quantification of intracellular A β O_s as measured by integrated fluorescent density of NU2 divided by area of MAP2 signal was conducted using ImageJ, n = 30 images per condition. Data were analyzed by ANOVA followed by post-hoc Dunnett's T3 multiple comparisons test. (*** denotes p < 0.001, **** denotes p < 0.0001). *1D.* NU-9 does not reduce neuronal binding of preformed A β O_s. Quantification of A β O puncta per μ m along the dendrites of mature hippocampal neurons following application of (left) 200 nM or (right) 30 nM preformed A β O_s with or without 30-minute pre-treatment with 3 μ M NU-9. Analysis was conducted using ImageJ, n = 30 images/condition. Data were analyzed by ANOVA followed by post-hoc Dunnett's T3 multiple comparisons test. (**** denotes p < 0.0001 using t-test).

experiments, this reduction ranged from 26-93%. These results robustly support the ability of NU-9 to prevent the accumulation of neuron-binding A β O.

To determine whether the reduction of dendritic A β O accumulation by NU-9 was the result of A β O retention at the cell body, we tested the effect of NU-9 on A β O levels in the cell body region. A β O levels in the cell body region were also reduced by NU-9 (Figure 2.1C, 57%, $p = 0.0002$). This indicates that NU-9 reduced overall buildup of A β O within cells and bound to dendrites.

The effect of NU-9 could be attributed to two potential causes. First, NU-9 might stimulate degradation of fully formed A β O or prevent their binding to neuronal receptors. Alternatively, NU-9 might disrupt a step in A β O formation. Therefore, to investigate whether NU-9 interferes with the binding of preformed A β O, we first pretreated neurons with NU-9, then applied one of two preparations of preformed A β O (200 nM or 30 nM)³¹⁰. The high concentration preparation of A β O contains both high molecular weight and low molecular weight species²⁰⁴. The population of the 30 nM A β O preparation contains a greater proportion of high molecular weight A β O^{311,312}. Pretreatment with NU-9 did not reduce the number of preformed A β O bound to dendrites in either condition ($p = 0.57$ for 200 nM, 0.35 for 30 nM, Figure 2.1D). This result supports the conclusion that NU-9 does not prevent binding or cause degradation of fully formed A β O, but rather interferes with a step in A β O formation.

2.2.2 NU-9 reduces A β O accumulation on neurons by a cell-based mechanism

To examine whether NU-9 directly interferes with A β O formation from monomer in solution, in the absence of neurons, neuronal culture media containing A β 42 monomer was incubated in the presence or absence of NU-9 and A β O levels were measured via dot blot. Pre-

treatment with NU-9 did not reduce A β O formation in fresh media ($p = 0.85$ for 3 μ M NU-9, 0.18 for 30 μ M NU-9, 0.13 for 300 μ M NU-9, Figure 2.2A). This result was also observed in conditioned media containing NU-9 ($p = 0.88$, Figure 2.2A) or in conditioned media from cells which had been pre-treated with NU-9 ($p = 0.54$). Thus, NU-9 does not act by directly blocking A β O formation nor by inducing the release of A β -degradative factors such as MMP-2 or MMP-9³¹³, but rather modulates a cellular pathway to reduce A β O accumulation.

To verify whether the effect of NU-9 occurs intracellularly, we tested whether NU-9 would still be effective at reducing dendritic A β O accumulation even if NU-9 were washed out from the extracellular media prior to the addition of A β 42 monomer. NU-9 remained able to reduce A β O bound to neurons even after washout ($p = 0.0004$, Figure 2.2B), further supporting a cell-based mechanism for the reduction of A β O accumulation by NU-9.

Given that NU-9 reduces A β O accumulation by a cell-dependent mechanism, we investigated whether dynamin-dependent endocytosis, which mediates internalization of A β species into neurons, is necessary for effectiveness of NU-9^{314,315}. To inhibit dynamin-dependent endocytosis, we pretreated neurons with 80 μ M dynasore. Unexpectedly, treatment with dynasore alone also prevented A β O buildup (75%, $p < 0.0001$, Figure 2.2C). This suggests that the buildup of a major population of A β O is dependent upon functional endocytosis.

We investigated whether NU-9 alters overall A β O levels or simply prevents the buildup of a particular neuron-binding proteoform. We probed the level of unbound A β O present in extracellular media collected from neurons treated with NU-9 and A β 42. In addition to the formation of neuron-binding A β O, monomeric A β 42 also produced unbound, extracellular A β O, which were detected by dot blot. We found that NU-9 did not significantly reduce the

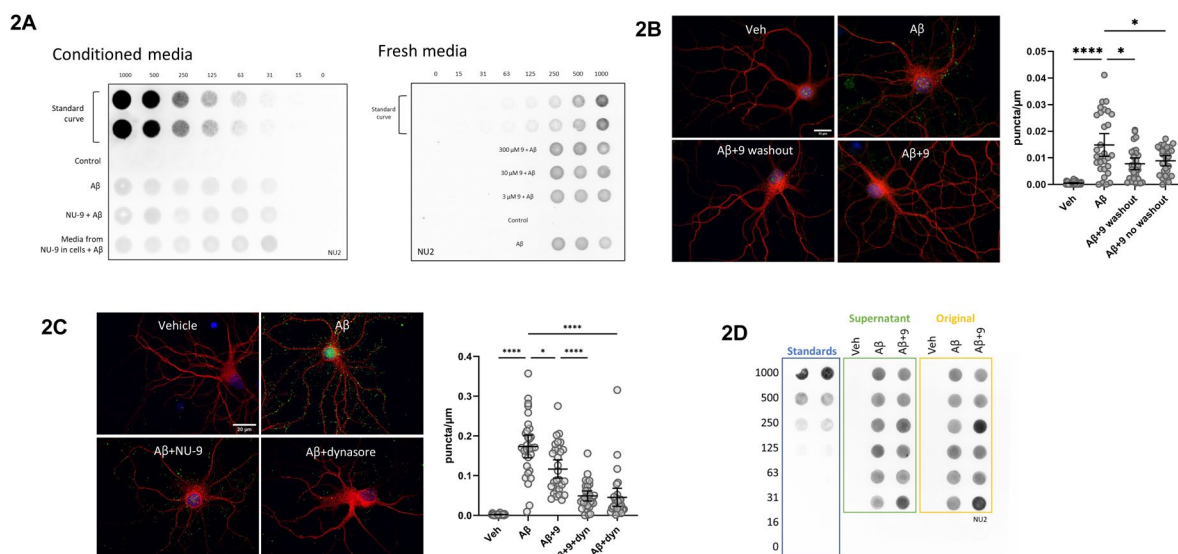


Figure 2.2 NU-9 reduces AβO accumulation on neurons by a cell-based mechanism.

2A. NU-9 does not reduce AβO formation from Aβ monomer in cell-free solution or from conditioned media derived from NU-9 treated cells. Dot blots probed for AβO abundance (NU2). The standard curve is 0-1000 fmol preformed AβOs ($r^2 = 0.99$ for both). All experimental solutions were prepared in triplicate. (Left) DMSO (control), Aβ, and NU-9 followed by Aβ were added for 30 min each to conditioned media. In the bottom row, cells were treated with NU-9 for 30 min, then extracellular media was removed, and Aβ was added to the media for 30 min. (Right) DMSO vehicle (control), Aβ, and NU-9 (3-300 μM) followed by Aβ were added to fresh culture media for 30 min each. **2B.** NU-9 reduces dendritic accumulation of AβOs even if washed out prior to Aβ addition. (Left) Representative images of neuron-bound AβOs (green, NU2 and red, MAP2). (Right) Puncta/length were analyzed using ImageJ, 30 images/condition. Data were analyzed by ANOVA with post-hoc Dunnett's T3 test. (* denotes $p < 0.05$, **** denotes $p < 0.0001$) Effectiveness of NU-9 after washout was observed in an additional bio-replicate. **2C.** AβO buildup is dependent on dynamin activity. (Left) Representative images of neuron-bound AβOs (green, NU2 and red, MAP2). (Right) Puncta/length were analyzed using ImageJ, 30 images/condition. Data were analyzed by ANOVA with post-hoc Dunnett's T3 test. (* denotes $p < 0.05$, **** denotes $p < 0.0001$). Prevention of AβO buildup by dynasore was observed in an additional bio-replicate. **2D.** NU-9 does not alter the number of unbound, extracellular AβOs. A dot blot labelled with NU2 was used to probe the level of unbound AβOs present in extracellular media pretreated for 30 min with NU-9, followed by application of Aβ for 30 min. The left column contains a standard curve from 0-1000 fmol preformed AβOs ($r^2 = 0.99$ for 125-1000 fmol). The middle section (green) contains extracellular media from cells treated with vehicle (Veh), Aβ, or NU-9 followed by Aβ (Aβ + 9), which were centrifuged to remove fibrils prior to application on the dot blot. Each of three bioreplicates was spotted in duplicate. The right column corresponds to the same media, uncentrifuged, in duplicate.

number of unbound, extracellular A β O_s in either supernatant ($p = 0.6$, Figure 2.2D) or uncentrifuged solution ($p = 0.3$). This finding supports the conclusion that NU-9 does not reduce total A β O levels but instead prevents buildup of a specific, neuron-binding proteoform.

2.2.3 Proteasome inhibition does not alter the effect of NU-9 on A β O accumulation

Because the proteasome is known to contribute to A β degradation, we tested whether NU-9 required functional proteasome activity to reduce A β O accumulation^{234,316,317}. We used 100 nM MG132 (30 min) to inhibit proteasome activity based on prior literature showing that this concentration inhibits neuronal proteasome activity with very minimal neurotoxicity³¹⁸. Proteasome inhibition had no effect on formation of A β O_s ($p = 0.19$, Figure 2.3A) or reduction of A β O accumulation by NU-9 ($p = 0.21$). The observation that NU-9 does not require proteasome activity to reduce A β O accumulation suggests that NU-9 does not act by directing A β species to the proteasome for degradation but may instead rely upon other mechanisms.

2.2.4 Lysosome inhibition prevents the effect of NU-9 on A β O accumulation

In addition to the proteasome, the lysosome is a major contributor to degradation of A β and A β O_s^{314,319,320}. We tested whether lysosomal activity was necessary for reduction of A β O accumulation. Inhibition of endo-lysosomal acidification using the v-ATPase inhibitor bafilomycin A (100 nM, 30 min pretreatment) prevented the effectiveness of NU-9 ($p = 0.0003$, Figure 2.3B). Matching these observations, vacuolin-1, which inhibits lysosomal maturation and exocytosis (1 μ M, 1 h pretreatment), also prevented the effect of NU-9 ($p = 0.0007$, Figure 2.3C). These results support the conclusion that NU-9 effectiveness is dependent upon the functioning of mature, acidic lysosomes.

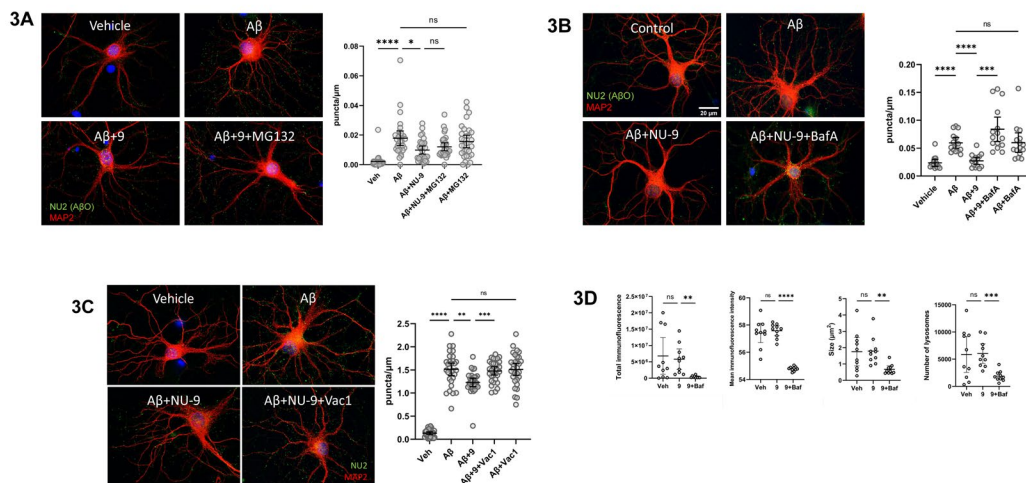


Figure 2.3 Lysosome inhibition prevents the effect of NU-9 on AβO accumulation 3A.

Proteasome inhibition did not alter AβO accumulation or effectiveness of NU-9. (Left) Representative images of AβOs (green, NU2) bound to dendrites (red, MAP2) of mature hippocampal neurons to which were applied 500 nM Aβ42, with or without 30-min pretreatment with 3 μM NU-9 and 30-min pretreatment 100 nM MG132. (Right) Quantification of AβO puncta per μm along the dendrites, which was conducted using ImageJ, n = 30 images/condition. Data were analyzed by ANOVA followed by post-hoc Dunnett's T3 multiple comparisons test (* denotes p < 0.05, **** denotes p < 0.0001). This result was observed in an additional bio-replicate. *3B. Effectiveness of NU-9 is dependent on endo-lysosomal acidification.* (Left) Representative images of neurons were pretreated first for 30 min with 100 nM bafilomycin A, then for 30 min with 3 μM NU-9, and were finally exposed for 30 min to 500 nM Aβ. AβOs were labeled with NU2 (green) and dendrites were visualized using MAP2 (red). Bafilomycin A prevented the effect of NU-9 (p = 6.98 E-6). This condition was not significantly different from Aβ treatment alone (p = 0.38), nor was Aβ + BafA (p = 0.37). (Right) Puncta/length were analyzed using ImageJ, n=15 images/condition. Data were analyzed by ANOVA, followed by a post-hoc Dunnett's T3 multiple comparisons test. (***) denotes p < 0.001, **** denotes p < 0.0001). Data from a second bio-replicate also showed NU-9 effectiveness was prevented in the presence of bafilomycin A. *3C. Effectiveness of NU-9 is dependent on lysosome maturation and exocytosis.* (Left) Representative images of AβOs (green, NU2) bound to dendrites (red, MAP2) of mature hippocampal neurons to which were applied 500 nM Aβ42 with or without 30-min pretreatment with 3 μM NU-9 and 1 h pretreatment 1 μM vacuolin-1. (Right) Quantification of AβO puncta per μm along the dendrites, which was conducted using ImageJ, n = 30 images/condition. Data were analyzed by ANOVA, followed by a post-hoc Dunnett's T3 multiple comparisons test (** denotes p < 0.01, *** denotes p < 0.001, **** denotes p < 0.0001 using t-test). An additional bio-replicate demonstrated the same trend. *3D. NU-9 does not increase lysosome acidity, size, or number.* Following 30 min treatment of NU-9, integrated fluorescent density of LysoTracker, indicating acidic lysosomes, was not altered (p = 0.73), although it was significantly reduced with the addition of bafilomycin A (p = 0.0039). This trend was observed across two bio-replicates. Lysosome number, size, and average intensity (correlates with acidity) were unchanged with NU-9 (p = 0.92, 0.94, 0.65).

To investigate whether NU-9 enhances lysosome acidity or turnover, LysoTracker was used to reveal acidic compartments, comprising lysosomes and late endosomes. The number, size, and average intensity, the last of which correlates with acidity, of these lysosomes were not altered by NU-9 treatment ($p = 0.99, 0.99, 0.87$, Figure 2.3D), although these values were significantly reduced by bafilomycin A, a lysosomal inhibitor ($p = 0.0008, 0.0045, < 0.0001$). Therefore, although the effectiveness of NU-9 to reduce A β O accumulation is dependent upon lysosome functioning, NU-9 does not directly enhance lysosome number, size, or acidity.

2.2.5 The effect of NU-9 is mimicked by cathepsin L inhibition, but NU-9 does not inhibit cathepsin L

We hypothesized that NU-9 may act via modulation of lysosomal enzymes. To test whether the effectiveness of NU-9 required cysteine cathepsins, we pretreated neurons for 24 h with the nonspecific cysteine cathepsin inhibitor E64 (10 μ M) prior to application of NU-9. Pretreatment with E64 alone significantly reduced A β O accumulation ($p < 0.0001$, Figure 2.4A), mimicking the effect of NU-9. We conclude that general cysteine cathepsin inhibition can prevent A β O buildup.

To test which cysteine cathepsin was responsible for the reduction of A β O accumulation mediated by nonspecific inhibition, we first tested the effect of cathepsin L inhibition on A β O accumulation. Cathepsin L expression is increased in the brains of individuals with AD, and both expression and activity of cathepsin L are enhanced upon treatment of cortical neurons with A β , leading to apoptosis³²¹⁻³²³. The specific cathepsin L inhibitor Z-FY-CHO (aka SB-412515, 10 μ M, 1 h) reduced A β O buildup ($p < 0.0001$, Figure 2.4B), indicating that cathepsin L inhibition

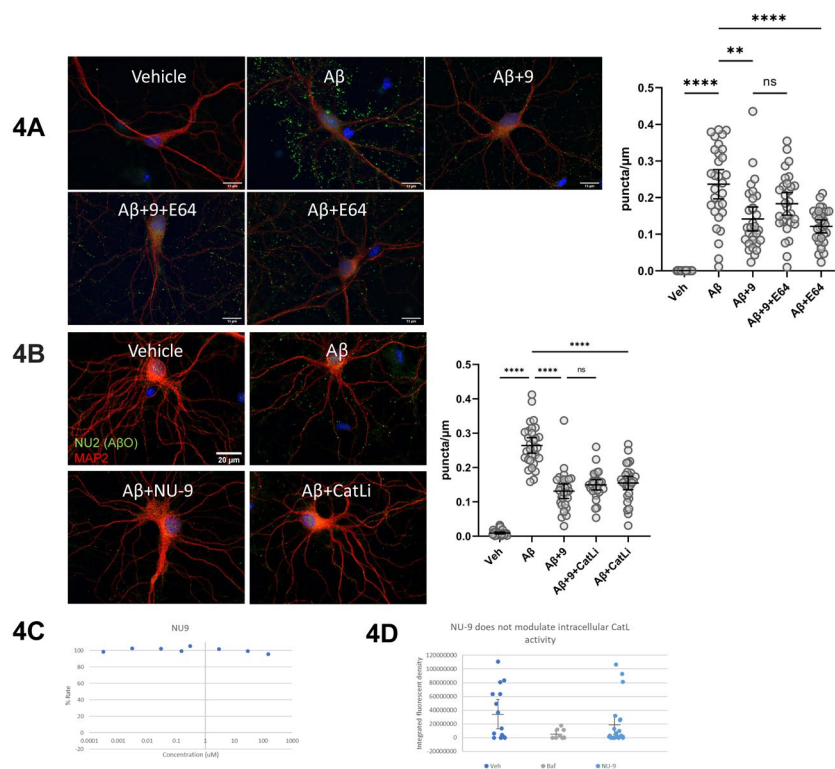


Figure 2.4 The effect of NU-9 is mimicked by cathepsin L inhibition, but NU-9 does not inhibit cathepsin L. *4A. Nonspecific cysteine cathepsin inhibition mimics the neuroprotective effect of NU-9 in a nonadditive manner.* (Left) Representative images of AβOs (green, NU2) bound to dendrites (red, MAP2) of hippocampal neurons to which were applied 500 nM Aβ42, with or without 30-min pretreatment with 3 μM NU-9 and 24 h pretreatment 10 μM E64. (Right) Quantification of AβO puncta per μm along the dendrites was conducted with ImageJ, n = 30 images/condition. Data were analyzed by ANOVA, followed by a post-hoc Dunnett's T3 test. (** denotes p < 0.01, **** denotes p < 0.0001). This trend was replicated in a second bio-replicate experiment. *4B. Specific inhibition of cathepsin L mimics the effect of NU-9.* (Left) Representative images of neurons that were pretreated first for 1 h with 10 μM cathepsin L inhibitor FY-CHO, then for 30 min with 3 μM NU-9, and finally for 30 min to 500 nM Aβ. AβOs (green, NU2) bound to dendrites (red, MAP2) were visualized by immunofluorescence. (Right) Puncta/length were analyzed using ImageJ, 30 images/condition. Data were analyzed by ANOVA, followed by a post-hoc Dunnett's T3 test. (**** denotes p < 0.0001). *4C. NU-9 is not a direct modulator of cathepsin L activity.* Percent activity for cathepsin L treated with 0.0003-150 μM NU-9 was calculated based on the cleavage rate of 7-AMC from Z-FR-AMC. No significant effect of NU-9 on cathepsin L activity was observed at any concentration. *4D. NU-9 does not modulate activity of intracellular cathepsin L.* Mature hippocampal neurons were treated with NU-9 for 30 min, then Magic Red was used to monitor intracellular cathepsin L activity. Cells were treated in 3 wells, and 9-22 images were analyzed per condition. Integrated fluorescent density for the lysosome inhibitor bafilomycin A (BafA) was significantly lower than vehicle (p = 0.011) but not for NU-9 (p = 0.34).

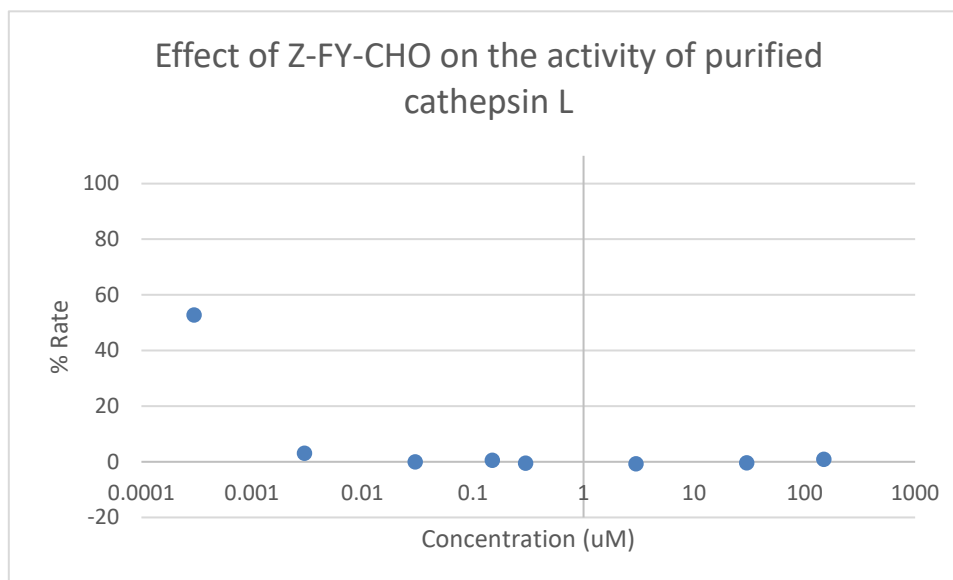


Figure 2.5 Control – inhibition of cathepsin L enzyme by cathepsin L inhibitor Z-FY-CHO. Effect of 0.0003-150 μM standard inhibitor Z-FY-CHO on the cleavage rate of 7-AMC from Z-FR-AMC by purified cathepsin L. Greater than 90% inhibition of enzyme activity was observed for concentrations 0.003 μM or higher.

could be responsible for the prevention of A β O accumulation mediated by cysteine cathepsin inhibition.

Based on this result, we further investigated whether NU-9 could act by inhibition of cathepsin L. First, we measured whether NU-9 was a direct inhibitor of cathepsin L by combining purified cathepsin L with its fluorogenic cathepsin L substrate Z-FR-AMC in the presence or absence of NU-9. No direct effect of NU-9 (0.0003-150 μM) was observed on the activity of purified cathepsin L ($p = 0.95$, Figure 2.4C, Figure 2.5). Therefore, we conclude that NU-9 is not a direct inhibitor of cathepsin L.

To monitor any indirect, intracellular effect of NU-9 on cathepsin L activity, we used its corresponding Magic Red assay kit, containing a cell-penetrant, fluorogenic substrate specifically cleaved by cathepsin L. Neurons were treated with NU-9. However, mean and total integrated fluorescence intensity was unchanged for NU-9 compared to vehicle ($p = 0.34$, Figure

2.4D). This result indicates that, although inhibition of cathepsin L produces a similar effect as NU-9, NU-9 does not directly or indirectly modulate activity of intracellular cathepsin L. Rather, we conclude that NU-9 and cathepsin L inhibitors may act independently to prevent A β O buildup.

2.2.6 Cathepsin B is necessary for the effect of NU-9, but NU-9 does not directly activate cathepsin B

In parallel with cathepsin L experiments, we also investigated whether the effectiveness of NU-9 depended on cathepsin B activity. Cathepsin B is connected to AD in several key ways. Cathepsin B is spatially associated with extracellular A β plaques in AD brain³²⁴, and cathepsin B trafficking to endosomes is also enhanced in the brains of AD patients³²⁵. Additionally, cathepsin B colocalizes with A β in secretory vesicles in a chromaffin cell model, where it is implicated in the production of A β from APP³²⁶. Across a variety of models of AD, several authors have described neuroprotective roles in which cathepsin B reduces A β accumulation³²⁷⁻³²⁹, while Hook et al. described neurodegenerative roles in which cathepsin B could contribute to A β production^{326,330,331}. To test whether inhibition of cathepsin B alters A β O accumulation or the effectiveness of NU-9 in our model, neurons were pretreated first for 24 h with 10 μ M of the specific cathepsin B inhibitor CA-074. Cathepsin B inhibition prevented the effect of NU-9 ($p = 0.016$, Figure 2.6A). These data support the conclusion that cathepsin B activity is essential for the effect of NU-9.

Accordingly, to determine whether NU-9 is an activator of cathepsin B, we conducted a cell-free assay in which NU-9 was combined with purified cathepsin B enzyme, and cleavage of

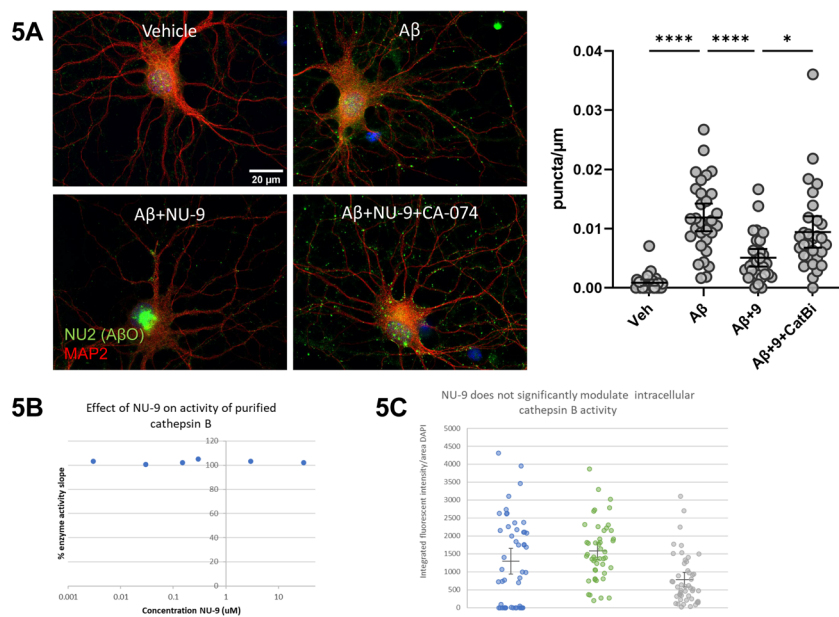


Figure 2.6 Cathepsin B inhibition blocks the effect of NU-9, but NU-9 does not directly activate cathepsin B. *5A. Effectiveness of NU-9 is dependent on cathepsin B.* (Left) Representative images of neurons that were pre-treated first for 24 h with 10 μM CA-074, then for 30 min with 3 μM NU-9, and were finally exposed for 30 min to 500 nM A β . (Right) Puncta/length were analyzed using ImageJ, 30 images/condition. Data were analyzed by ANOVA, followed by a post-hoc Dunnett's T3 multiple comparisons test. (* denotes $p < 0.05$, **** denotes $p < 0.0001$). CA-074 prevented the effect of NU-9 ($p = 0.016$). *5B. NU-9 has minimal direct effect on the activity of purified cathepsin B.* Percent activity of purified cathepsin B was calculated based on the rate of cleavage of the fluorogenic cathepsin B substrate Z-RR-AMC to 7-AMC. A very modest direct effect of NU-9 (0.0003-30 μM) was observed on the activity of purified cathepsin B ($p = 0.0076$). *5C. NU-9 has no effect on intracellular cathepsin B activity.* Mature hippocampal neurons were treated with NU-9 for 30 min, then Magic Red was used to monitor intracellular cathepsin B activity. Three wells per condition were treated, and all fields were analyzed, 48 images per condition. Integrated fluorescent density was significantly lower for bafilomycin A treated cells than for vehicle ($p = 0.013$) but not for cells treated with NU-9 ($p = 0.19$).

the fluorogenic cathepsin B substrate Z-RR-AMC was monitored. A negligible direct effect of NU-9 (0.0003-30 μM) was observed on the activity of purified cathepsin B enzyme (Figure 2.6B, Figure 2.7).

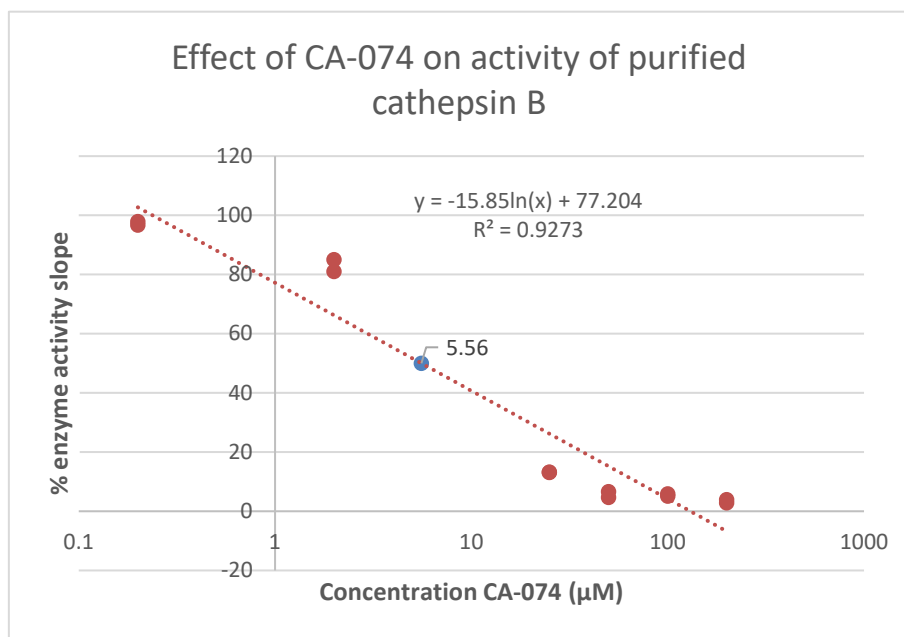


Figure 2.7 Control – inhibition of cathepsin B by CA-074. For the known cathepsin B inhibitor CA-074, increasing inhibition of enzyme activity was observed at concentrations 2 μM and above. The IC_{50} was estimated at 5.56 μM CA-074 in this assay.

Since NU-9 had minimal direct effect on cathepsin B activity, we investigated whether NU-9 had an indirect, downstream effect on cathepsin B activity within the neuronal environment. A cathepsin B-specific Magic Red substrate was used to monitor the effect of NU-9 treatment on intracellular cathepsin B activity. NU-9 did not significantly alter intracellular cathepsin B activity ($p = 0.19$, Figure 2.6C). Based on these results, we conclude that, while NU-9 promotes a cathepsin B-dependent mechanism to prevent $\text{A}\beta\text{O}$ accumulation, NU-9 does not directly or indirectly activate cathepsin B. Instead, it likely acts on a target that is cathepsin B-dependent.

2.2.7 NU-9 rescued memory performance in preliminary experiments

Given the suppression of A β O buildup effected by NU-9, we investigated whether NU-9 treatment in 5xFAD mice would protect their memory. 5xFAD mice possess 5 mutations associated with familial AD and rapidly develop A β O and A β plaque pathology beginning at 2-4 months of age^{201,332,333}. Behavioral deficits in memory function are observed by 4-5 months of age²⁰¹. In 5xFAD mice, removal of A β O by intranasal injection of an A β O-selective antibody was previously shown to provide protection against memory loss²⁰¹.

To test for potential protective effects of NU-9, Dr. Maíra Bicca treated 10-month-old 5xFAD mice for about one month with 20 mg/kg NU-9 by oral gavage. In a preliminary experiment, Dr. Bicca observed that 3 out of the 4 animals treated orally with NU-9 retained memory function in a combined test of novel object recognition and novel location recognition, while all 5 animals treated with vehicle control failed (Figure 2.8). This result indicates that reduction of A β O accumulation of NU-9 has the potential to mediate neuroprotection such that memory function is protected. Future studies will be conducted to probe this potential memory protection by NU-9 using a larger cohort and to monitor whether NU-9 can protect against the development of *in-vivo* pathology.

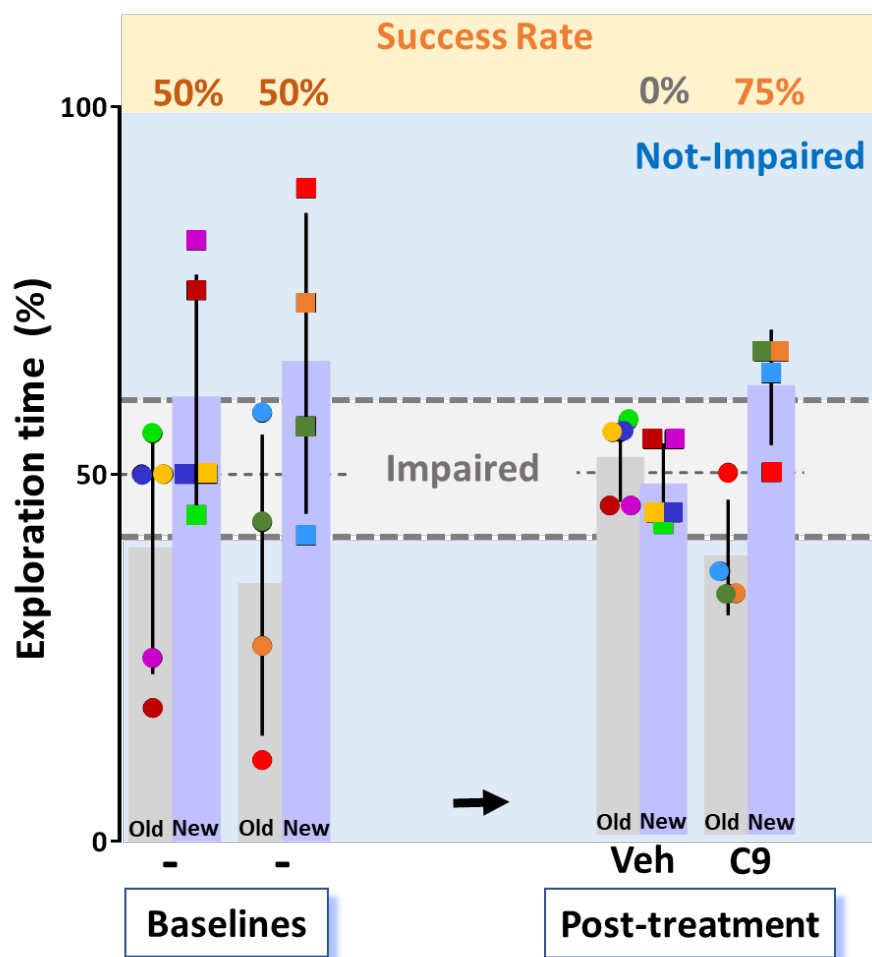


Figure 2.8 NU-9 rescued memory performance in preliminary experiments. Dr. Maíra Bicca tested memory performance in 5xFAD mice. The quantification of exploration time for new versus old objects, comparing baselines and post-treatment animals orally dosed with vehicle and NU-9 (C9) for one month. Animals that had higher interaction time with the new object were defined as not-impaired, successful results. A fifth NU-9 treated animal was excluded from post-treatment analysis because it was considered an outlier due to preferential interaction with the old object.

2.3 Discussion

2.3.1 Summary

In this work, we identified the ability of the small molecule compound NU-9 to prevent the accumulation of neuron-binding A β O_s. This molecule was previously shown to provide protection in ALS models, indicating potential translation of this paradigm to other proteopathies. Reduction of A β O formation by NU-9 ranged from 26-93%. The mechanism of NU-9 involves a cellular pathway that is dependent on intact lysosomal and cathepsin B activity. Results additionally provide new insight into the formation of A β O_s and their ability to reach cell surface targets, an intracellular trafficking pathway which appeared to be cathepsin L- and dynamin-dependent. Efficacy of NU-9, which acts cellularly, suggests its potential use as a neuroprotective agent in reducing the ability of A β to form AD-causing A β O_s.

2.3.2 NU-9 previously protected upper motor neurons against ALS proteopathies

NU-9 is a small molecule that was originally developed to prevent aggregation of mutant SOD1 for protection against ALS. ALS is a neurodegenerative disease in which aggregates of TDP-43 and SOD1 are associated with the degeneration of motor neurons, resulting in muscle weakness³⁰⁵. TDP-43 and SOD1 can form both large aggregates and smaller oligomers that propagate in a prion-like manner, which may represent major instigators of neurodegeneration in ALS³³⁴⁻³³⁷. The efficacy of NU-9 was previously established in two different translational animal models of ALS^{306,307}. One model expressed mutant SOD1 and the other expressed mutant TDP-43. Each of these aggregation-prone proteins are individually implicated in ALS, and expression of either protein in rodents causes neurodegeneration of upper motor neurons and loss of limb function. In each model, NU-9 protected upper motor neurons, and preserved limb function. In

the SOD1 model, levels of misfolded protein were also measured by immunofluorescence and were found to be reduced. These results indicated an ability of NU-9 to mitigate ALS proteopathy. However, the exact mechanism by which NU-9 acts has remained unclear, and the generalizability of NU-9 to combat other proteopathies aside from ALS had not been previously studied. In this work, we evaluated the ability of NU-9 to prevent buildup of a key oligomer formed in Alzheimer's disease and investigated the cellular mechanism by which it acts.

2.3.3 A β O_s cause neurodegeneration in AD

In AD, aggregation-prone A β peptide accumulates in soluble oligomers known as A β O_s^{54,92,97,98,100}, which cause AD pathology. A β O_s are elevated in the brains of individuals with AD^{140,154,155,157-159,163,164,294,295} and correlate with memory impairment^{140,158,162-164}. A β O_s induce tau phosphorylation, activation of astrocytes and microglia, synapse degeneration, and memory loss^{179,181-184}. Preventing A β O buildup by antibody treatment or anti-aggregation therapy protects against memory loss^{190-192,298,299}. In this work, we investigated the ability of NU-9 to prevent A β O buildup.

2.3.4 NU-9 prevents the buildup of neuron-binding A β O_s

In the context of AD-related oligomers, we observed that A β monomers formed A β oligomers after application to cells for even a brief period. These A β O_s bound to neuronal dendrites in a punctate manner, and some were associated with the cell body region. NU-9 protected against that buildup of A β O_s. NU-9 required cells to reduce A β O buildup and remained effective even when washed out prior to introduction of A β monomer. NU-9 was effective when monomer was added to cells but did not block the binding of preformed A β O_s to

cells. Our results support the conclusion that NU-9 acts on a cellular target to prevent the formation of neuron-binding A β O.

The reduction of A β O formation by NU-9 ranged from 26-93% across experiments. This range is attributed to a limitation of this model, which involves the application of exogenous, monomeric A β to neurons in aqueous media. Formation of A β O occurs rapidly in this environment⁹⁶. We hypothesize that a minority of the A β O buildup on neurons results from the very rapid oligomerization that occurs when A β is added to aqueous media. Given that NU-9 acts on a cellular target to prevent A β O buildup from A β , extracellularly-formed A β O would not be affected by NU-9. Depending on the experiment, minor differences in timing might enable faster extracellular oligomerization, reducing the observed effectiveness of NU-9. In AD, where a high proportion of A β is formed intracellularly, in trafficking vesicles, it is predicted that NU-9 might provide more complete and consistent suppression of A β O buildup.

We determined that the effect of NU-9 was lysosome and cathepsin B-dependent. NU-9 required lysosome acidity and intact endo-lysosomal fusion. The lysosomal enzyme, cathepsin B, was also essential to the effectiveness of NU-9. Thus, we conclude that NU-9 prevents proteopathy by a lysosome- and cathepsin B-dependent protective mechanism capable of blocking the formation of neuron-binding A β O. This novel effect of NU-9 indicates potential therapeutic application to AD and supports the conclusion that NU-9 inhibits a general mechanism of neurodegenerative proteopathy.

2.3.5 NU-9 may restore trafficking of A β to active lysosomes to prevent buildup of neuron-binding A β O_s

In AD patients and disease models, endo-lysosomal trafficking and lysosome function is disrupted^{338,339}, and A β accumulates in the late endosome and multi-vesicular bodies^{92,101,102,105,107,113,115,314,340}. This disrupted trafficking is implicated in the formation of A β O_s^{103,106}. In fact, disruption of trafficking by Rab5 activation has been shown to reproduce key factors of AD pathology³⁴¹. Additionally, genetic studies in late-onset Alzheimer's disease have identified numerous risk genes involved in endo-lysosomal trafficking³⁴²⁻³⁴⁶. Given that NU-9 reduces the buildup of neuron-binding A β O proteoforms by a mechanism that is intracellular, and lysosome- and cathepsin B-dependent, we hypothesize that NU-9 restores the trafficking of A β species to active lysosomes, where the formation of cell-binding A β O_s can be blocked by cathepsin B (Figure 2.9). Cathepsin B has been shown to proteolytically cleave A β ^{327,347}, and enhancement of cathepsin B levels by chemical modulation or viral delivery reduced A β deposits and provided functional protection in AD models³²⁷⁻³²⁹. Lysosome acidification is also protective in AD, indicating that the lysosome is a critical site for modulation of A β O formation³²⁰. NU-9 could promote trafficking to active lysosomes by activation of Rab7, Rab12, Rab9, or JNK-interacting protein 3³⁴⁸⁻³⁵⁰, or their downstream effectors such as Rab-interacting lysosomal protein (RILP)³⁵¹. Modulation of trafficking by NU-9 represents a novel avenue to protect neurons against A β O formation. Additionally, these results provide new insight into key features of a trafficking mechanism that could be leveraged to provide protection against multiple diseases.

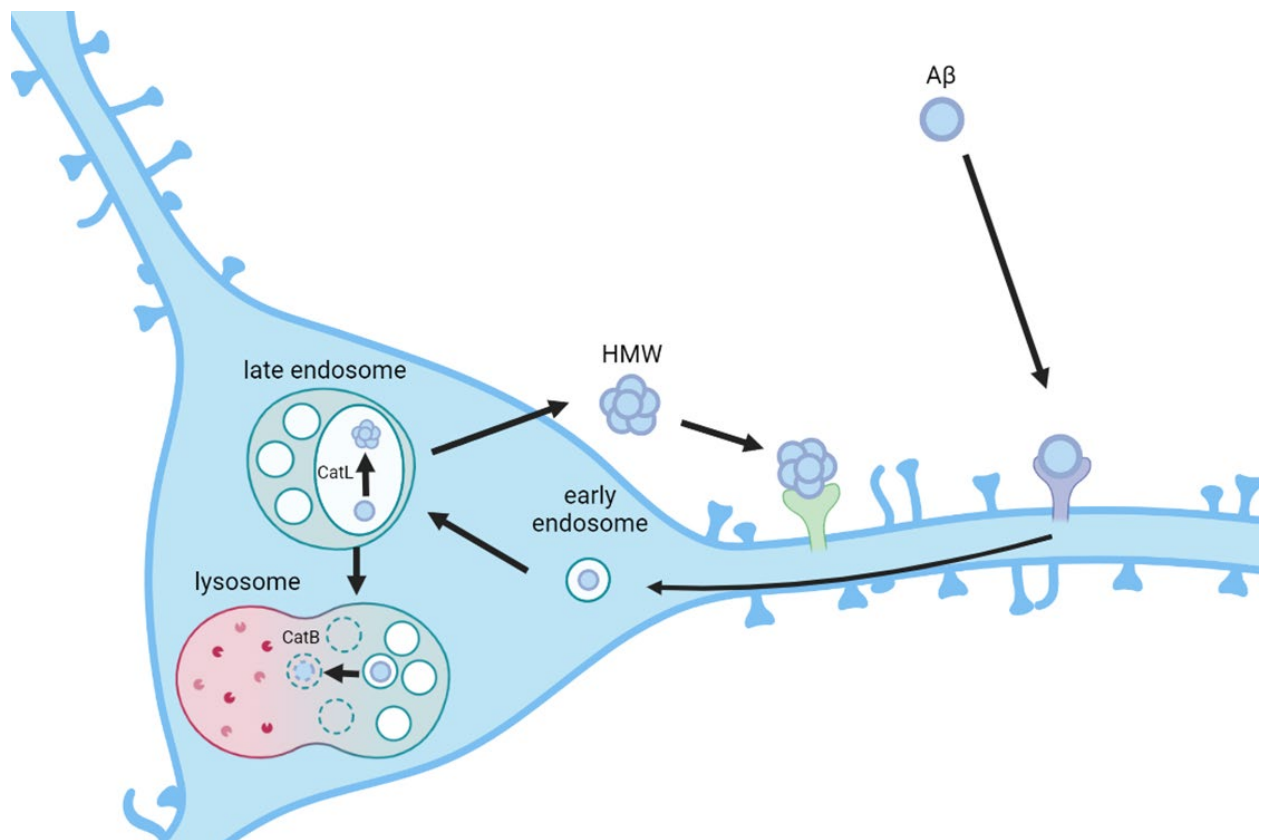


Figure 2.9 Proposed mechanism: NU-9 restores trafficking of A β species to active lysosomes. The proposed mechanism of action of NU-9 involves restoration of A β trafficking to active lysosomes, where cathepsin B (CatB)-dependent processes can prevent formation of neuron-binding A β O. Additionally, the proposed mechanism of formation of neuron-binding A β O in this model involves internalization of A β , trafficking, and cathepsin L (CatL)-dependent A β O formation, and release to bind dendrites. Neuron-binding A β O are proposed to comprise a high molecular weight (HMW) A β O. Figure created with BioRender.com.

2.3.6 Alternative possible mechanisms for NU-9

Alternative mechanisms for NU-9 could involve promotion of cathepsin B trafficking to the lysosome by stabilization of mannose-6-phosphate receptors, which deliver newly synthesized pro-cathepsins to the late endosome for maturation and delivery to lysosomes³⁵².

However, this mechanism is unlikely, because these receptors are also responsible for delivery of

cathepsin L, which our results implicated in A β O formation, to late endosomes. Alternatively, NU-9 may activate an A β -modulating enzyme or chaperone, such as an endothelin-converting enzyme, matrix metalloproteinase, or phospholipase D family member 3 (PLD3) to suppress the formation of neuron-binding A β O_s³⁵³⁻³⁵⁵. However, cathepsin-B dependence of a particular intracellular A β -modulating enzyme or chaperone is not clear. As another possibility, cathepsin B may prevent formation of a key A β O formation mediator such as GM1 ganglioside, maintaining manageable basal levels for NU-9 to inhibit. Cathepsin B also protects against buildup of intracellular cholesterol, which has also been reported to contribute to A β O formation and buildup³⁵⁶. However, these alternative explanations are less likely because cathepsin B inhibition alone did not increase A β O buildup significantly. As an additional conclusion, the cathepsin B-dependence of NU-9 also suggests that this compound acts via a mechanism specific to neurons, as cathepsin B has been shown to degrade A β specifically in neurons³⁵⁷. Therefore, NU-9 is hypothesized to promote endo-lysosomal trafficking of A β in neurons, thereby preventing the accumulation of neuron-binding A β O_s.

2.3.7 Neuron-binding A β O buildup from exogenous A β is dynamin-dependent

Our results further shed light on the mechanism of A β O formation in this model. Prior literature supported dynamin-dependent endocytosis as a key mechanism for the internalization of A β species in neurons^{314,315,358}. Our results show that the buildup of neuron-bound A β O_s is dynamin-dependent. One limitation of this work was the use of the standard dynamin inhibitor, dynasore, which is known to cause off-target effects, including alteration of cholesterol levels. Cholesterol alterations could disrupt A β O formation or the formation of A β O-binding lipid rafts independently of endocytosis. Future experiments to confirm the effect of dynamin versus

cholesterol will be informative to clarify this point. However, the effect of dynasore to block dynamin-dependent endocytosis of A β species has been well established. As such, our results support the conclusion that the formation of neuron-binding A β O_s relies on dynamin-dependent endocytosis. Several literature reports state that A β O_s most likely form intracellularly in disease upon concentration in late endosomes or lysosomes, which can then be released from cells to bind at synapses^{92,101,102}. Our findings support this literature and provide neuronal evidence that intracellularly formed A β O_s comprise a major sub-population of neuron-binding, disease-relevant A β O species. This new mechanistic insight raises the possibility that inhibition of A β endocytosis could provide a therapeutic avenue to prevent the formation of neuron-binding A β O_s.

2.3.8 Cellular A β O formation is cathepsin-L dependent

Another key insight obtained into the mechanism of cellular A β O formation was a dependence upon activity of cathepsin L. We observed that cathepsin L inhibition prevented the buildup of neuron-binding A β O_s. Boland et al. demonstrated that expression and activity of cathepsin L both are enhanced upon treatment of cortical neurons with A β ³²³. Further, Islam et al. noted that cathepsin L activation leads to cleavage of lamin B and caspase 3, degrading nuclear structure and instigating apoptosis³²². We hypothesize that cathepsin L may contribute to A β O formation by impairment of lysosomal function due to nuclear destabilization in response to A β treatment. Regardless of the mechanism, our work provides the first evidence that cathepsin L activity is necessary for A β O buildup. These results thereby offer new insight into the mechanism of A β O accumulation. Further, these findings support the use of cathepsin L inhibition as a possible intervention to prevent A β O buildup.

2.3.9 Future directions

Future directions of this work could provide additional insight into the precise details of cellular A β O formation, the mechanism by which NU-9 inhibits A β O buildup, and the effects of NU-9 on endogenous formation of A β O. Regarding cellular A β O formation, proteomic or other structural analysis could be used to identify which A β O are prevented from forming when dynamin is inhibited. This would provide insight into the structural features of the neuron-binding A β O that form by an intracellular mechanism. Additionally, future experiments could be used to establish whether cathepsin L contributes to A β O buildup by cleavage of lamin B and caspase 3. These investigations would help to illuminate additional effectors that can be targeted to protect neurons in AD.

To identify the exact target of NU-9, a photoaffinity pulldown experiment could be used. This experiment will clarify the exact mechanism by which NU-9 inhibits proteopathy. Identification of the target will also provide a basis for structure-guided optimization to develop more potent molecules. To identify whether NU-9 mediated protection against the formation of neuron-binding A β O results in functional protection of memory and AD-relevant pathology, the effect of NU-9 will be tested on a larger cohort of 5xFAD model mice. Additionally, the effects of NU-9 on buildup of physiologically relevant A β O could be tested in the chick retina. In chick retina, transient A β O expression occurs during embryonic development¹⁵¹.

Finally, future experiments could be pursued to determine the breadth of oligomeric proteins altered by NU-9. Genc et al. demonstrated that NU-9 was capable of preventing buildup of misfolded SOD1 in upper motor neurons in a transgenic ALS model⁶⁰. Our present work demonstrates that NU-9 also inhibits the accumulation of neuron-binding A β O in a cell model

of AD. Future experiments to determine whether NU-9 also protects against formation of oligomers of α -synuclein, phosphorylated tau, or huntingtin will help to illuminate the extent to which NU-9 can be used to protect against neurodegeneration in general.

2.3.10 Potential therapeutic application of NU-9

Our results demonstrated the ability of NU-9 to inhibit the buildup of A β O_s, an effect which suggests a potential therapeutic application. Robust evidence from animal models and clinical trials indicates that the removal of A β O_s can slow or stop cognitive loss in AD^{190-192,298,299}. As such, prevention of A β O buildup by NU-9 would be a valuable therapeutic tool. To that point, one post-mortem study found that more than half of individuals diagnosed with probable AD have mixed pathology, including both A β plaques and tau tangles but also TDP-43 aggregates and/or α -synuclein aggregates³⁵⁹. In cases of mixed pathology, the additional proteopathies may contribute to neurodegeneration. The ability of NU-9 to target shared mechanisms of protein oligomerization could therefore be a powerful asset for the effective treatment of mixed pathology in neurodegeneration.

Further, the mechanistic information obtained in this work could be used to inform the potential therapeutic use of NU-9. For example, given that NU-9 is lysosome dependent, a potential synergistic effect could be achieved with the use of NU-9 in combination with lysosome activators. Additionally, NU-9 could be used to block the intracellular formation of new A β O_s in combination with an A β O-neutralizing agent that would simultaneously remove pre-existing extracellular A β O_s. Lastly, the fact that NU-9 prevents the buildup of neuron-binding A β O_s but does not block binding of pre-existing A β O_s suggests that this compound

could serve as a preventative agent to provide protection in early disease such as mild cognitive impairment.

2.3.11 Conclusion

In conclusion, a potential therapeutic against formation of cell-binding A β O_s was identified and a lysosome-dependent mechanism involving differential roles for cathepsin B and cathepsin L was elaborated. These findings will be valuable towards understanding the shared mechanisms of unstructured protein accumulation in various neurodegenerative diseases and begin to provide novel insight into interventions that might be effective against multiple diseases.

2.4 Materials

Materials used in this research and the commercial sources are as follows: 1,1,1,3,3,3-hexafluoro-2-propanol (HFIP) (Sigma-Aldrich, 52517), 7-amino-4-methylcoumarin, 99% (Sigma-Aldrich 257370-100MG), 96-well plates (Greiner Bio-One 655076), 96-well polystyrene poly-D-lysine microplate (Fisher Scientific 07-000-190), amyloid beta (Peptides International PAM-4349) anti-tubulin β -3 (TUBB3, Fisher Scientific 501029522), bafilomycin A1 (Sigma-Aldrich B1793-2UG), bovine serum albumin (Pierce 23209), Bradford assay reagent (Thermo Scientific 23238), Brij[®] L23 solution (Sigma-Aldrich B4184), CA-074 (Cayman Chemical 24679), cathepsin L from human liver (Fisher Scientific 50-489-704), cover glass 12 mm (Fisher Scientific 12-545-80P and 12-545-81P), CPCA-MAP2 (EnCor Biotechnology CPCA-MAP2), culture dishes 35 mm (Fisher Scientific 08-772A), dimethyl sulfoxide (Sigma-Aldrich D2650-5X5ML), dynasore (Cayman Chemical 164062), E18 rat tissue (Transnetyx SDEHCV), E64 (Sigma-Aldrich 324890-1MG), formaldehyde solution 37% (Sigma-Aldrich F8775-500ML), goat anti chicken IgY secondary antibody Alexa Fluor 568 (Thermo Fisher Scientific A11036),

goat anti-chicken IgY secondary antibody Alexa Fluor 488 (Molecular Probes A11039), goat anti-mouse IgG secondary antibody Alexa Fluor 488 (Fisher Scientific A11029), goat anti-mouse IgG secondary antibody Alexa Fluor 568 (Fisher Scientific A11004), Ham's F12 medium (Caisson Labs HFL05-500ML), Hibernate E minus calcium (Transnetyx HECA), Hibernate® EB Complete (Transnetyx HEB), human amyloid beta (1-42) (Peptides International, PAM-4349), L-glutamic acid (Calbiochem 3510), LysoTracker Red DND 99 (Thermo Fisher Scientific L7528), MG132 (Millipore Sigma 474787-10MG), microcentrifuge tubes (MIDSCI AVX-T-17-LC and AVX-T-06-LC), NbActiv1® (Transnetyx NB1), NbActiv4® (Transnetyx NB4 and NB4PR500), Neurobasal media (Thermo Scientific 21103049), nitric acid (Fisher Scientific A200-500), nitrocellulose membrane (GE 10600003), normal goat serum (Fisher Scientific ICN19135680), papain (Sigma-Aldrich P4762), peroxidase-linked anti-mouse-IgG secondary antibody (Fisher Scientific NA931), poly-D-lysine (Sigma-Aldrich P6407), Prolong Diamond mountant (Thermo Fisher Scientific P36862), SuperSignal West Femto Maximum Sensitivity Substrate (Fisher Scientific PI34095), Triton X-100 (Sigma-Aldrich T9284-500ML), Tween-20 (Sigma-Aldrich P1379), vacuolin-1 (Cayman Chemical 20425), Z-Arg-Arg-7-amido-4-methylcoumarin hydrochloride (Sigma-Aldrich C5429-5MG), Z-FR-AMC (Cayman Chemical 34045), Z-FY-CHO aka SB-412515 (Cayman Chemical 23249).

2.5 Methods

2.5.1 A β film preparation

A β films were originally prepared according to the method of Lambert, et al and Chromy, et al^{91,95,310}. The resulting 0.451 mg A β films were stored at -80 °C over desiccant until use.

Miniature A β films were prepared from 0.451 mg films by a modified version of the previous

procedure. To 0.451 mg films was added 1.25 mL ice-cold HFIP using a Hamilton syringe. The vial was tilted and incubated for 1 h at RT, and then chilled on ice prior to aliquoting 100 μ L per tube into 0.6 mL microcentrifuge tubes on ice. HFIP was evaporated as previously described, and the resulting aliquots of 36 μ g A β were stored at -80 °C over desiccant until use.

2.5.2 Amyloid beta oligomer preparation

For experiments using preformed oligomers, A β O_s were prepared according to the method in Lambert, et al³¹⁰. For the 200 nM concentration, A β O_s were prepared at approximately 1 μ M in Ham's F12 media and exact concentration was calculated by the Bradford assay. This solution was diluted to 200 nM in conditioned media for cell treatment to account for potential loss of A β to the plastic during formation from monomer in the dish. For the 30 nM concentration, oligomers were formed according to the procedure in Velasco, et al.³¹¹ in warm Neurobasal media. For cell treatment, media was replaced with this solution.

2.5.3 Hippocampal neuron cell culture

1 pair of combined E18 Sprague-Dawley rat hippocampus, cortex, and sub-ventricular zone tissue was obtained fresh from Transnetyx and cultured according to the manufacturer's protocol, based on the procedures from Brewer et al.^{360,361}. Cells were diluted to 0.11-0.22 million/mL and plated at 0.15 mL/cover slip directly onto sterile poly-D-lysine coated 12 mm circular coverslips, which were prearranged 4/dish in 35 mm culture dishes. This yielded a density of approximately 15,000 cells/cm². Cells were fed 4 days after plating by half-media exchange with NbActiv1, and subsequently every 2-3 days by half-media exchange with NbActiv1.

2.5.4 Hippocampal neuron cell treatment

Mature hippocampal neurons at 18-25 div were pretreated first with any inhibitors of interest including: dynasore (80 μ M, 30 min), MG132 (100 nM, 30 min), bafilomycin A1 (100 nM, 30 min), vacuolin-1 (1h, 1 μ M), E64 (10 μ M, 24h), Z-FY-CHO aka SB-412515 (10 μ M, 1h), CA-074 (10 μ M, 24h), or the corresponding DMSO vehicle in conditioned media. In some cases, two pretreatments with inhibitors were carried out one after another. These interventions were followed by 30 min incubation with 3 μ M NU-9 (or alternative, stated concentrations) or DMSO vehicle, and finally by 30 min application of 500 nM A β or 30-200 nM A β O_s and the corresponding DMSO, neurobasal, or F12 vehicle. At all stages, previous compounds were not removed. To add subsequent treatments, half of the media was removed from each dish, and a 2x solution of the next treatment was prepared in that conditioned media, which was then added back to the dish and mixed to apply the treatment at the desired concentration. For immunofluorescence experiments, cells were washed with sterile PBS prior to fixation with formaldehyde. For biochemical experiments of extracellular, unbound A β O_s, media was removed from each dish after mixing well, and analyzed fresh or was flash-frozen and stored at -80 °C prior to analysis.

2.5.5 Immunofluorescence

After washing with sterile PBS, coverslips were fixed by addition of an equal volume of 3.7% formaldehyde solution for 10 min, followed by replacement with 3.7% formaldehyde for 10 min. Coverslips were washed three times with PBS and blocked with 5% normal goat serum, 0.1% Triton X-100 in PBS overnight at 4 °C or for 1h at RT. Primary antibodies NU2 (1-2 μ g/mL, in-house) and CPCA-MAP2 (1:10,000) were added in 10% blocking buffer overnight at

4 °C. Occasionally, other antibodies were used instead of MAP2 for labeling neuronal processes, including anti-tubulin β -3 (1:2000).

Coverslips were then washed three times with PBS and secondary antibodies, goat anti-mouse Alexa Fluor 488 or 568 (1:2000) and goat anti-chicken Alexa Fluor 568 or 488 (1:2000) were added in a solution of 10% blocking buffer in PBS, for 3h, at RT, in the dark. Coverslips were washed three times and mounted in Prolong Diamond Antifade mountant with DAPI.

Images were collected using a Leica DM6B fluorescent microscope using the 63x objective. Using the Leica LAS-X software, 3D deconvolution was applied for 3 iterations, and subsequently maximum projections were obtained for each image.

2.5.6 Analysis of A β O binding assay

A β O binding analysis was conducted on immunofluorescent images in which a structural reference antibody, most commonly MAP2, but also including β -3 tubulin, was used as an indicator of neuronal processes. ImageJ was used for analysis, using macros included in the Appendix. Briefly, tiff images were assigned random numbers to avoid bias during analysis, and then cell bodies were manually traced and deleted for each image to eliminate signal from nonspecific antibody accumulation in the cell body. Then, the signal from different wavelengths was split. To calculate total dendrite length in each image, a Gaussian blur was applied to the MAP2 signal, and the signal above an equal threshold for each image was skeletonized, and the total length of the skeleton was measured. To calculate the total A β O puncta along processes, again a Gaussian blur was applied to the dendrite signal, and the signal above an equal threshold was selected. Then, the signal was dilated to encompass the area around the dendrites by 15 dilations. The area around the dendrites was used as a selection, and within the selection area,

ImageJ particle analysis and summary was used to count the NU2 puncta above an equal threshold for each image. Thresholds were chosen based on one or two positive and negative control images. Total NU2 puncta were divided by the total dendrite length to calculate the A β O puncta/micron.

2.5.7 Cell-free incubation of A β

For experiments using fresh NbActiv1 media: NU-9 or an equal volume of DMSO vehicle was added to fresh media and incubated for 30 min, 37 °C in the absence of cells. For experiments with conditioned media: NU-9 was added to one dish of cells, while conditioned media from other dishes was removed and NU-9 or DMSO vehicle was added and incubated for 30 min, 37 °C in the absence of cells. Then, media from the NU-9 treated dish was removed to a cell-free microcentrifuge tube, and 500 nM A β or an equal volume of DMSO vehicle was applied to all solutions, mixed well with a pipet, and incubated in a cell-free environment for 30 min, 37 °C. Following this treatment, all tubes were placed on ice, centrifuged at 14,000 rcf, 10 min, 4 °C, to remove any fibrils, and the top 80% was used for analysis.

2.5.8 Dot blot biochemical assay of A β

Samples were diluted 25-30x using additional media, and 200 μ L of each was quickly loaded on a pre-wet nitrocellulose membrane using a Whatman Minifold dot blot system. For the standard curve, standard solutions at 0-5 nM of preformed F12 A β O were prepared in duplicate and loaded at 200 μ L per well to achieve a curve from 0-1000 fmol per spot. A vacuum was applied to concentrate samples on the solution, and then 200 μ L Tris-buffered saline (20 mM Tris, 150 mM NaCl, pH 7.4, TBS) was used to wash all wells of the manifold and then vacuum was re-applied. The membrane was allowed to dry briefly, and subsequently a blocking solution

comprised of 5% milk was made in TBS with 0.1% Tween-20 (TBS-T) and applied for 1h, RT, on a rocking shaker. The membrane was next incubated with primary antibody solution of 1-2 $\mu\text{g}/\text{mL}$ of NU2 for 90 min, RT, and was washed 3 x 10 min each, with TBS-T, prior to application of 1:20,000-1:40,000 peroxidase-linked anti-mouse-IgG secondary antibody for 1 h, RT, on a rocking shaker. Finally, the membrane was washed 3 x 10 min each, with TBS-T and 3 times, quickly, with doubly-deionized water. West Femto Maximum Sensitivity chemiluminescent substrate was applied according to the manufacturer's instructions, at half-strength or full-strength, as needed, and membranes were imaged using a Sapphire Biomolecular Imager.

2.5.9 Lysosome characterization using LysoTracker

In conditioned media, bafilomycin A1 (100 nM, 1 h) was applied to cells, followed by NU-9 (3 μM , 30 min). Then, media was replaced with warm, transparent NbActiv4 media, containing LysoTracker Red DND 99 used according to the manufacturer's instructions, at 75 nM for 30 min. Cells were washed 1x into transparent NbActiv4. Immediately prior to imaging with the 5x objective on a Leica DM6B fluorescent microscope, each coverslip of cells was inverted onto a glass slide. Imaging was conducted quickly to avoid coverslips drying out.

2.5.10 Cathepsin B purified activity assay

Conditions were based on a protocol published by Sigma-Aldrich³⁶² and assays developed by Barrett and coworkers^{363,364}. 0.1% Brij solution was prepared from Brij L23 in doubly-deionized water. Stocks of test compound NU-9 and the standard inhibitor CA-074 were prepared by serial dilution into 0.1% Brij solution. Assay buffer, 0.1% Brij solution, and compound solutions were added to a black, flat-bottom 96-well plate. A fresh solution of 5 μM

7-amino-4-methylcoumarin (7-AMC) in 0.1% Brij was added to create a standard curve from 0.4-02 μM . A fresh solution of the fluorogenic substrate, Z-Arg-Arg-7-amido-4-methylcoumarin hydrochloride (Z-RR-AMC), was prepared in 0.1% Brij solution and added to the assay plate at 60 μM . The assay plate was subsequently warmed to 40 $^{\circ}\text{C}$ prior to addition of the enzyme solution. The enzyme solution was added at 0.13 U/mL, wells were mixed, and the formation of the fluorogenic substrate was monitored with a Synergy Neo 2 plate reader at an excitation of 348 nm and emission of 440 nm every 20 sec over 30 min.

2.5.11 Cathepsin L purified activity assay

Assay conditions were developed based on the method of Barrett, Mason, and coworkers^{364 365}. Stock solutions of NU-9 and the standard inhibitor Z-FY-CHO were prepared by serial dilution in doubly-deionized water and diluted into the assay buffer in a 96-well plate at final concentrations of 0.0003-150 μM . To prepare a standard curve, solutions of 7-AMC were diluted into a 96-well assay plate for final concentrations 0-2 μM in assay buffer. Substrate stock was prepared by dissolving N-[(phenylmethoxy)carbonyl]-L-phenylalanyl-N-(4-methyl-2-oxo-2H-1-benzopyran-7-yl)-L-argininamide, trifluoroacetate salt (Z-FR-AMC) to 1 mM in DMSO. The substrate solution was added to the 96-well assay plate at 1 μM Z-FR-AMC. Purified cathepsin L enzyme from human liver was added at 25 ng/mL into 0.1% Brij solution containing 1 mM DTT and incubated for 40 min at 4 $^{\circ}\text{C}$ to activate the enzyme. Then, the enzyme was further diluted in activating solution to prepare an enzyme solution at 8.7 ng/mL. The assay plate was mixed well and preincubated without the enzyme for 5 min at 30 $^{\circ}\text{C}$. Then, activated cathepsin L enzyme was added into the 96-well plate for a final concentration of 0.87 ng/mL, approximately 2.3 $\mu\text{U/mL}$ based on manufacturer analysis. Cleavage of substrate to the

fluorogenic product 7-AMC was monitored using a Synergy Neo 2 plate reader with excitation at 348 nm and emission at 440 nm every 40 sec over 30 min.

2.5.12 Intracellular cathepsin activity assays

For cathepsin activity assays only, neurons were grown in a sterile, clear poly-D-lysine-coated 96-well plate. Dissection and dissociation were carried out as previously described, and E18 hippocampal neurons were plated at 20,000-40,000 cells/well in 100 μ L media. Cells were fed by addition of 100 μ L NbActiv1 media after 4 days, then every 2-3 days by $\frac{1}{2}$ media exchange with fresh NbActiv1. Cells were used at 21-25 div. For experiments, cells were treated in conditioned media, first with 100 nM bafilomycin A1 for 30 min at 37 $^{\circ}$ C, then 3 μ M NU-9 was added for another 30 min at 37 $^{\circ}$ C. Magic Red reagents for CatB and CatL were solubilized according to the manufacturer's instructions, then diluted to the recommended concentration in transparent NbActiv4 media. This freshly made Magic Red-containing media was used to replace treatment media, and the plate was incubated for 30 min at 37 $^{\circ}$ C. In some experiments, Hoescht 33342 was added at 0.1 mg/mL for 5 min at 37 $^{\circ}$ C to label nuclei. Cells were washed 1x with warm, clear NbActiv4 media prior to imaging using the 40x objective of a Molecular Devices ImageXpress High Content Imaging Robotic Platform. During imaging cells were maintained at 37 $^{\circ}$ C in the microscope.

2.5.13 Novel object and novel placement recognition assay

Twelve 5xFAD mice were bred on the slow-onset background. These animals received either vehicle control or NU-9 by gavage (20 mg/kg) daily for one month. Locomotion and memory performance were evaluated prior to treatment, by measuring rearings and crossings, and using the novel location recognition and novel object recognition assays, and animals were

evenly distributed into treatment and vehicle groups^{366,367}. In these assays, animals were first habituated for 6 min to an open-field testing arena made of polyvinyl chloride with dimensions of 21 × 21 × 12". A visual cue was attached to one wall of the arena. Animals first were presented with two plastic objects during a 6 min training session. Next, to assess novel object recognition, one object was replaced with a novel object. Finally, to assess novel location recognition, the novel object was displaced. The percentage of time spent interacting with each object was quantified by the experimenter. Following treatment, a novel object was displaced as a measure of both hippocampus- and cortex-dependent memory.

CHAPTER 3:
DISRUPTION OF AMYLOID BETA OLIGOMER ACCUMULATION AND TAU
PHOSPHORYLATION BY NNOS INHIBITION

CHAPTER 3: DISRUPTION OF AMYLOID BETA OLIGOMER ACCUMULATION AND TAU PHOSPHORYLATION BY NNOS INHIBITION

3.1 Introduction: Alzheimer's disease and nNOS

3.1.1 A β O_s trigger tau phosphorylation and neurodegeneration

Alzheimer's disease (AD) is the most common cause of dementia, which afflicts approximately 1 in 9 people age 65 and older². The histopathological diagnosis of AD is based on the presence of amyloid β (A β) plaques and neurofibrillary tangles of hyperphosphorylated tau protein³⁶⁸. However, the presence of A β plaques does not ensure AD development, and the density of A β plaques does not correlate well with cognitive decline³⁶⁹. Rather, soluble oligomers of A β (A β O_s) instigate neurodegeneration^{54,174-178,181-184}. A β O levels can be used to detect AD in very early stages and correlate with cognitive impairment throughout disease^{140,158,162-164}. A β O_s cause neurodegeneration in multiple ways, including by instigating oxidative and nitrosative stress, triggering inflammation, impairing autophagic machinery, and, importantly, inducing phosphorylation of tau protein^{54,286,370-372}.

The binding of extracellular A β O_s to neuronal receptors triggers intracellular signaling cascades that result in aberrant post-translational modification of proteins^{373,374}. While these modifications are typically important for modulating protein activity to maintain homeostasis, aberrant post-translational modifications can lead to cellular dysfunction. For example, aberrant cysteine nitrosylation of several proteins is observed in AD brains, causing the activation of multiple tau kinases and the inhibition of a key chaperone; these post-translational modifications may contribute to tau hyperphosphorylation, synapse damage, and further protein aggregation^{286,370}. Additionally, the binding of A β O_s to receptors triggers intracellular tau

hyperphosphorylation^{197,375}. Hyperphosphorylation alters the function of tau, leading to mislocalization, aberrant protein interactions, and eventual formation of the characteristic neurofibrillary tangles³⁷⁵⁻³⁷⁹. Thus, hyperphosphorylated tau mediates a substantial portion of downstream A β O-induced neurotoxicity³⁸⁰⁻³⁸². However, the mechanisms by which A β O binding triggers intracellular tau phosphorylation and cysteine nitrosylation have not been well elucidated.

3.1.2 Connection between nNOS and A β O binding

Mechanistically, A β Os are known to activate the N-methyl-D-aspartate receptor (NMDAR), a ligand-gated calcium channel (Figure 3.1)^{216,383,384}. One of four drugs currently

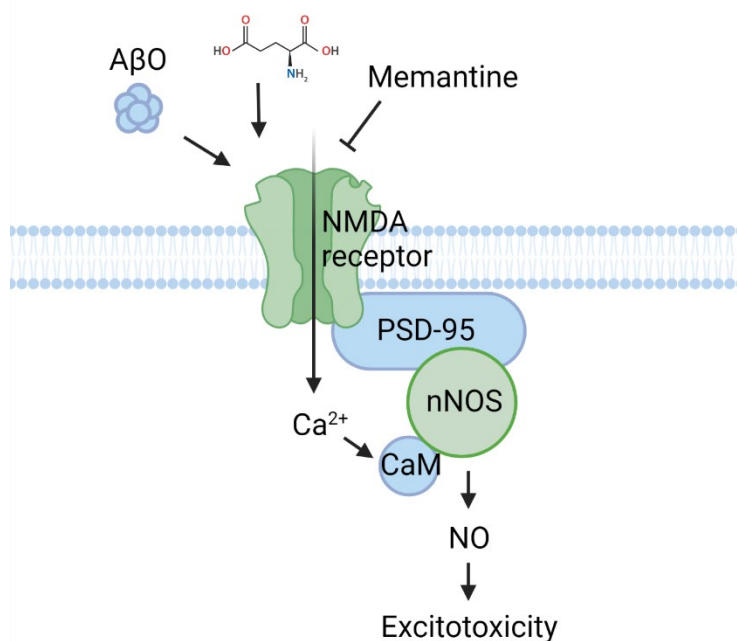


Figure 3.1 Mechanism of NMDAR and nNOS-dependent excitotoxicity. A β Os and glutamate activate the N-methyl-D-aspartate receptor (NMDAR), causing local calcium ion influx. Memantine is an NMDAR inhibitor. Because neuronal nitric oxide synthase (nNOS) is physically linked to the NMDAR via postsynaptic density protein 95 (PSD95), the local calcium influx enables calmodulin (CaM) to activate nNOS, which produces nitric oxide (NO) that contributes to excitotoxicity downstream. Created with BioRender.com.

used to treat AD, memantine, is an NMDAR antagonist that inhibits acute downstream reactive oxygen species formation and calcium influx following exposure to A β O_s²⁸⁴. Throughout the course of AD, in addition to NMDAR activation, dysregulation of other calcium channels, such as the ryanodine receptor, also contribute to increasing intraneuronal calcium in AD^{385,386}. The excitotoxicity following A β O-induced calcium influx could be mediated by neuronal nitric oxide synthase (nNOS). nNOS is physically linked to the NMDAR via postsynaptic density protein 95 (PSD95)^{387,388}. When the NMDAR is activated, the subsequent local calcium influx enables calmodulin to activate nNOS³⁸⁹⁻³⁹².

3.1.3 Physiologic and pathologic roles of nNOS

Activation of nNOS causes increased production of nitric oxide (NO), which under normal conditions allows a functional response: activation of soluble guanylate cyclase, triggering cyclic guanosine monophosphate (cGMP)-mediated downstream activation of protein kinase G and cAMP response element-binding protein (Figure 3.2)³⁹³⁻³⁹⁶. These processes underlie the normal signaling functions of nNOS, which include long-term potentiation and blood vessel dilation³⁹⁷. In early AD, increased activation of nNOS has been proposed to provide a compensatory mechanism by which neurons enhance synaptic signaling³⁸⁵. However, over the long term, overactivation of nNOS mediates excitotoxicity by excess cysteine nitrosylation and tyrosine nitration of protein targets and by contributing to nitrosative stress^{370,398}. For example, in a mouse model of glutamate-induced excitotoxicity, disruption of the PSD95/nNOS interaction rescued neurons from cell death^{399,400}. Additionally, a nonselective inhibitor that targeted multiple isoforms of nitric oxide synthase (NOS) and NMDAR activity was also neuroprotective against glutamate-induced excitotoxicity⁴⁰¹. Overall, these results point to nNOS as a mediator of

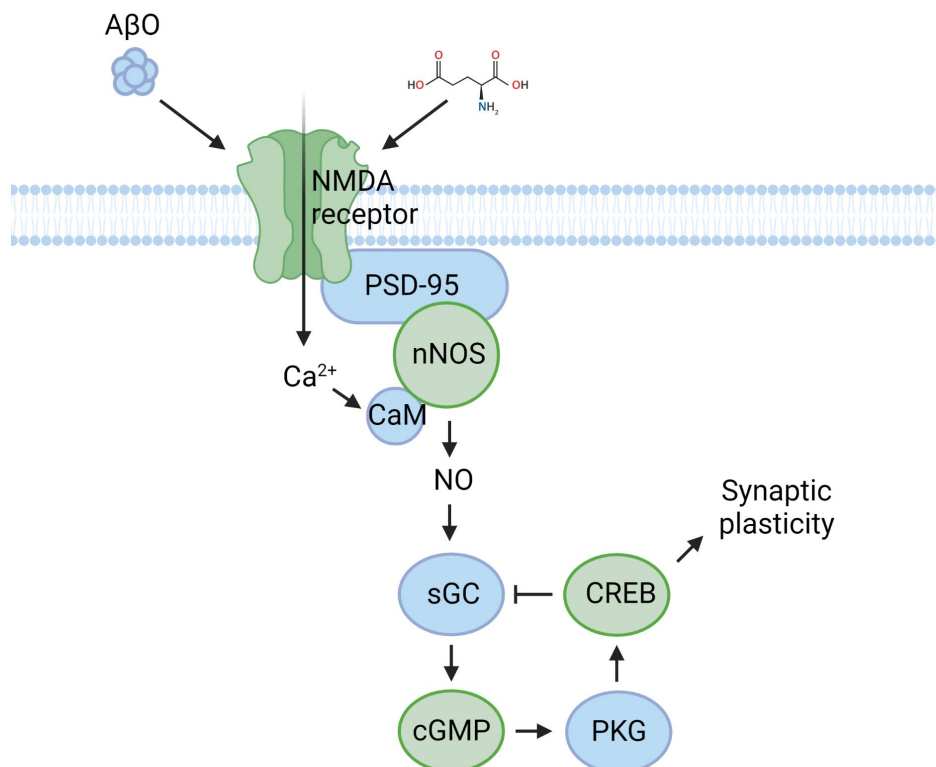


Figure 3.2 Mechanism of physiological NMDAR/nNOS signaling. Physiological levels of glutamate and possibly amyloid beta oligomers AβOs activate the NMDAR to trigger local calcium influx, which activates neuronal nitric oxide synthase (nNOS) via calmodulin (CaM) binding. Activated nNOS produces nitric oxide (NO), which activates soluble guanylate cyclase (sGC), triggering cyclic guanosine monophosphate (cGMP)-mediated downstream activation of protein kinase G (PKG) and cAMP response element-binding protein (CREB), which mediate synaptic plasticity. Created with BioRender.com.

neurodegeneration downstream of NMDAR activation and dysregulated calcium influx.

However, it is currently unclear whether nNOS activation overall plays a neuroprotective or neurodegenerative role in AβO-induced AD pathology.

3.1.4 Evidence for the overactivation of nNOS in AD

The loss of nNOS-expressing neurons in the hippocampus of AD patients suggests that nNOS overactivation may contribute to AD neurodegeneration^{402,403}. Evidence for nNOS

overactivation in the AD brain includes excess nitrosylation of cysteines^{286,404-406}. Although nitrosylation of cysteine targets serves a functional role at physiological levels, overactivation of this pathway has been implicated in neuronal dysfunction. Also increased in the AD brain is the chemically distinct, NO-dependent nitration of protein tyrosine residues⁴⁰⁷. Work by Lüth and coworkers suggests that nNOS is responsible for tyrosine nitration in neurons, while other isoforms of NOS including inducible NOS (iNOS) and endothelial NOS (eNOS), produce the majority of NO in glial cells⁴⁰⁸. However, iNOS is capable of producing higher levels of NO, which may diffuse from where it is produced in glial cells to have downstream consequences in neurons³⁹⁷. As such, the relative contribution of nNOS to NO-dependent changes in the AD brain remains unknown.

3.1.5 Potential targets of nNOS in AD

Several targets altered by nitric oxide in AD could be triggered by nNOS overactivation (Figure 3.3). Two prominent tau kinases, glycogen synthase kinase-3 β ²⁸⁵ and cyclin-dependent kinase 5²⁸⁷, are both activated by nitric oxide. Additionally, activation of the small G protein Dexas1 by S-nitrosylation is implicated in A β O-induced synapse loss^{409,410}. Further, S-nitrosylation of the chaperone protein disulfide isomerase is observed in AD, and the resultant inhibition of chaperone activity would be expected to accelerate protein aggregation²⁸⁸. Alternatively, nitric oxide also triggers zinc release, which can stabilize A β O formation^{289,290}. By modulating these targets, nNOS overactivation could be involved in promoting A β O-induced tau phosphorylation, synaptic spine loss, and AD-relevant protein aggregation. However, the role of nNOS in contributing to these forms of AD-relevant neuronal damage has not been established.

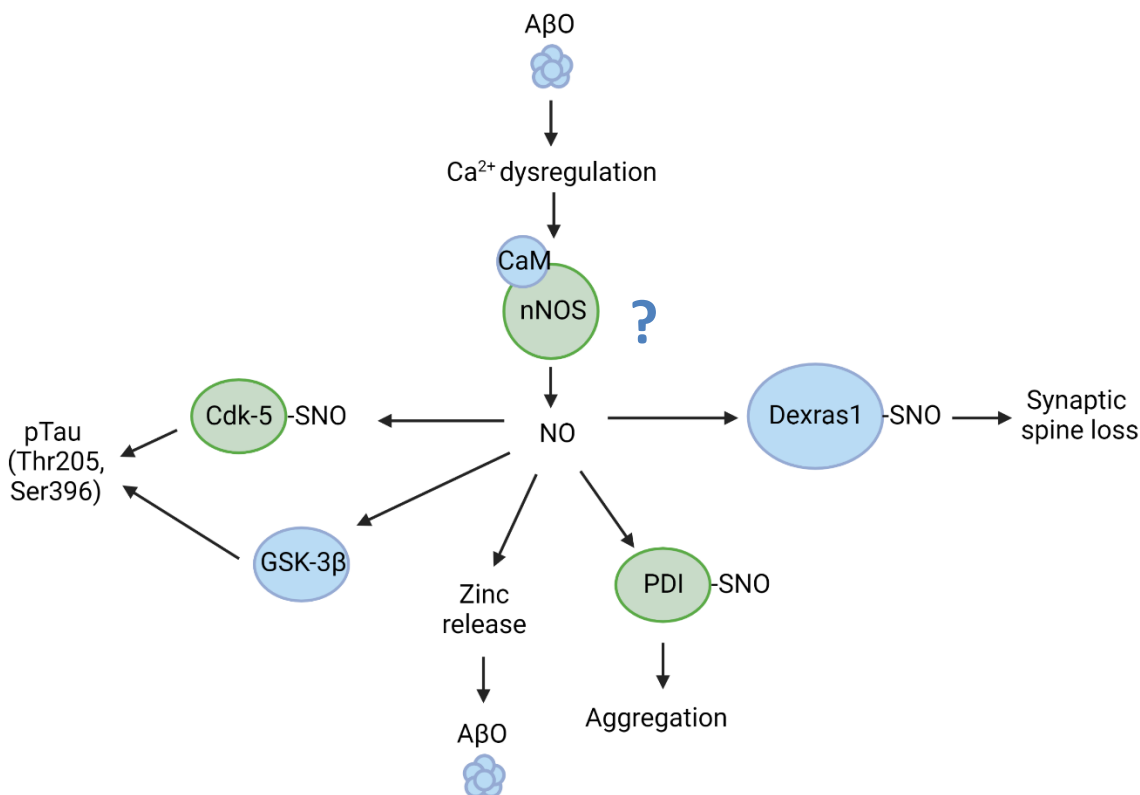


Figure 3.3 Potential mechanisms of nNOS-mediated neurodegeneration. Amyloid beta oligomers (A β O)s trigger calcium dysregulation in neurons, which could lead to neuronal nitric oxide synthase (nNOS) overactivation, which would generate excess nitric oxide (NO). Nitric oxide activates the tau kinases glycogen synthase kinase-3 β (GSK-3 β) and cyclin-dependent kinase 5 (Cdk-5). NO also activates the small G protein Dexras1 by S-nitrosylation, which leads to synapse loss. NO can inhibit the protein disulfide isomerase (PDI) by S-nitrosylation and can trigger zinc release, which can contribute to aggregation and A β O formation. Created with BioRender.com.

3.1.6 nNOS inhibitors

Highly selective inhibitors of nNOS have not been previously applied to the study of AD, and as such, present a novel tool for the interrogation of this system. Sensitive, selective competitive inhibitors for nNOS over other NOS isoforms have been developed in the Silverman lab, but most exhibited low membrane-penetrance, limiting their ability to reach the brain in

*vivo*⁴¹¹. These inhibitors began as mimics of arginine, the endogenous substrate for NOS, and were further optimized via “scaffold-hopping” to thiophene-carboximidamide, aminopyridine, and aminoquinoline-based inhibitors.

3.1.7 Development of nNOS inhibitors

Like arginine, these nNOS inhibitors typically use a guanidine-like head moiety to form a salt bridge with Glu597 and hydrogen bond with Trp592. Although arginine binds identically into the active site of each isoform, specificity over endothelial NOS (eNOS) has been achieved by designing inhibitors that preferentially fit into the differently-shaped, more electronegative pocket of nNOS, as defined by the replacement of eNOS Val104 with Met341 in nNOS, and the replacement of eNOS Asn366 with Asp602 in nNOS⁴¹¹⁻⁴¹³. Specificity over inducible NOS (iNOS) has been achieved by taking advantage of the more flexible, hydrophilic nNOS active site. Using these strategies, several hundred-fold selectivity for nNOS over other NOS isoforms has been achieved. Sensitivity has been optimized to nanomolar levels by installing amine tail groups that interact with one or both heme propionates, in analogy to the binding of the N-terminal nitrogen of arginine, and by installing groups on the linker that form hydrogen bonds or van der Waals interactions with additional active site residues including Tyr567, Tyr 593, Asn574, Met575, and Tyr711^{412,414,415}.

3.1.8 Low bioavailability of nNOS inhibitors

Although these inhibitors have achieved low-nanomolar sensitivity and several hundred-fold selectivity for nNOS over other NOS isoforms, many have exhibited low membrane-penetration, hampering their potential to reach the brain. To access the brain, drugs must pass through the blood-brain barrier (BBB), the layer of endothelial cells surrounding all capillaries in

the brain⁴¹⁶. Endothelial cells in the BBB are connected by tight junctions and express a high number of efflux transporters, reducing paracellular transport and enforcing efficient removal of efflux transporter substrates. Low membrane penetrance is a common issue for arginine-mimic based compounds, which have high basicity and total polar surface area, as well as several hydrogen bond donors⁴¹³. These properties confer sensitivity but are unfavorable for membrane permeability. As such, several attempts to increase permeability have led to decreased sensitivity or selectivity^{417,418}.

3.1.9 Prodrug approach to nNOS inhibitors

The prodrug approach is ideally suited to solve the problem of low membrane penetrance. A prodrug is a modified version of a drug that is converted to the active form *in vivo*⁴¹⁹. Using prodrugs, membrane permeability can be optimized by tuning lipophilicity and pKa, and by masking hydrogen-bond donors. Prodrugs may also be used to target molecules directly to the tissue of interest by taking advantage of transporters expressed only in the BBB or cleavage enzymes expressed only in the brain that will liberate the active molecule. Finally, prodrugs may also be used to “lock-in” active molecules within the brain, by unmasking a polar group following movement across the blood-brain barrier⁴²⁰. Major prodrugs for amines include carbamate, N-oxide, and oxodioxolenyl compounds⁴²¹. Conjugated amino acids and sugars have also been used as prodrugs to take advantage of active transport into the brain by the large neutral amino acid (LAT-1) and glucose (GLUT1) transporters. To test the viability of a prodrug approach to improve membrane penetrance of nNOS inhibitors, in this work several simple carbamate prodrugs were synthesized, and their penetrance was tested.

3.1.10 Non-prodrug optimization of nNOS inhibitors

However, simultaneous non-prodrug structural modifications of nNOS inhibitors by a coworker in the Silverman group, Dr. Ha Do, also yielded promising improvements in BBB-permeability⁴¹⁵. An aminopyridine compound with a fluorobenzene linker and dimethylamine tail showed improved permeability while retaining sensitive and selective nNOS binding. These results support the hypothesis that non-prodrug modifications, especially those that decrease tail amine pKa or mask available tail hydrogen bonds, provide a useful avenue toward improving BBB-permeability of nNOS inhibitors. In this work, this improved inhibitor with favorable permeability, HD-3-86, was used to test the effect of nNOS on tau phosphorylation and other AD-relevant damage in neurons.

3.1.11 Research objective

Although significant evidence supports a potential role for nNOS in mediating A β O-induced tau phosphorylation and other features of AD pathology, thus far the exact role of the neuronal isoform of nitric oxide synthase has not been established in these pathways. Highly selective inhibitors of nNOS have not been previously applied to the study of AD, and as such, present a novel tool for the interrogation of this system. Therefore, in this work I applied a specific inhibitor of nNOS for the first time to a model of A β O-induced tau phosphorylation to determine whether nNOS activity was necessary for A β O-induced tau phosphorylation, to measure whether nNOS activity contributed to A β O buildup from A β monomer, and to test the effect of nNOS inhibition on synaptic puncta density.

3.2 Results

3.2.1 Synthesis of carbamate prodrugs for nNOS inhibitors

To prepare carbamate prodrugs of an nNOS inhibitor, compounds **1**, **2**, and **3** (methyl, ethyl, and benzyl carbamate derivatives of HD-I-86) were synthesized from the parent compound using the corresponding methyl, ethyl, or benzyl chloroformate with triethylamine (Figure 3.4). For the synthesis of compound **4**, due to the higher pKa of the pyridine-connected amine compared to the tail amines, which were previously protected, a more potent base, sodium hydride, was used for deprotonation.

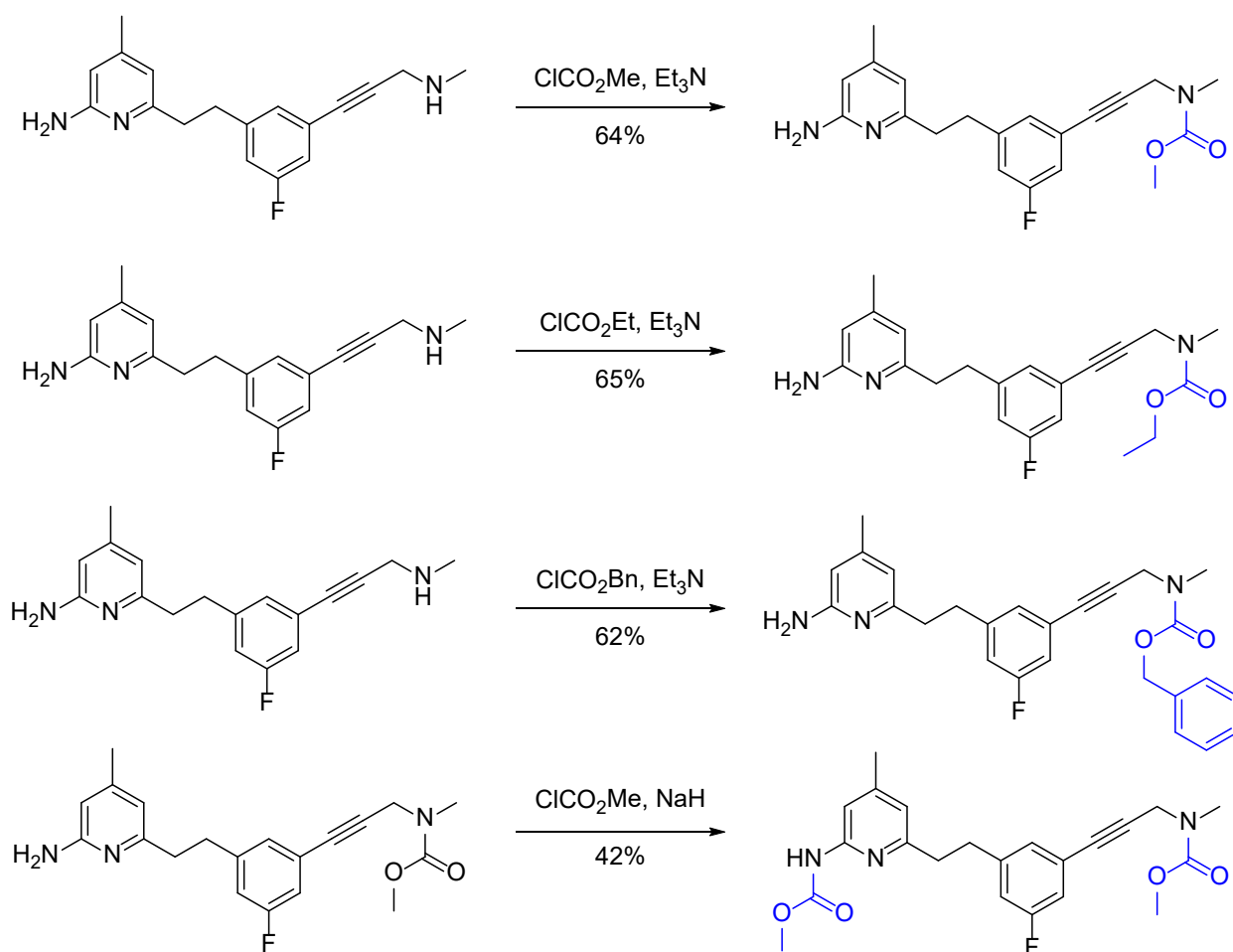


Figure 3.4 Synthesis of (1) methyl, (2) ethyl, (3) benzyl, and (4) dual methyl carbamate derivatives of HD-1-86.

3.2.2 Passive permeability of *n*NOS inhibitor carbamate prodrugs was reduced

The parallel membrane permeability assay (PAMPA) was used to measure passive permeability of each compound through brain lipids⁴²². Effective permeability (P_e) values for each compound, presented in Table 3.1, were calculated via established methods based on the transfer of each compound through a brain lipid-infused membrane⁴²³. In this assay, some fraction of compound may not pass through but may simply be retained within the membrane (%R).

As seen in Table 3.1, the effective permeability of compound **1** was the same as that of HD-I-86. Compounds **2** and **3** had lower effective permeabilities than HD-I-86. Additionally, high membrane retention was observed for these compounds. Since retention decreased for compound **2** when its concentration was reduced, the lack of permeability may partly reflect poor solubility. Taken together, these results indicate that even for some simple carbamate prodrugs of HD-I-86, lipophilicity became too high for effective membrane penetration.

Table 3.1 PAMPA-BBB results for compounds 1-3

Compound	P_e (Effective permeability)	%T (Transfer)	%R (Membrane retention)
Verapamil (+)	20.9 ±1.7 E-6	35.7	19.3
Theophylline (-)	0.15 ±0.01 E-6	0.799	0.249
HD-I-86 (200µM)	15.2 ±0.6 E-6	33.7	15.8
1 (200µM)	15.2 ±0.6 E-6	12.8	67.9
2 (200µM)	7.3 ±2.21 E-6	3.01	88.7
2 (100µM)	10.0 ±0.8 E-6	9.77	66.3
3 (200µM)	6.0 ±1.15 E-6	1.20	94.9

3.2.3 Permeability predictions for prodrugs of HD-1-86

Permeability trends for compounds **1-3** were accurately represented by a six-parameter model developed by Wager and coworkers^{424,425}. This model uses lipophilicity, molecular

weight, total polar surface area, number of hydrogen-bond donors, and pK_a to calculate a score of CNS drug-likeness, referred to as a CNS multi-parameter optimization (MPO) score ranging from zero to six. A compound with a CNS MPO score of six is generally predicted to be very drug-like, including good penetration of the blood-brain barrier, while one with a score of zero is predicted not to be drug-like, including poor blood-brain barrier penetration. Predicted data for prodrug derivatives of HD-I-86 are shown in Table 3.2.

Table 3.2 CNS MPO scores for compounds 1-6

Compound	ClogP	ClogD	MW	TPSA	HBD	pK_a	CNS MPO score
HD-I-86	3.62	1.58	297.38	50.94	3	8.74	4.48
1	3.85	3.05	355.41	68.45	2	8.16	4.47
2	4.21	3.41	369.44	68.45	2	8.16	4.04
3	5.57	4.77	431.51	68.45	2	8.16	2.91
4	3.43	3.41	400.48	93.65	1	12.93	3.18
5	8.54	7.13	530.02	57.51	2	8.83	2.09
6	4.41	3.05	418.52	57.26	2	12.08	3.33

As with the changes in measured permeability, the CNS MPO score for compound **1** was similar to that of HD-I-86, and compounds **2** and **3** display progressively worse scores (Figure 3.5). For compound **4**, the dual carbamate, permeability is predicted to be slightly better than that of compound **3**, but worse than the parent compound.

Additional compounds **5** and **6** had been designed as Schiff base and dihydropyridine derivatives of HD-I-86, respectively, comprising other common CNS prodrug moieties (Figure 3.6). Unfortunately, these compounds are predicted to exhibit similar or worse passive permeability than the carbamate derivatives, likely due to their high lipophilicity and molecular weight (Table 3.2). Therefore, these additional prodrug modifications were not pursued.

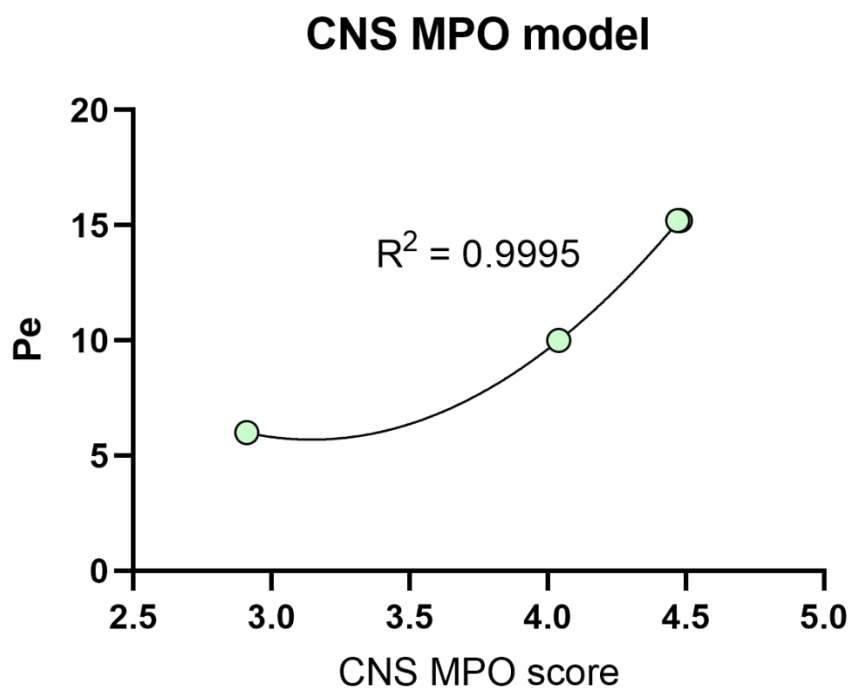


Figure 3.5 Central nervous system multi-parameter optimization (CNS-MPO) score correlates with measured permeability (P_e). P_e values for methyl, ethyl, benzyl carbamate prodrugs, and the parent compound were correlated to CNS MPO scores by an exponential growth curve ($R^2 = 0.9995$).

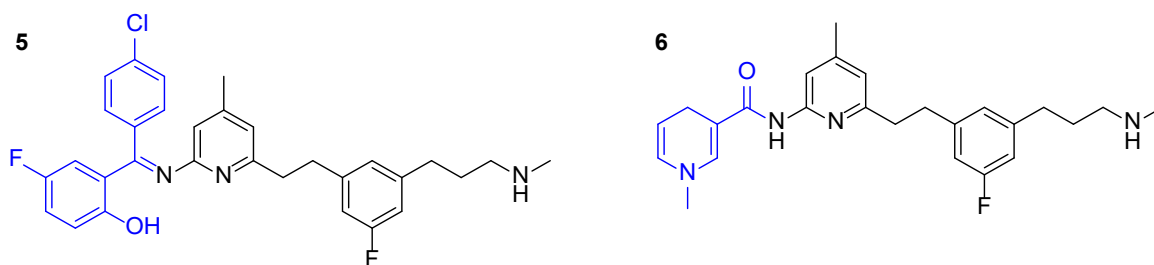


Figure 3.6 Proposed Schiff base (5) and dihydropyridine (6) derivatives of HD-I-86.

3.2.4 Neuronal production of nitric oxide radicals can be prevented by NOS inhibition

To explore the effect of NOS inhibition in hippocampal neurons, an assay to monitor NO production in neurons was established using the fluorescent dye diaminofluorescein-FM diacetate (DAF-FM DA)^{426,427}. L-Glutamate and D-serine, co-agonists of the NMDAR, were administered to neurons as a positive control for nNOS activation⁴²⁸. An increased trend in the integrated fluorescent intensity was observed in the treated condition as compared to the control, indicating glutamate-induced NO production (Figure 3.7, 540x, ns).

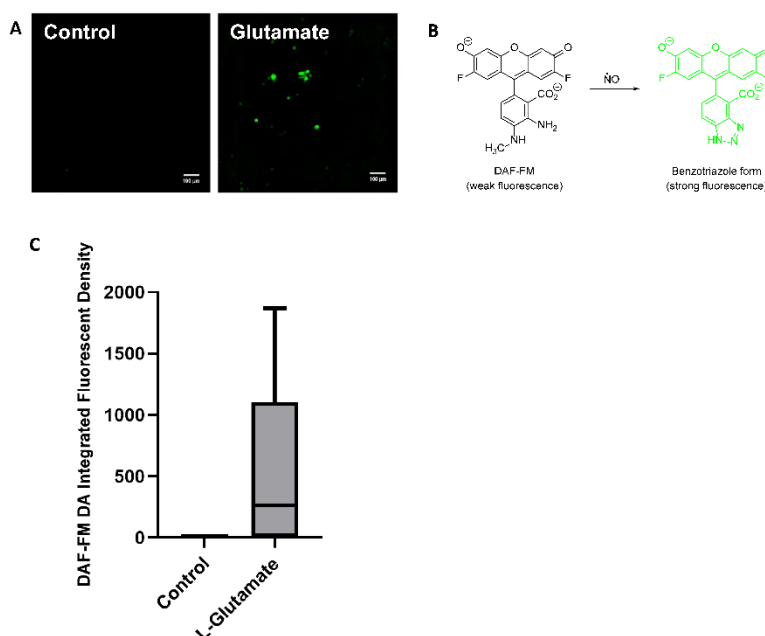


Figure 3.7 Glutamate induces NO production. (A) Representative images of rat hippocampal cells incubated with DAF-FM DA and treated with conditioned media as a control or 100 μ M L-glutamic acid and 10 μ M D-serine. Cells were excited at 495 nm and imaged at 515 nm using the 10x objective. (B) Reaction of DAF-FM with NO. (C) Immunofluorescent integrated fluorescent density in control and glutamate treated wells, normalized to intensity in control wells. Data were combined from n=3 experiments, n=2 wells each. Integrated fluorescent density had an increased trend of 541x in the L-glutamate treatment ($p = 0.13$ due to high standard deviation).

The general NOS inhibitor N^G-nitro-L-arginine methyl ester (L-NAME) was used as a negative control for NO production. L-NAME pretreatment showed a trend toward reduction of integrated fluorescence intensity, reflecting the suppression of NO production by NOS inhibition (Figure 3.8A, 100%, ns).

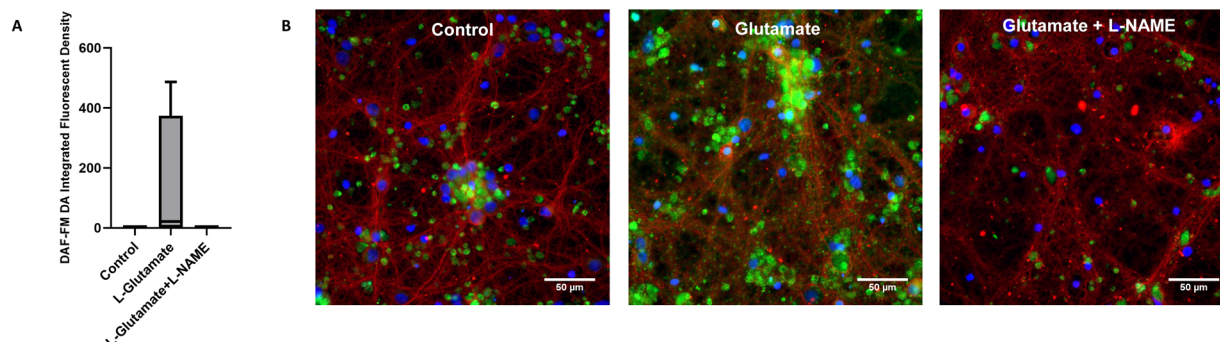


Figure 3.8 NOS inhibition prevents glutamate NO production. (A) Immunofluorescent integrated fluorescent density from rat hippocampal neurons imaged following incubation with DAF-FM DA (80 μM) for 2 hours, then treated with conditioned media, 100 μM L-glutamic acid and 10 μM D-serine, or pre-incubated with 200 μM L-NAME before incubation with 100 μM L-glutamic acid and 10 μM D-serine. Signal was normalized to intensity in control wells. Images used for quantification were collected using a 10x microscope objective in live cells, 4 images per well were averaged, and data were combined from n=2 experiments (data also included in figure 3.7), n=2 wells each. Integrated fluorescent showed a trend toward reduction by L-NAME (100%, $p = 0.4047$ due to high standard deviation). (B) Representative images of rat hippocampal cells treated as described in (A) and then labeled with β-III-tubulin antibody and DAPI and imaged at high magnification.

An isoform of NOS found in immune cells, iNOS, can produce large amounts of NO³⁹⁷. Since this signal could significantly mask nNOS activation, I verified that most NO production stimulated by glutamate was occurring in neurons, and not in nearby glial cells. I detected NO using DAF-FM DA, then fixed and labeled cells with an antibody against β-III tubulin to selectively stain neurons. Results indicated that most glutamate-stimulated NO production occurs in neurons (Figure 3.9, median 66%).

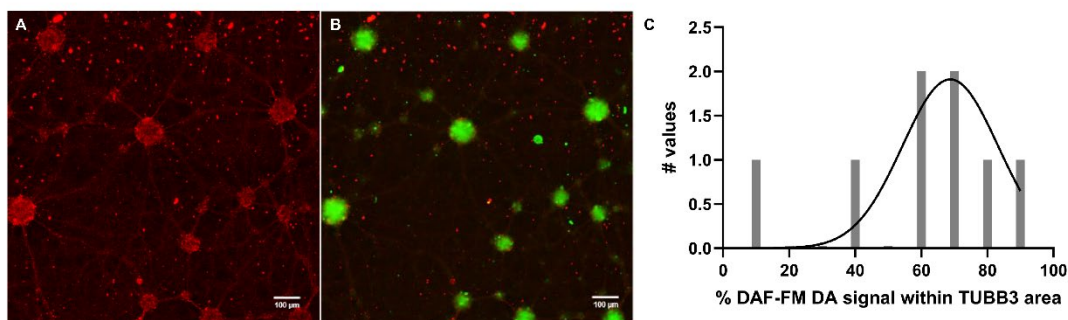


Figure 3.9 Nitric oxide production in neurons. Rat hippocampal neurons were incubated with DAF-FM DA (80 μ M) for 2 hours, then 100 μ M L-glutamic acid and 10 μ M D-serine, and finally labeled with β -III tubulin. Neurons were imaged at Cy5 and FITC ranges with an ImageXPress microscope using the 10x objective. (A) Neurons were labeled using β -III tubulin (TUBB3, red). (B) Merged signal from β -III tubulin (red) and NO (green) are shown. (C) A histogram of % DAF-FM DA signal found within neuronal (TUBB3) area. Median value 66% of NO was produced in neurons.

Finally, higher-magnification images were obtained (Figure 3.8B). The blue fluorescent 4',6-diamidino-2-phenylindole (DAPI) stain was added to mark nuclei. NO production was detected in numerous 3-10 μ m oval regions close to the cell body in many cells, and with diffuse cell-body staining in some cells. These observations are consistent with the description of nNOS subcellular distribution by Roth et al., who observed brain nNOS localized in some cases to mitochondrial membranes, or in a more diffuse cellular distribution⁴²⁹.

3.2.5 Cellular expression of nNOS was variable across cell culture

An antibody for nNOS (3G6B10) was used to measure cell-to-cell trends in expression of nNOS. I observed a 5-fold variation in nNOS expression across different cells (Figure 3.10). This suggests that some cells may be more vulnerable to any nNOS-mediated neurodegeneration.

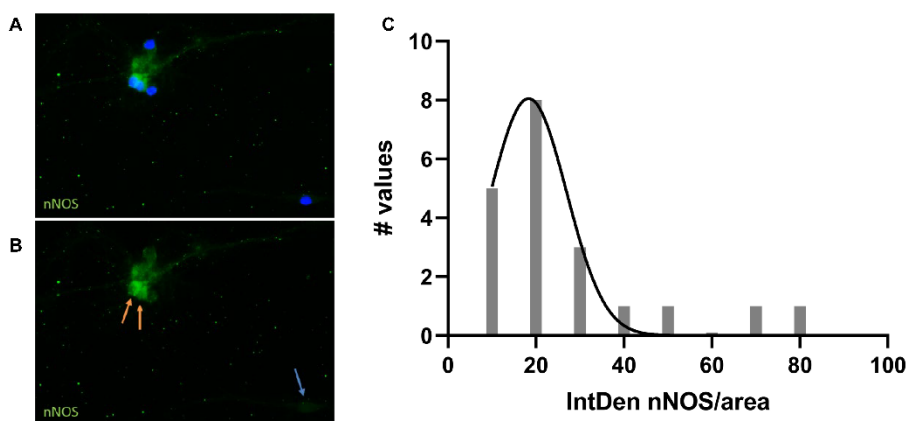


Figure 3.10 nNOS expression is varied throughout neuron culture. Images of neuronal cell culture labeled with anti-nNOS antibody (green) with DAPI (blue) (A) or without DAPI shown (B). Cells were imaged at 60x. Some cells exhibited high nNOS expression (orange arrows), while others had low expression levels (blue arrow). (C) A histogram was used to quantify expression levels of nNOS throughout the cell culture in terms of integrated fluorescent density of nNOS antibody divided by area. The minimum value was 8.75, the maximum was 79.8, and the median was 21.7. Data were collected from $n = 31$ regions of interest from a total of 9 images.

3.2.6 Inhibition of nNOS blocked A β O-induced tau phosphorylation at Thr205 and pSer396

Therefore, to determine whether nNOS activation was required to mediate A β O-induced tau phosphorylation, mature neurons were treated with vehicle or 500 nM A β O, with or without 100 μ M nNOS inhibitor (HD-3-86, 30 min pretreatment) and probed for A β O binding (NU4) and tau phosphorylation at Thr205. Although it did not alter A β O binding (Figure 3.11a, c, ns), nNOS inhibition significantly prevented downstream tau phosphorylation at Thr205 (Figure 3.11b, 108% reduction, $p < 0.0001$). In a separate experiment, in a separate neuron culture, nNOS inhibition also prevented tau phosphorylation at Ser396 (Figure 3.12, 97%, $p < 0.0001$). Based on these results, we conclude that nNOS is required for tau phosphorylation at both Thr205 and Ser396, two AD-relevant phosphorylation sites.

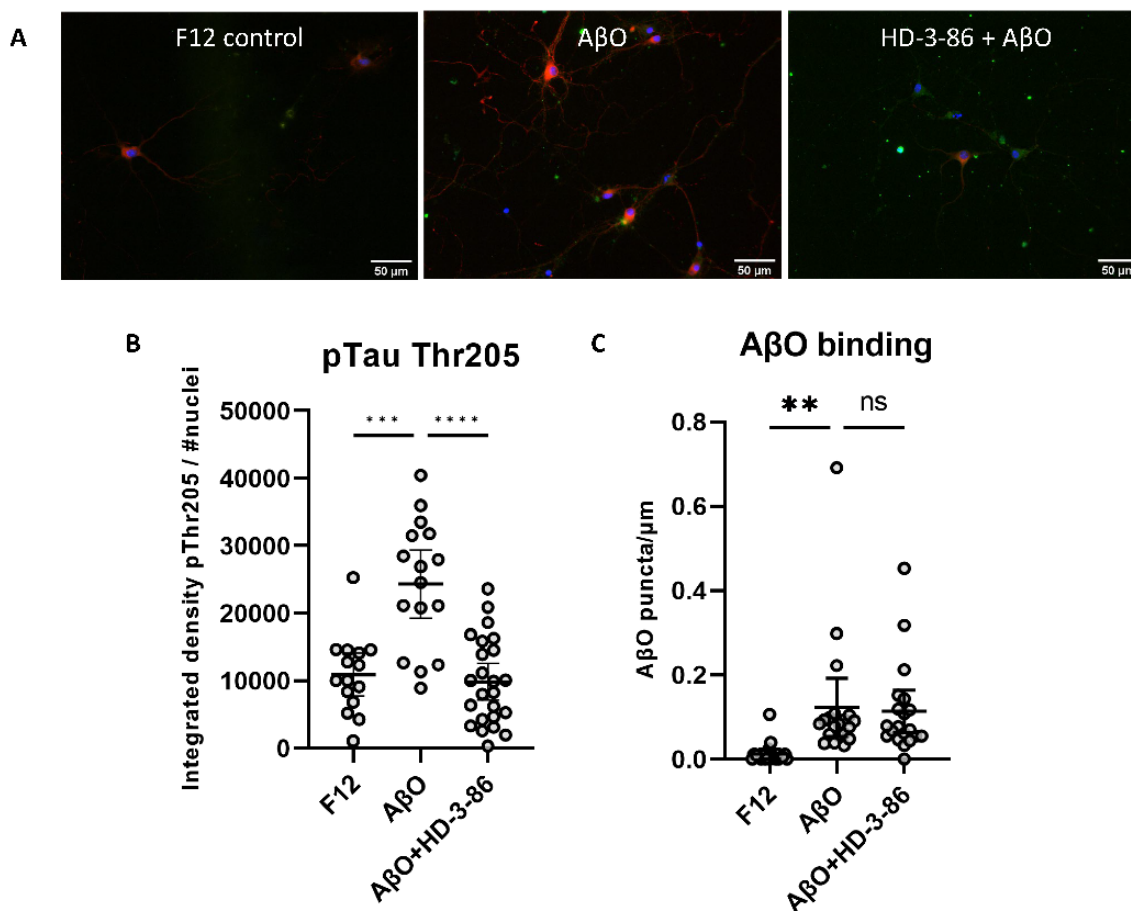


Figure 3.11 nNOS inhibition blocks pTau (Thr205). (A) Representative images of neurons were pre-treated with HD-3-86 (100 μ M), then treated with 500 nM A β O for 4 h. Cells were stained for A β O (NU4, green), tau phosphorylated at Thr205 (pThr205, red), and nuclei (DAPI, blue) and mounted on slides before imaging using a 20x objective. (B) Tau phosphorylation at Thr205 was quantified based on integrated fluorescent density of pThr205 antibody divided by number of nuclei per image (n=15-24 images per condition). Tau phosphorylation at Thr205 was significantly increased in the A β O condition (p = 0.0001) and significantly reduced in the A β O+HD-3-86 condition (108%, p<0.0001). (C) A β O puncta per micron along processes were quantified from n = 18-19 images per condition, collected using a 63x objective. The A β O condition demonstrated significantly more A β O puncta than F12 vehicle (p <0.0001), and A β O binding was not reduced in the A β O+HD-3-86 condition (ns).

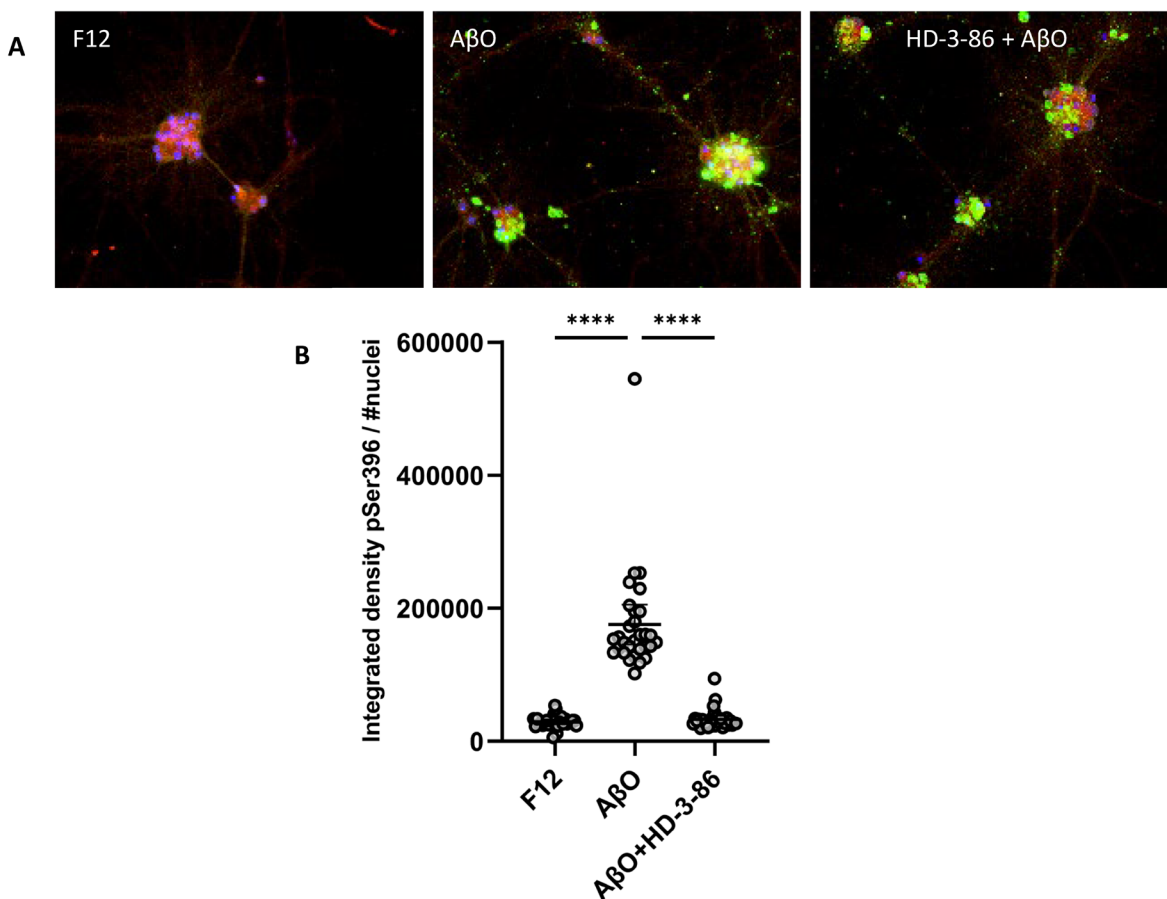


Figure 3.12 nNOS inhibition blocks pTau (Ser396). (A) Representative images of neurons were pre-treated with HD-3-86 (100 μ M) or vehicle, then treated with 500 nM A β O or vehicle for 6 h. Cells were stained for A β O (NU2, green), tau phosphorylated at Ser396 (pSer396, red), and nuclei (DAPI, blue) and mounted on slides before imaging with a 20x objective. (B) Integrated fluorescent density of pSer396 divided by number of nuclei were analyzed for 30 images in each condition. A β O-treated cells displayed significantly more pTau than F12 vehicle-treated cells ($p < 0.0001$). HD-3-86 pre-treated cells had significantly lower levels of pTau than A β O-treated cells (97%, $p < 0.0001$).

3.2.7 nNOS inhibition increases synaptic puncta from baseline

In AD, the degeneration of synaptic spines correlates closely with memory loss^{51,430-432}.

Therefore, to determine whether nNOS inhibition could alter the number of synaptic spines on neurons, phalloidin staining was used to label filamentous actin, which is highly enriched in synapses. Treatment with the nNOS inhibitor HD-3-86, even in the presence of crosslinked

A β O_s, induced an increase in synaptic spine density (Figure 3.13, intensity increased 1.5-fold, $p = 0.0499$). This supports the conclusion that nNOS inhibition could protect or even enhance synapses.

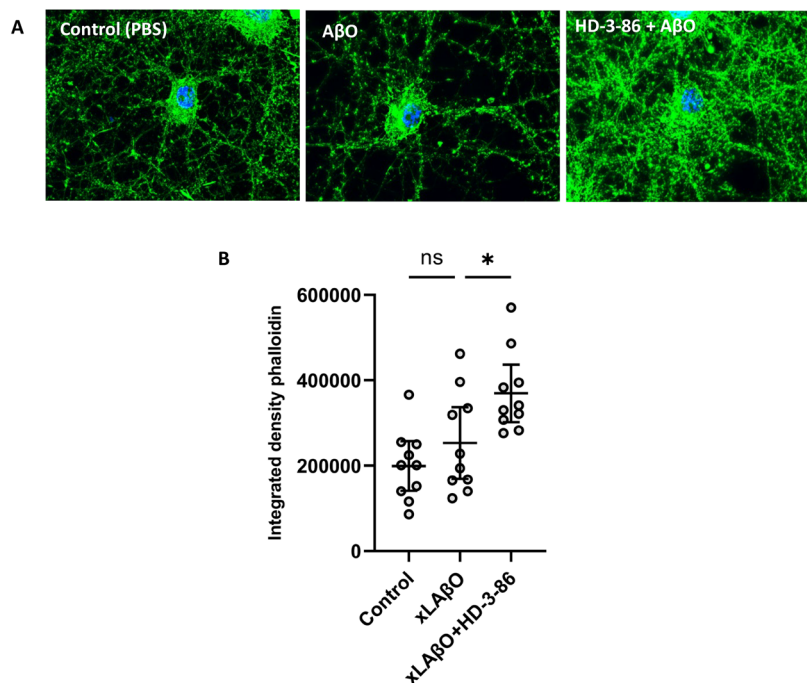


Figure 3.13 nNOS inhibition increased synaptic puncta. (A) Representative images of neurons pre-treated with HD-3-86 (100 μ M), then treated with 500 nM A β O for 1 h. Cells were stained for filamentous actin (phalloidin, green) and nuclei (DAPI, blue) and mounted on slides before imaging with a 63x objective. (A) Analysis of integrated fluorescent density of phalloidin was conducted using $n = 10$ images per condition. HD-3-86 pre-treated cells demonstrated an increase in integrated fluorescent density (1.5x, $p = 0.0499$).

3.2.8 nNOS inhibition reduces A β -derived A β O buildup

Given prior experiments (Chapter 2) showing that the small molecule NU-9 protected neurons from A β O buildup when A β monomer was applied, we also tested the effect of nNOS inhibition on A β O buildup along neurons using the same assay. In two separate experiments using different cell cultures, nNOS inhibition reduced A β O buildup (Figure 3.14, 54%, $p = 0.0057$). This

supports the conclusion that nNOS inhibition protects cells not only from A β O-induced tau phosphorylation, but also from upstream A β O buildup.

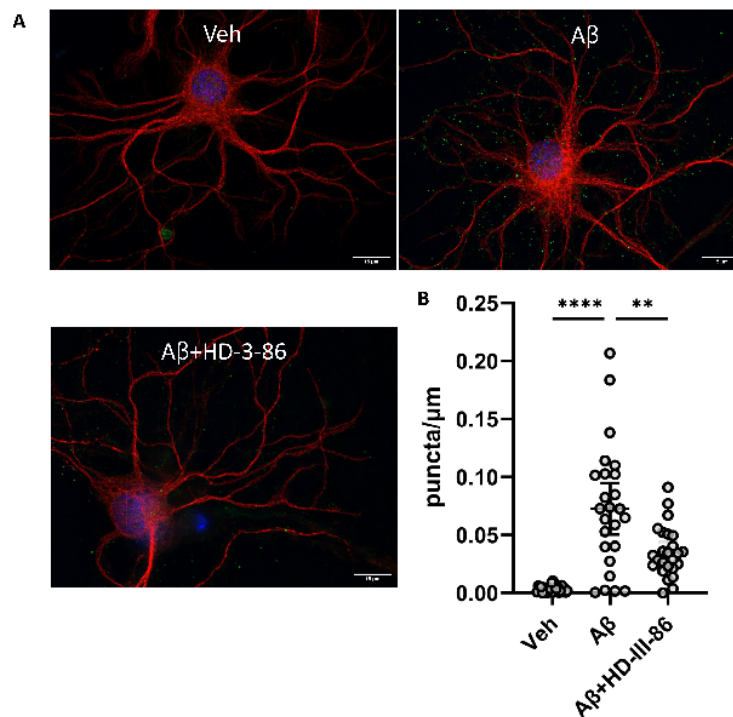


Figure 3.14 nNOS reduces A β -derived A β O buildup. (A) Representative images of cells pre-treated with HD-3-86 (100 μ M, 30 min), then A β monomer (500 nM, 30 min), labeled for dendrites (MAP2, red), A β O (NU2, green), and nuclei (DAPI, blue). (B) Analysis of A β O puncta per micron along dendrites were quantified in $n = 30$ images per condition. A β O buildup was observed in the A β monomer condition ($p < 0.0001$) and was significantly prevented by nNOS inhibition (54%, $p = 0.0057$). This same trend was observed in a replicate experiment in a separate cell culture.

3.3 Discussion

3.3.1 Summary of results

In this work, I first synthesized carbamate prodrugs for nNOS inhibitors in an attempt to improve permeability without compromising sensitive and selective inhibition. Unfortunately, we found that these modifications did not improve passive permeability, indicating an upper

limit for lipophilicity. However, an nNOS inhibitor analog synthesized by Dr. Ha Do demonstrated improved permeability. I therefore used that permeable analog to test the biological effects of nNOS inhibition in neuronal cells.

The results I obtained in this study suggest that NMDAR-stimulated NO production in neurons could be prevented by NOS inhibition and that the majority of NO production was localized to cell body-adjacent regions within neurons. Additionally, cellular expression of nNOS varies across hippocampal cell culture, and A β O-induced tau phosphorylation at pThr205 and pSer396 is dependent upon nNOS activity. Finally, nNOS inhibition increased the number of synaptic spines on neurons and suppressed A β -derived A β O buildup. Taken together, these results identify nNOS activity as a contributor to A β O buildup in neurons and A β O-induced tau phosphorylation, and support nNOS inhibition as a potential therapeutic strategy to protect against these pathologic hallmarks of AD.

3.3.2 Mechanisms of interest

The obtained results suggest several potential mechanisms for nNOS-dependent tau phosphorylation, synapse growth suppression, and A β oligomerization. In these mechanisms, significant evidence indicates the involvement of NO, but the role of nNOS has not previously been established. First, two major tau kinases are activated by nitric oxide: cyclin-dependent kinase 5 and glycogen synthase kinase-3 β . Once tau is phosphorylated, Fyn kinase likely contributes to enhancement of nNOS-dependent tau phosphorylation. In addition to phosphorylation, we hypothesize a potential role for nNOS in triggering tau acetylation by GAPDH nitrosylation. S-nitrosylation of Dexras1 could also be involved in propagating effects of nNOS activation, including tau phosphorylation. To suppress synapse growth, we hypothesize

that nNOS may be involved in suppressing mTOR activity downstream of the NMDAR. Finally, nNOS may contribute to A β oligomerization by triggering release of zinc, or by inhibition of the chaperone protein disulfide isomerase. These proposed mechanisms lay a foundation for potential future experiments to identify the role of downstream effectors in nNOS-dependent, AD-related processes.

3.3.3 nNOS-dependence of tau phosphorylation at Thr205 – a potential role for Cdk5

Our results demonstrate that A β O-induced tau phosphorylation at Thr205 is nNOS-dependent. We hypothesize that S-nitrosylation of cyclin-dependent kinase 5 (Cdk5), a tau kinase, is the mechanism by which nNOS mediates A β O-induced tau phosphorylation at Thr205 (Figure 3.15). The tau phosphorylation site at Thr205 comprises a major phosphorylation target of Cdk5. S-nitrosylation of Cdk5, which is elevated in AD²⁸⁷, enhances the activity of Cdk5. Qu et al. demonstrated that application of A β to neurons triggers S-nitrosylation of Cdk5, which could potentially be mediated by nNOS downstream of NMDA receptor activation, and which caused downstream synaptic spine loss²⁸⁷. Conversely, a mutation of Cdk5 that prevented nitrosylation, as well as a nitric oxide synthase inhibitor, resulted in protection against synaptic spine loss²⁸⁷. In AD, expression of the Cdk5 activator protein p25 is increased; p25 formation can be triggered when A β binding at synapses causes intracellular calpain activation^{433,434}. Town et al. also found that A β -induced Cdk5 overactivation can cause tau hyperphosphorylation, but this effect was attributed to calpain-mediated increases in p25^{287,433,435-438}. Given our results, nNOS-dependent S-nitrosylation of Cdk5 may be a major contributor to A β O-induced tau phosphorylation. Future studies to identify whether nNOS inhibition diminishes A β O-induced Cdk5 S-nitrosylation, and whether nNOS inhibitors are still able to prevent A β O-induced tau

phosphorylation at Thr205 in the presence of constitutively active Cdk5, could further support this possible explanation.

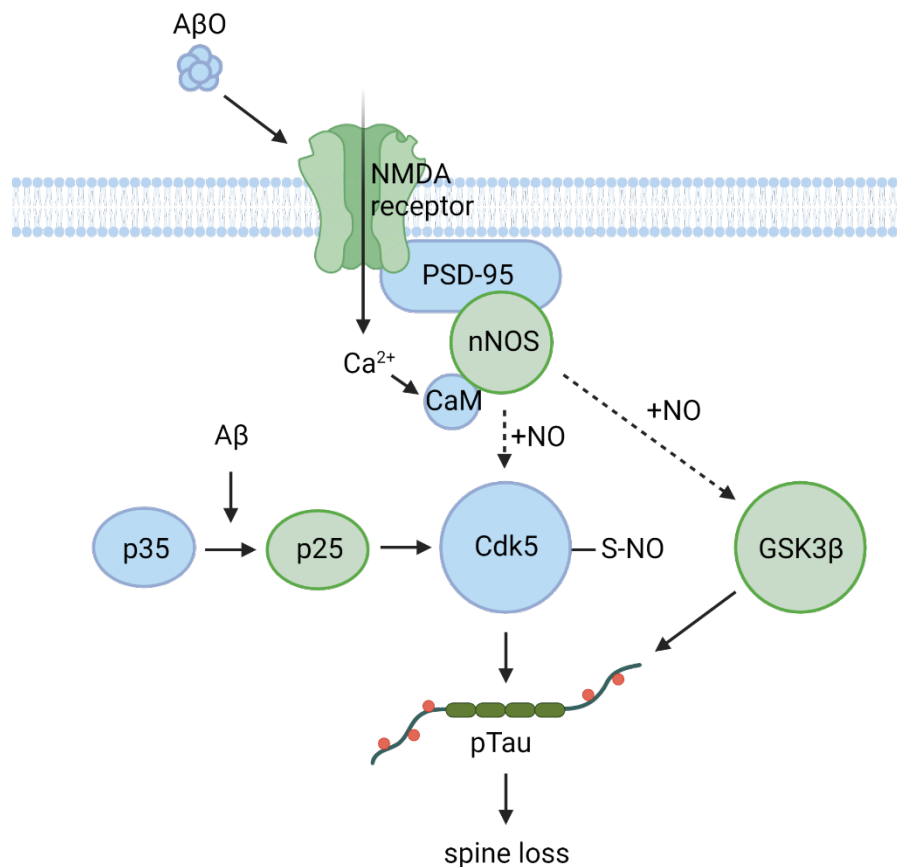


Figure 3.15: Activation of tau kinases. AβOs trigger N-methyl-D-aspartate (NMDA) receptor-mediated calcium influx, which enables calmodulin (CaM) binding to activate neuronal nitric oxide synthase (nNOS), which produces nitric oxide (NO). This could cause S-nitrosylation of cyclin-dependent kinase 5 (Cdk5), a tau kinase, activating it to enable increased production of phosphorylated tau (pTau) and synaptic spine loss. Aβ also causes increased formation of p25, which also activates Cdk5 from p35. NO production by nNOS could also activate glycogen synthase kinase-3β (GSK3β), another tau kinase. Dashed lines indicate hypothesized pathways. Created with BioRender.com.

3.3.4 nNOS-dependence of tau phosphorylation at Ser396 – a potential role for GSK-3β

Our experiments also show that AβO-induced tau phosphorylation at Ser396 is nNOS-dependent. This result implicates nNOS-dependent activation of a second tau kinase, glycogen

synthase kinase-3 β (GSK-3 β , Figure 3.15)^{285,439}. Ser396 is a major phosphorylation target of GSK-3 β . Zhang et al. determined that application of NO to neurons resulted in GSK-3 β -dependent tau phosphorylation at Ser396/404⁷⁴. Additionally, the distribution of active GSK-3 β in the AD brain matches patterns of tau phosphorylation⁴⁴⁰. Further, inhibition of GSK-3 β and knockdown of GSK-3 β expression both protected neurons against A β -induced tau phosphorylation^{441,442}. Future studies to determine whether nNOS inhibitors are still able to prevent A β O-induced tau phosphorylation at Ser396 in the presence of constitutively active GSK-3 β would establish whether nNOS-dependent tau phosphorylation at this site relies on activation of GSK-3 β .

3.3.5 Potential Fyn kinase contribution to nNOS signaling

As previously discussed, we observed that nNOS is necessary for A β O-induced tau phosphorylation at two key AD-relevant sites. Tau hyperphosphorylation causes tau to detach from microtubules and redistribute from the axon to the cell soma and dendrites^{443-445 375,376,446-449}. There, tau tethers Fyn to the PSD-95 scaffold protein, which facilitates phosphorylation of the NMDAR by Fyn, enhancing PSD-95/NMDAR stability (Figure 3.16). Ittner et al. found that Fyn was necessary for A β -induced neurotoxicity⁴⁴⁹⁻⁴⁵¹. Given that nNOS is physically and functionally linked to the NMDAR by PSD-95, this enhanced association likely contributes to the observed nNOS-dependent AD-relevant processes we observed. Future experiments to determine whether Fyn is necessary for tau phosphorylation at both Ser396 and Thr205, and whether nNOS inhibition prevents Fyn-mediated NMDAR phosphorylation would help to establish the interaction of Fyn with this newly established role for nNOS.

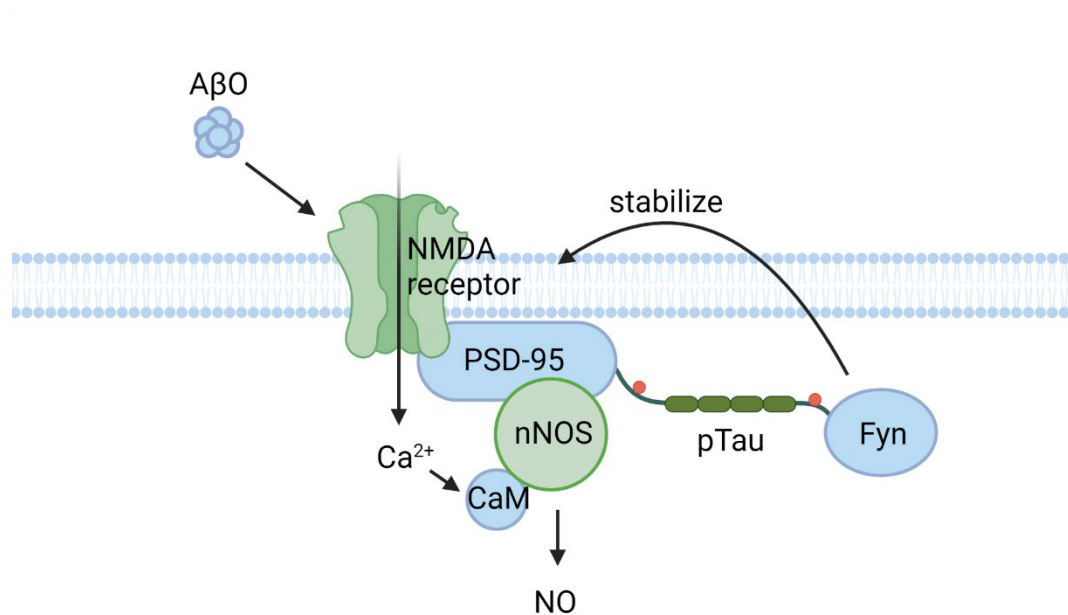


Figure 3.16 Potential Fyn contribution to nNOS signaling. Hyperphosphorylated tau (pTau) tethers the kinase fyn to the post-synaptic density 95 (PSD-95) scaffold protein, where it can phosphorylate the N-methyl-D-aspartate (NMDA) receptor to stabilize the interaction of the NMDAR and PSD-95. This may enhance activation of neuronal nitric oxide synthase (nNOS) by calmodulin (CaM) when NMDAR activation causes local calcium influx. Created with BioRender.com.

3.3.6 Potential role of nNOS in tau acetylation

Recently, in addition to phosphorylation, acetylation of tau has been identified as a post-translational modification which is elevated in AD brains⁴⁵². Acetylation impairs tau function and contributes to aggregation and toxicity mediated by tau⁴⁵³⁻⁴⁵⁷. Sen and coworkers showed that, in cortical neurons, Aβ stimulates nitrosylation of GAPDH, a modification which is also enhanced in the brains of AD patients⁴⁵⁸. Nitrosylated GAPDH activates the tau acetylase p300 and concurrently inhibits the tau deacetylase SIRT1; as a result, tau acetylation is enhanced via a nitrosylation-dependent pathway (Figure 3.17). Conversely, use of the GAPDH nitrosylation inhibitor omigapil prevented Aβ-induced tau acetylation and memory impairment in mice. These observations suggest that nNOS could also contribute to pathogenic tau acetylation. Future

experiments to determine the effect of nNOS inhibition on tau acetylation would help to establish whether nNOS is necessary for A β O-induced tau acetylation.

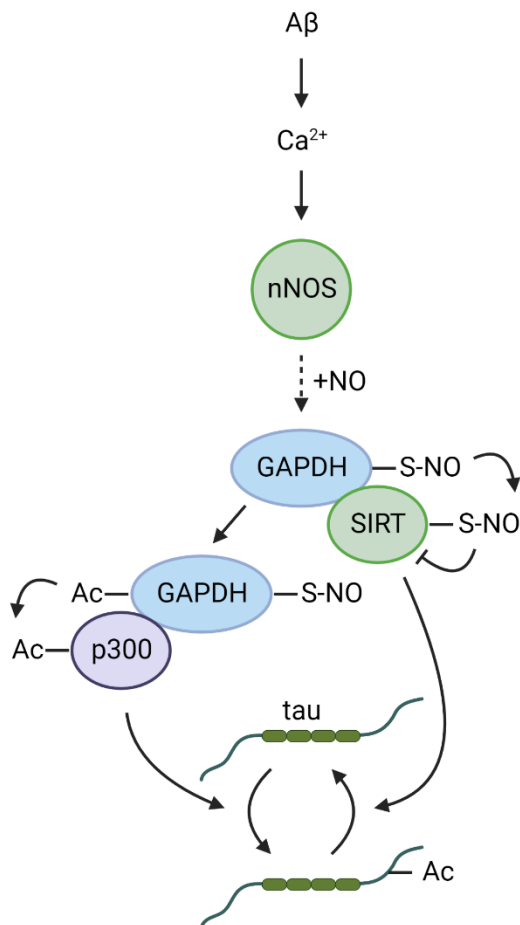


Figure 3.17 Tau acetylation. A β stimulates calcium influx into neurons, which activates neuronal nitric oxide synthase (nNOS) to produce nitric oxide (NO) which could nitrosylate glyceraldehyde-3-phosphate dehydrogenase (GAPDH). Nitrosylated GAPDH acetylates p300, enabling it to acetylate tau. By trans-nitrosylation, GAPDH also inhibits the tau deacetylase (sirtuin 1) SIRT1, reducing tau de-acetylation. Dashed lines indicate hypothesized pathways. Created with BioRender.com.

3.3.7 Dexas1 activation and tau nitration as potential effects of nNOS

Another adaptor protein, the C-terminal PDZ ligand of nitric oxide synthase (CAPON/NOS1AP) also acts as a scaffold to promote interaction of nNOS with additional

targets (Figure 3.18)⁴⁵⁹. Binding of nNOS to CAPON is triggered by NMDAR activation and has been shown to help potentiate NMDAR signaling⁴⁶⁰. CAPON expression is upregulated in CA1 pyramidal cells of the AD brain, and CAPON deficiency ameliorated AD-related phenotypes in an AD model mouse^{410,461}. One ligand coupled to nNOS by CAPON is Dexas1. Zhang et al. demonstrated that A β species enhance the nNOS-CAPON interaction, leading to nitrosylation of Dexas1⁴⁰⁹. Dexas1 S-nitrosylation triggers damage to mitochondria, causing A β -induced neurodegeneration in their model. Further, Hashimoto et al. reported that tau binds to CAPON, and that nNOS-CAPON interaction allows increased nitration of tau at Tyr29, promoting tau phosphorylation⁴¹⁰. Therefore, future experiments to establish whether Dexas1 nitrosylation and tau Tyr29 nitration are prevented by nNOS inhibition would further demonstrate whether these are features of nNOS-dependent neurodegeneration.

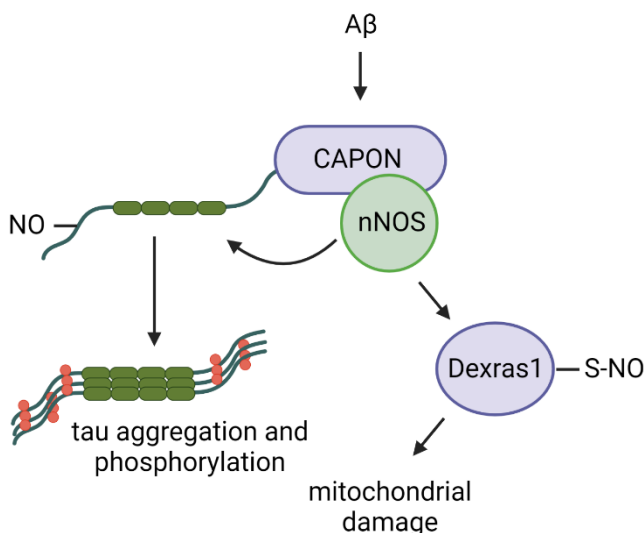


Figure 3.18 CAPON and Dexas1 activation. A β triggers increased interaction of the C-terminal PDZ ligand of nitric oxide synthase (CAPON) with neuronal nitric oxide synthase (nNOS). This interaction enables nitrosylation of Dexas1. S-nitrosylation enables Dexas1 to damage mitochondria. Tau also binds to CAPON, and nNOS-CAPON interaction allows increased nitration of tau at Tyr29, promoting tau aggregation. Created with BioRender.com.

3.3.8 nNOS increases the number of synapses

We also observed that nNOS inhibition stimulates an increase in synaptic spines. This result is not unexpected considering reports that inhibition of the NMDAR using memantine or ketamine also promotes spine formation⁴⁶²⁻⁴⁶⁴. Li et al. demonstrated that the mechanism for this synaptic spine formation involves activation of the mTOR pathway⁴⁶². However, adding complexity to this regulatory pathway, Ruddy et al. reported that, while acute NMDAR inhibition increases spine density, long-term administration at low levels reduces spine density⁴⁶⁵. This may explain the reduction in spine density that is observed in NMDAR knockout animals⁴⁶⁶. As such, future studies to determine the long-term effects of nNOS inhibition on spine density will be of interest. Additional studies to identify whether synaptic spine increases stimulated by nNOS inhibitors are mTOR activity-dependent will help to illuminate the details of this pathway.

3.3.9 nNOS inhibition can prevent A β O buildup from monomer

Our results demonstrating that nNOS inhibition can reduce dendritic A β O buildup from monomer in cell culture match observations by Deshpande et al. showing that synaptic formation of A β O is activity-dependent, and that targeting to synapses can be prevented by NMDAR inhibitors⁴⁶⁷. They implicated release of zinc as a potential mediator of this A β O formation, given that zinc can stabilize certain A β O species²⁸⁹. Bossy-Wetzel et al. showed that NO can stimulate release of free zinc to the cytoplasm²⁹⁰. Future experiments to determine whether nNOS inhibitors alter zinc release in neurons, and whether addition of excess zinc could prevent the protective effect of nNOS inhibition would establish whether nNOS acts by preventing zinc-dependent A β O formation. Alternatively, S-nitrosylation of protein disulfide isomerase (PDI), a

chaperone which prevents protein aggregation, has also been observed in AD²⁸⁸. Therefore, future studies to measure the effect of nNOS inhibition on PDI S-nitrosylation would help to establish whether this modification is also nNOS-dependent.

3.3.10 Potential therapeutic applications of nNOS inhibitors

In conclusion, this work establishes a role for the activation of nNOS in A β O-induced tau phosphorylation, A β O formation, and modulation of spine morphology. Although alterations of calcium homeostasis induced by A β O have previously been reported⁴⁶⁸, and nitrosylation and nitration are implicated in AD pathology^{285,287-290,409,410}, a direct role for nNOS in this mechanism has not been previously established. Our work suggests that nNOS inhibition could provide a strategy to block A β O-related neurodegeneration. Important considerations for therapeutic application of nNOS inhibitors will be the effect of long-term administration, and the identification of an appropriate therapeutic window in which normal function is preserved, but aberrant signaling is prevented. These results demonstrate that multiple forms of AD neurodegeneration are nNOS-dependent and can be disrupted by specific inhibition of nNOS.

3.4 Methods

3.4.1 Synthesis

Reactions were performed in oven-dried glassware using anhydrous solvents. Column chromatography was conducted using a CombiFlash instrument and Teledyne ISCO columns. Thin-layer chromatography (TLC) was used to monitor reactions using EMD Millipore silica gel 60 F254 coated plates (1057150001). NMR experiments were carried out on a Bruker Avance III 500 MHz spectrometer, using a DCH CryoProbe, and a SampleXpress autosampler. NMR values

are reported in ppm. Deuterated chloroform was used as the solvent with a standard chemical shift. Peaks are denoted as singlet (s), doublet (d), triplet (t), quartet (q), or multiplet (m).

Coupling constants are reported in Hz. Mass spectra were collected on an Agilent HPLC and Thermo Scientific MS instrument with a quadrupole detector and APCI ionization.

Compound **1** was prepared by reaction of HD-1-86 (0.12g, 0.40 mmol, 1 equiv) with methyl chloroformate (0.038g, 0.040 mmol, 1 equiv) in triethylamine (0.068 mL, 0.48 mmol), DCM (1.21 mL) and MeOH (0.13 mL) with stirring. The crude product was purified by flash chromatography using a gradient of 0-20% MeOH in DCM. A solid white powder was obtained after solvent evaporation (0.092 g, 64%). ^1H NMR (500 MHz, CDCl_3) δ 7.10 (s, 1H), 6.94 (m, 2H), 6.43 (s, 1H), 6.25 (s, 1H), 4.28 (s, 2H), 3.72 (s, 3H), 3.00 (s, 3H), 2.95 (s, 4H), 2.28 (s, 3H). **APCI-MS** (M^+) 356/357.

Compound **2** was prepared by reaction of HD-1-86 (0.05 g, 0.1 mmol, 1 equiv) with ethyl chloroformate (0.020 g, 0.18 mmol, 1.1 equiv) in triethylamine (0.028 mL, 0.20 mmol), DCM (0.50 mL), and MeOH (0.056 mL) with stirring. The crude product was purified by flash chromatography using a gradient of 0-20% MeOH in DCM. A beige solid was obtained by solvent evaporation (0.039 g, 65%). ^1H NMR (500 MHz, CDCl_3) δ 7.07 (m, 3H), 6.54 (s, 1H), 6.38 (s, 1H), 4.45 (s, 2H), 4.31 (q, $J = 21.1$ Hz, 2H) 3.14 (s, 3H), 3.06 (d, $J = 7.8$ Hz, 4H), 2.38 (s, 3H), 1.41 (t, 3H, (t, $J = 14.3$ Hz)). ^{13}C NMR (126 MHz, CDCl_3) δ 163.80, 163.52, 163.33, 161.37, 155.90, 154.68, 151.13, 142.72, 127.82, 124.45, 116.60, 116.42, 116.02, 115.85, 113.52, 109.39, 85.18, 82.63, 77.04, 61.79, 38.77, 35.69, 35.01, 21.66, 14.68.

Compound **3** was prepared by reaction of HD-1-86 (0.05 g, 0.17 mmol, 1 equiv) with benzyl chloroformate (0.032 g, 0.18 mmol, 1.1 equiv) in triethylamine (0.028 mL, 0.20 mmol, 1

equiv), DCM (0.5 mL), and methanol (0.11 mL) with stirring. The crude product was purified by flash chromatography using a gradient of 0-20% MeOH in DCM. A yellow oil was obtained by solvent evaporation (0.037 g, 62%). ^1H NMR (500 MHz, CDCl_3) δ 7.30 – 7.16 (m, 5H), 7.12 – 6.72 (m, 3H), 6.12 (d, J = 13.2 Hz, 2H), 5.03 (s, 2H), 4.18 (d, J = 28.7 Hz, 2H), 2.90 (s, 3H), 2.79 (s, 2H), 2.73 (s, 2H), 2.06 (s, 3H). ^{13}C NMR (126 MHz, CDCl_3) δ 207.04, 163.29, 161.34, 157.28, 155.65, 151.50, 143.82, 136.60, 128.51, 128.06, 126.98, 124.19, 124.17, 116.30, 116.11, 116.04, 115.87, 114.12, 107.76, 84.82, 82.94, 67.46, 65.24, 38.97, 37.77, 35.26, 34.22, 33.38, 30.94, 21.24.

Compound **4** was prepared by reaction of compound **1** (0.021 g, 0.058 mmol, 1 equiv) with methyl chloroformate (0.022 g, 0.23 mmol, 4 equiv) and sodium hydride (0.0028 g, 0.069 mmol) in 0.29 mL THF with stirring. The crude product, a brown solid, was purified by flash chromatography with a gradient of 0-80% ethyl acetate in hexanes. The pure product was obtained by solvent evaporation (0.010 g, 42%). ^1H NMR (500 MHz, CDCl_3) δ 7.64 (s, 1H), 7.03 (s, 1H), 6.92 (d, J = 8.9 Hz, 1H), 6.82 (d, J = 9.4 Hz, 1H), 6.60 (s, 1H), 4.31 (s, 2H), 3.77 (s, 3H), 3.72 (s, 3H), 2.99 (s, 3H), 2.93 (dd, J = 10.2, 6.7 Hz, 2H), 2.90 – 2.83 (m, 2H), 2.29 (s, 3H). ^{13}C NMR (126 MHz, CDCl_3) δ 163.29, 161.33, 153.55, 150.80, 127.71, 119.21, 116.27, 116.09, 115.94, 115.77, 110.46, 82.86, 82.84, 77.27, 77.02, 76.76, 60.40, 52.97, 52.51, 35.05, 33.33, 21.44, 14.20. **APCI-MS** (M^+) 452.

3.4.2 PAMPA-BBB assay

The parallel membrane permeability assay for blood-brain barrier penetration was used by Dr. Ha Do to measure passive permeability of each compound through brain lipids⁴²². Effective permeability values for each compound, presented in Table 3.1, were calculated based

on the transfer of compound from a donor to an acceptor well through a lipid-infused membrane using Equation 1⁴²³. In this formula, A corresponds to the cross-sectional area of the membrane, ε_a to the membrane porosity, V_A and V_D to the volumes of the donor and acceptor wells, t to the incubation time, τ_s to the time required to saturate the membrane, $C_A(t)$ to the concentration detected in the acceptor well after incubation, and $C_D(0)$ to the original concentration of compound added to the donor well. R represents the fraction of compound that is retained in the membrane and was calculated as shown in Equation 2 below.

Equation 1

$$P_e = -\frac{2.303}{A \cdot \varepsilon_a \cdot (t - \tau_s)} \cdot \frac{V_A \cdot V_D}{V_A + V_D} \cdot \log \left[1 - \left(\frac{V_A + V_D}{(1 - R)V_D} \cdot \frac{C_A(t)}{C_D(0)} \right) \right]$$

Equation 2

$$R = 1 - \frac{C_d V_d + C_a V_a}{C_d(0) V_d}$$

3.4.3 Neuron culture in phenol red-free media for NO assays

1 pair of combined E18 Sprague-Dawley rat hippocampus, cortex, and sub-ventricular zone tissue was obtained fresh from Transnetyx (SDEHCV) and cultured according to the manufacturer's protocol, based on the procedures from Brewer et al.^{360,361}. Cells were diluted to 0.2-0.4 million/mL and plated at 100 μ L/well directly onto sterile pre-coated 96-well plates (Fisher Scientific 07-000-190). This yielded a density of approximately 20,000-40,000 cells/well. Cells were fed every seven days by addition of 35-50 μ L phenol red-free NbActiv4 (Transnetyx NB4 and NB4PR500).

3.4.4 DAF-FM DA assay for NO production in neurons

Nitric oxide (NO) production in neurons was measured using the fluorescent dye diaminofluorescein-FM diacetate (DAF-FM DA, Thermo Fisher Scientific D23844) according to the previous protocols by Nott and Kolarow^{426,427}. DAF-FM DA was added to cells in transparent conditioned media (80 μ M, 37 °C, 2h, dark). Cells were subsequently washed twice with Hanks' Balanced Salt Solution. In some experiments, the general NOS inhibitor N^G-nitro-L-arginine methyl ester (L-NAME) or vehicle was applied (200 μ M, 30 min, 37 °C, dark). Then 100 μ M L-glutamate and 10 μ M D-serine were applied in transparent conditioned media (5 h, 37 °C)⁴²⁸. Live cells were imaged using the ImageXPress microscope in the Northwestern High-Throughput Analysis Laboratory at 10x objective. The total integrated fluorescence intensity for each well was quantified using ImageJ.

To co-stain for neurons, the cells were next fixed by addition of 3.7% formaldehyde 1:1, 10 min, and subsequent replacement of this mixture with 3.7% formaldehyde for 10 min. Cells were then blocked using 10% normal goat serum in PBS with 0.1% Triton X-100 for 30-45min,

RT. A primary mouse antibody against β -III tubulin (Promega G712A, 1:2000), which selectively stained neurons, was applied in blocking buffer at 4 °C overnight. After washing, this antibody was visualized using the Alexa 647 goat anti-mouse antibody (Invitrogen A11029, 1:2000, 3h, RT, dark). In some cases, blue fluorescent 4',6-diamidino-2-phenylindole (DAPI) stain was added as well to mark nuclei. These were imaged using the ImageXPress microscope in the Northwestern High-Throughput Analysis Laboratory at 10x and 40x objectives.

3.4.5 Neuron culture on coverslips for immunofluorescence of fixed cells

1 pair of combined E18 Sprague-Dawley rat hippocampus, cortex, and sub-ventricular zone tissue was obtained fresh from Transnetyx (SDEHCV) and cultured according to the manufacturer's protocol, based on the procedures from Brewer et al.^{360,361}. Cells were diluted to 0.11-0.22 million/mL and plated at 0.15 mL/coverslip directly onto sterile poly-D-lysine (Sigma-Aldrich P6407) coated 12 mm circular coverslips (Fisher Scientific 12-545-80P or 12-545-81P), which were prearranged 4/dish in 35 mm culture dishes (Fisher Scientific 08-772A). This yielded a density of approximately 15,000-30,000 cells/cm². Cells were fed 4 days after plating by half-media exchange with NbActiv1 (Transnetyx NB1) and subsequently every 2-3 days by half-media exchange with NbActiv1.

3.4.6 Cell treatment and immunofluorescent detection of pTau levels

Neurons were pretreated at 12-21 *div* with 100 μ M HD-3-86 or DMSO vehicle as control. A β Os, made according to the protocol of Lambert et al., or F12 media vehicle as control (Caisson Labs HFL05) were added to cells for 4-6 h, 37 °C³¹⁰. For immunofluorescence, cells were fixed by addition of an equal volume of 3.7% formaldehyde solution (Sigma-Aldrich F8775-500) for 10 min, followed by replacement with 3.7% formaldehyde for 10 min.

Coverslips were washed three times with PBS and blocked with 5% normal goat serum (Fisher Scientific ICN19135680), 0.1% Triton X-100 (Sigma-Aldrich T9284-500ML) in PBS for 1 h at RT. Primary antibodies NU4 (1:2000, Klein lab), anti-tau pThr205 (1:500, GeneTex GTX31124), anti-tau pSer396 (1:500, Thermo Fisher Scientific 710298), and/or anti-nNOS (1:500 based on Figure 3.19, Thermo Fisher Scientific 372800) were applied overnight in blocking buffer at 4 °C.

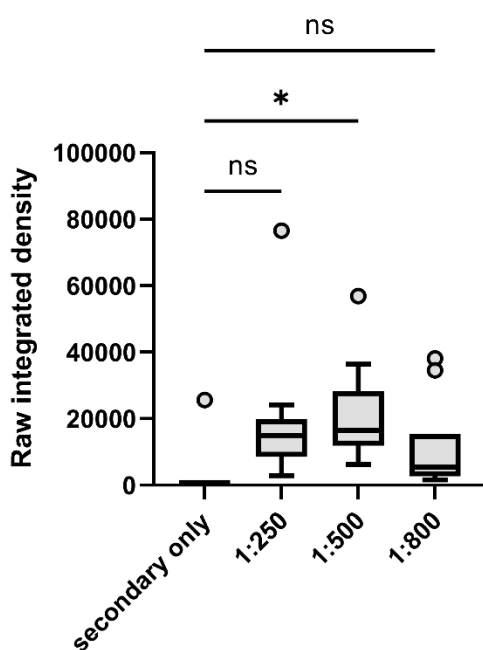


Figure 3.19 nNOS antibody titration. Quantification of raw integrated fluorescent density from three dilutions of nNOS antibody (1:250, 1:500, 1:800) that were compared to a secondary only staining condition. nNOS signal was significantly different from secondary only at 1:500 ($p = 0.0153$). Image analysis was conducted in ImageJ and data were analyzed using one-way ANOVA with post-hoc Dunnett's T3 multiple comparisons test.

Coverslips were then washed three times with PBS and secondary antibodies, goat anti-mouse Alexa Fluor 488 (1:2000, Fisher Scientific A11029) and goat anti-rabbit Alexa Fluor 568 (1:2000, Thermo Fisher Scientific A11036) were added in a solution of 10% blocking buffer in PBS, 3 h at RT in the dark. Coverslips were washed three times and mounted in Prolong Diamond Antifade mountant with DAPI (Thermo Fisher Scientific P36862).

3.4.7 A β O-induced pTau formation – method optimization/troubleshooting

Some inconsistencies with the tau phosphorylation assays were observed over time. The best results were often obtained using fresh antibody, and some batches of antibody failed to show A β O-induced tau phosphorylation. After initial freeze-thaw, the antibody against pSer396 (Thermo Fisher Scientific 710298) failed to show tau phosphorylation (data not shown), suggesting that aliquoting to avoid freeze-thaws is crucial for its use.

For this analysis, crosslinked A β O (xLA β O) were used due to their higher observed binding to cells. xLA β O were prepared according to the method of Cline et al., followed by 6 rounds of buffer exchange into PBS to remove excess reagents and to enrich A β O¹³⁸. The AT8 antibody (Thermo Fisher Scientific MN1020), which detects tau phosphorylation at Thr205, was initially found to detect small but significant increases in tau phosphorylation when 500 nM xLA β O was administered to mature cells at 21 *div* for 6 h (Figure 3.20a, $p = 0.0006$, 1.4x). Additional tests of different aliquots, which likely experienced different amounts of freeze/thawing, showed no A β O-induced tau phosphorylation for one aliquot (Figure 3.20b, $p = 0.82$), while a significant increase was observed for another aliquot (Figure 3.20c, $p = 0.0083$, 4.4x). This result supports the conclusion that different aliquots of the same antibody might label phosphorylated tau with different efficacy, likely due to a loss of efficacy after multiple freeze-

thaws. For this reason, antibodies were then routinely aliquoted to prevent high numbers of freeze-thaw cycles.

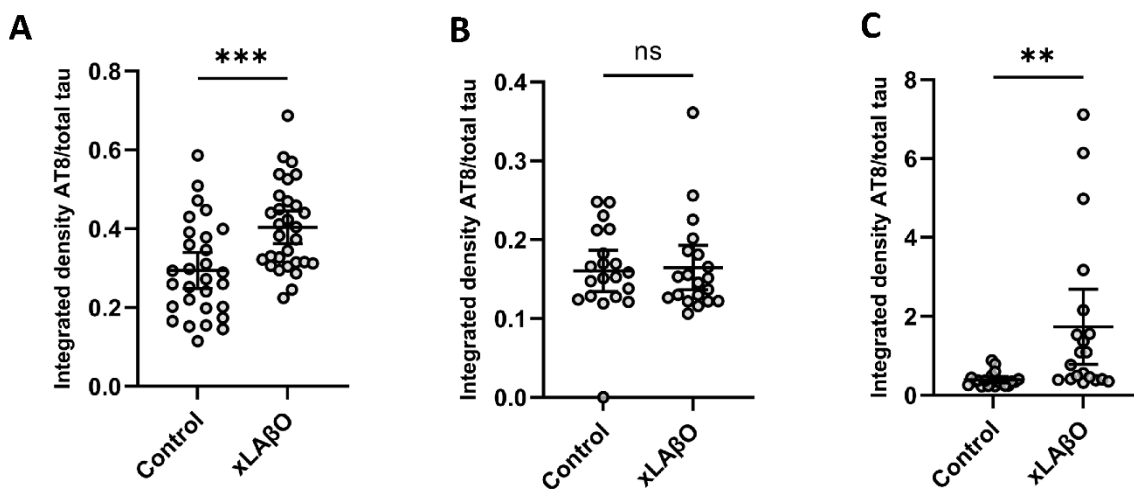


Figure 3.20 AT8 optimization. (A) Using AT8, cells were treated with 500 nM xLABO, 6h. Analysis of integrated fluorescent density of AT8 signal divided by integrated fluorescent density of total tau was used to calculate tau phosphorylation (n = 29-30 images/condition from 3 CS). A modest, but significant increase in tau phosphorylation was detected (1.4x, p = 0.0006) In a follow-up experiment, cells were treated with 500 nM xLABO, 6h, and tau phosphorylation was measured using different antibody aliquots in (B) and (C), resulting in different outcomes as measured by integrated fluorescent density of AT8 signal divided by integrated fluorescent density of total tau (n = 20 images/condition from 2 CS). No significant difference was observed in (B), but a significant increase upon treatment was observed using (C) (4.4x, p = 0.0083).

3.4.8 Synaptic spine measurement with phalloidin

Neurons at 21 *div* were pretreated with 100 μ M HD-3-86 or DMSO vehicle as control. A β O_s or F12 media (Caisson Labs HFL05) vehicle as control were added to cells for 30 min at 37 °C. Cells were washed with PBS, and were then fixed by addition of an equal volume of 3.7% formaldehyde solution (Sigma-Aldrich F8775-500) for 10 min, followed by replacement with 3.7% formaldehyde for 10 min. Cells were washed with PBS, and then permeabilized with 0.5% Triton X-100 (Sigma-Aldrich T9284-500ML) in PBS for 5 min at RT. Cells were washed again

with PBS, and then phalloidin reconstituted at 14 μ M in 100% methanol was applied to cells at 100 nM in PBS for 30 min at RT in the dark. Coverslips were washed three times with PBS and mounted in Prolong Diamond Antifade mountant with DAPI (Thermo Fisher Scientific P36862). Slides were stored protected from light at 4 °C for less than 2 weeks prior to imaging.

3.4.9 *A β O binding assay*

Mature hippocampal neurons at 21-22 *div* were pretreated first for 30 min with 100 μ M HD-3-86 or the corresponding DMSO vehicle in conditioned media. Then 500 nM A β or DMSO vehicle was applied for 30 min. To add A β , half of the media was removed from each dish, and a 2x solution of the next treatment was prepared in that conditioned media, which was then added back to the dish and mixed well. For immunofluorescence, cells were washed with sterile PBS prior and subsequently fixed by addition of an equal volume of 3.7% formaldehyde solution (Sigma-Aldrich F8775-500) for 10 min, followed by replacement with 3.7% formaldehyde for 10 min. Coverslips were washed three times with PBS and blocked with 5% normal goat serum (Fisher Scientific ICN19135680), 0.1% Triton X-100 (Sigma-Aldrich T9284-500ML) in PBS for 1 h at RT or 4 °C overnight. Primary antibodies NU2 (1:2000, Klein lab) and anti-MAP2 (1:10,000, EnCor Biotechnology CPCA-MAP2) were applied overnight in blocking buffer at 4 °C. Coverslips were then washed three times with PBS and secondary antibodies, goat anti-mouse Alexa Fluor 488 (1:2000, Fisher Scientific A11029) and goat anti-chicken Alexa Fluor 568 (1:2000, Thermo Fisher Scientific A11041) were added in a solution of 10% blocking buffer in PBS for 3 h at RT in the dark. Coverslips were washed three times and mounted in Prolong Diamond Antifade mountant with DAPI (Thermo Fisher Scientific P36862).

Quantification was conducted on immunofluorescent images in which a structural reference antibody, most commonly MAP2, but also including β -3 tubulin, was used as an indicator of neuronal processes. ImageJ was used for analysis, using macros included in the Appendix. Briefly, tiff images were assigned random numbers to avoid bias during analysis, and then cell bodies were manually traced and deleted for each image to eliminate signal from nonspecific antibody accumulation in the cell body. Then, the signal from different wavelengths was split. To calculate total dendrite length in each image, a Gaussian blur was applied to the MAP2 signal, and the signal above an equal threshold for each image was skeletonized, and the total length of the skeleton was measured. To calculate the total A β O puncta along processes, again a Gaussian blur was applied to the dendrite signal, and the signal above an equal threshold was selected. Then, the signal was dilated to encompass the area around the dendrites by 15 dilations. The area around the dendrites was used as a selection, and within the selection area, ImageJ particle analysis and summary were used to count the NU2 puncta above an equal threshold for each image. Thresholds were chosen based on one or two positive and negative control images. Total NU2 puncta were divided by the total dendrite length to calculate the A β O puncta/micron.

3.4.10 Microscopy

NO imaging was conducted using a Molecular Devices ImageXpress High Content Imaging Robotic Platform in the High-Throughput Analysis Laboratory at Northwestern University. Fixed fluorescent images were collected using a Leica DM6B Fluorescent Microscope in the Biological Imaging Facility at Northwestern University.

CHAPTER 4:
BLOCKAGE OF AMYLOID BETA OLIGOMER BINDING USING NUSC1
MEGAMOLECULES

CHAPTER 4: BLOCKAGE OF AMYLOID BETA OLIGOMER BINDING USING NUSC1 MEGAMOLECULES

4.1 Introduction:

4.1.1 Neutralization of A β O_s provides neuroprotection

In individuals with Alzheimer's disease (AD) small, soluble clusters of A β peptide called amyloid beta oligomers (A β O_s) accumulate in the brain over the course of disease^{296,297}. A β O_s instigate other features of AD pathology, including tau hyperphosphorylation, inflammation, synapse degeneration, and memory loss^{165-169,179,181-184}. Neutralization and removal of A β O_s by antibody treatment protects against memory loss in AD mouse models^{298,299}.

Several clinical trials have tested antibodies that bind and remove A β , measuring their effectiveness to treat AD dementia^{186,187}. However, most of these antibodies remove monomeric and fibrillar A β , rather than A β O_s. As such, therapeutic efficacy has been limited¹⁸⁸. Additionally, because A β serves a physiological function to maintain integrity of blood vessel walls, nonspecific removal of all A β species likely contributes to the adverse effects of brain edema and hemorrhage (ARIA)⁴⁶⁹⁻⁴⁷². However, two of the antibodies tested in clinical trials, aducanumab and lecanemab, bind to a subset of species that includes A β O_s somewhat more selectively¹⁸⁹⁻¹⁹². Accordingly, these species showed modest efficacy to protect memory. Highly selective A β O_s-specific antibodies are therefore predicted to provide a powerful protection of memory function against AD dementia.

4.1.2 Application of scFv technology to antibody therapy

However, the use of antibody therapies for neuroprotection suffers from several inherent challenges. Firstly, full-sized immunoglobulin G (IgG) antibodies have a high molecular weight, which may hamper their ability to penetrate the blood-brain barrier (BBB)⁴⁷³⁻⁴⁷⁵. Additionally, the crystallizable fragment (Fc) region of a full-length IgG antibody activates microglial inflammation and immune responses by the complement system, which would be harmful within the environment of the brain⁴⁷⁶⁻⁴⁷⁸. These features likely also contribute to adverse effects associated with the AD antibodies previously tested in clinical trials⁴⁶⁹⁻⁴⁷².

Single-chain variable fragment (scFv) antibodies, which consist of just the variable fragment, with one variable heavy and one variable light chain connected by a covalent linker, provide a solution to these problems⁴⁷⁹. ScFv antibodies are about five times smaller than full-sized IgG antibodies, retain specific binding ability, and demonstrate more rapid pharmacokinetics than full-sized antibodies, along with an absence of inflammation or immune response^{473,480}. An additional advantage of scFv antibodies is that, in contrast to full-sized IgG antibodies, their small size and lack of glycosylation means scFv antibodies can be produced at lower cost in microbial systems. As such, scFv antibodies could provide a valuable therapeutic tool to clear A β O from the AD brain.

4.1.3 Nusc1 is an A β O-specific scFv antibody fragment

Using biopanning to screen a human phage-display library, our colleagues Velasco and Sebollela et al. identified the A β O-binding scFv antibody Nusc1^{311,481}. Nusc1 binds specifically to A β O larger than 50 kDa, which comprise major neuron-binding proteoforms. Nusc1 detected A β O bound in a punctate pattern along hippocampal dendrites in neuronal culture. It also

differentiated tissue from APP/PS1 AD model mice compared to wild-type and distinguished human AD brain tissue from that of age-matched controls. Nusc1 protected hippocampal neurons in culture from A β O-induced tau phosphorylation and prevented the production of reactive oxygen species.

Our collaborators Selles et al. tested neuroprotection by Nusc1 in two AD mouse models: one where A β O_s were injected intracerebroventricularly and one in the APP^{swe}/PS1 Δ E9 genetic model⁴⁸². In both models, adeno-associated viral vector (AAV)-expression of Nusc1 protected memory function. Given its robust protection of cellular and memory function in AD models, Nusc1 presents a valuable potential therapeutic intervention against A β O-induced damage in AD.

4.1.4 Megamolecule technology for antibody fragments

Although scFv antibodies are typically taken up into the brain more rapidly and efficiently than full-sized IgG antibodies, a potential drawback for therapeutic use is that these small fragments are less thermodynamically stable and are cleared from circulation more rapidly^{473,474,480,483}. Potential solutions to this problem include AAV expression or combination of multiple scFvs⁴⁸⁴. The two most common strategies to combine scFvs are the use of tandem scFvs and diabodies⁴⁸⁴⁻⁴⁸⁷. However, development of tandem scFvs requires extensive structural optimization to ensure bioactivity, and synthesis of diabodies does not produce precisely defined populations. A third strategy, the use of megamolecules, can also be used to combine multiple scFvs, producing precisely defined, modular structures that are still up to 1.5x smaller than full-sized IgG antibodies and still absent the inflammatory and immune-reactive Fc region. The combination of multiple scFvs into megamolecules would enhance avidity⁴⁸⁸, optimize stability

by masking hydrophobic regions⁴⁸⁹, and have the potential to include central nervous system-targeting elements⁴⁹⁰.

To implement megamolecules, our collaborators Modica et al. developed a new platform for the precise preparation of modular megamolecules²⁹¹⁻²⁹³. The platform uses fusion proteins in which the protein of interest is fused with a particular enzyme, such as cutinase, and linked to other fusion proteins with synthetic linkers (Figure 4.1). The specific reactivity of the chosen

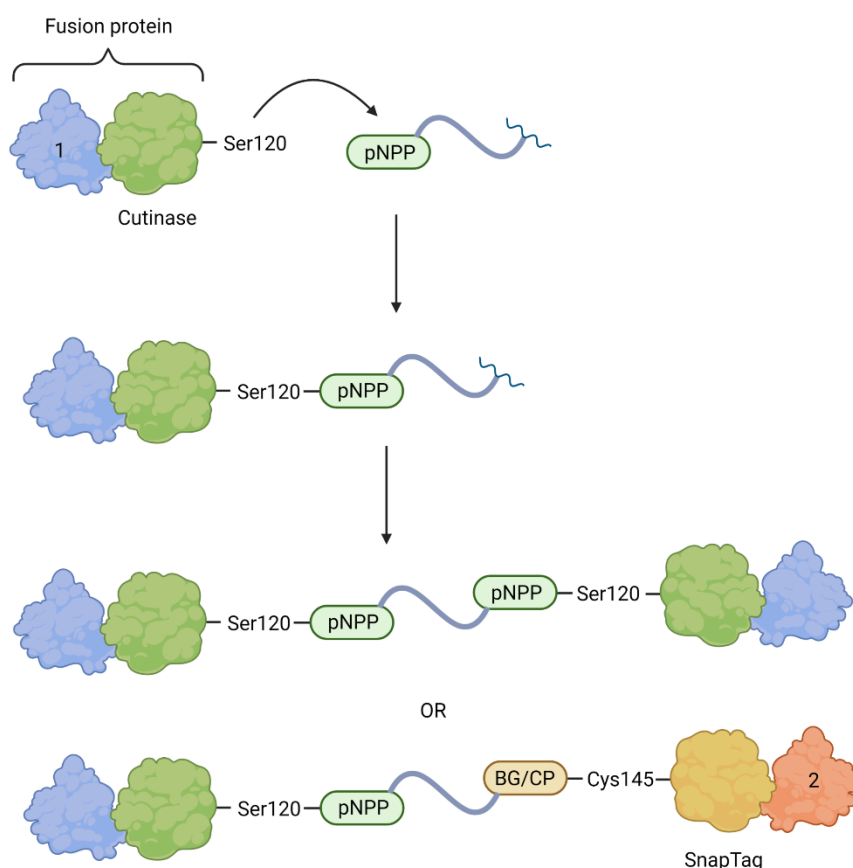


Figure 4.1 Megamolecule synthesis overview. A hypothetical fusion protein containing a protein of interest (1) linked to cutinase reacts with a p-nitrophenyl phosphonate (pNPP) group on the synthetic linker. This generates an ether connection to the linker. This can be used to create a symmetrical dimer, or to link another protein of interest (2) by reaction of SnapTag with benzylguanine (BG) or chloropyrimidine (CP) on the linker. Figure created with BioRender.com.

enzyme enables selective binding to each end of the linker. One end of the linker contains a p-nitrophenyl phosphonate (pNPP), which will specifically react with the cutinase Ser120, producing an ester which attaches the cutinase-based fusion protein to the linker and simultaneously inactivates the cutinase. At the other end, the linker may contain another phosphonate, to create a symmetrical megamolecule. Alternatively, it may contain a benzylguanine group, which enables attachment of a SnapTag-based fusion protein to the linker, with simultaneous inactivation of the SnapTag enzyme. For fragment antibodies, this megamolecule platform could be used to improve stability by masking hydrophobic regions, optimize avidity by increasing valency, attach central nervous system-targeting moieties, and precisely combine multiple fragment antibodies to enable multiple biological effects.

4.1.5 Application of megamolecules to Nusc1

Our collaborators in the Mrksich group, Justin Modica and Alexandra Barajas, generated three monospecific megamolecules of increasing valency using Nusc1-cutinase fusion proteins (Figure 4.2). First, they prepared a monomeric Nusc1-cutinase fusion protein. Then, they used symmetrical linkers with p-nitrophenyl phosphonate groups at each end to produce dimer and trimer species. These species were predicted to exhibit increasing avidity with increasing valency, which would translate to an enhanced ability to bind and neutralize disease relevant A β Os. Therefore, our objective in this work was to measure megamolecule binding to cell-bound A β Os and to characterize the differential ability of increasing n-mer megamolecules to neutralize A β Os. We found that megamolecules can bind to and clear cell-bound A β Os in neuron culture more effectively at higher valency. In particular, across the range of concentrations tested, the Nusc1 dimer demonstrated a robust ability to bind and neutralize A β Os specifically, even at 10-

fold lower concentration than monomer. This work provides a proof of concept for the use of Nusc1 in megamolecules to bind and neutralize A β O_s.

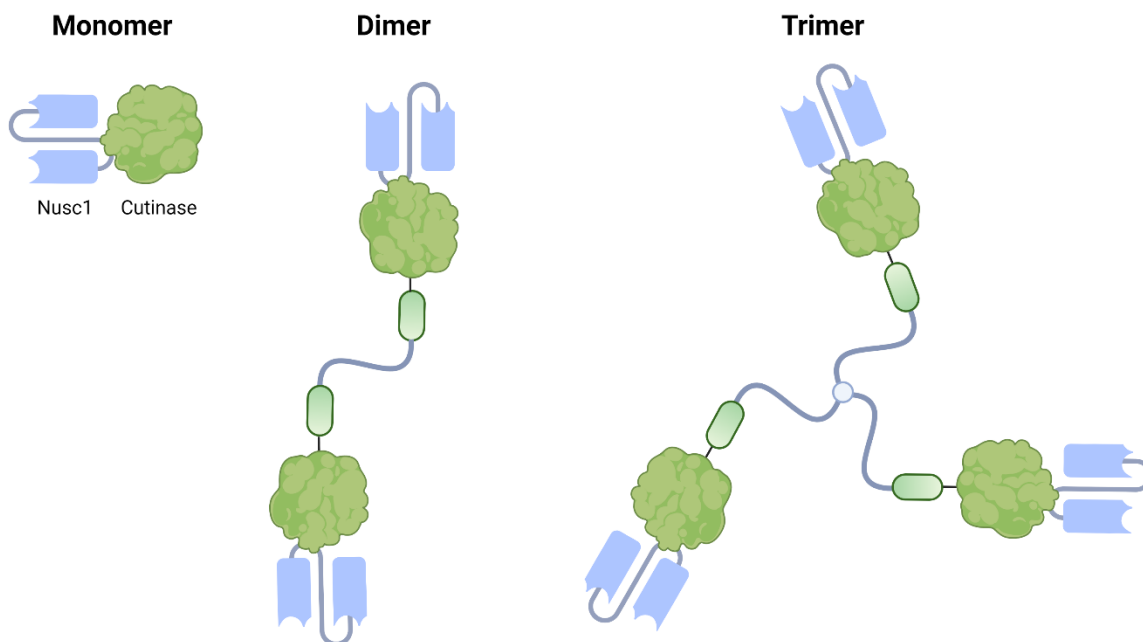


Figure 4.2 Monomer, dimer, and trimer megamolecules of Nusc1. Monomer is a fusion protein of Nusc1 with cutinase. Dimer has a divalent linker with pNPP groups at either end. Trimer has a trivalent linker with pNPP groups at all ends. Figure created with BioRender.com.

4.2 Results

4.2.1 Megamolecules bind to cell-bound A β O_s in neuron culture

Given that the original Nusc1 scFv detects the punctate binding of high molecular weight (>50 kDa) A β O_s along dendrites in neuronal culture, it was important to verify whether Nusc1 megamolecules were also capable of binding cell-bound, high molecular weight A β O_s. To test this, we applied crosslinked A β O_s (xLA β O_s), which are stabilized at >50 kDa⁴⁹¹, to mature hippocampal neurons (500 nM xLA β O, 1 h). Then the cells were fixed with formaldehyde, and

immunofluorescent labeling was conducted using Nusc1 megamolecules. For a full list of labeling conditions screened, see section 4.4.4. Megamolecules were diluted according to the number of Nusc1 units present on each. Monomer was used at 0.2 μM , dimer was diluted twofold to 0.1 μM , and trimer threefold to 0.07 μM . For secondary labeling, because Nusc1 contains a polyhistidine (His) tag, a green-fluorescent anti-His tag antibody was used to label megamolecules.

Under these conditions, all three megamolecules detected A β O bound to cells (Figure 4.3). Dimer and trimer identified a higher number of A β O puncta compared to vehicle than monomer (Figures 4.3 and 4.4, 2.0 ± 1.4 for monomer, 140 ± 58 for dimer, 92 ± 94 for trimer).

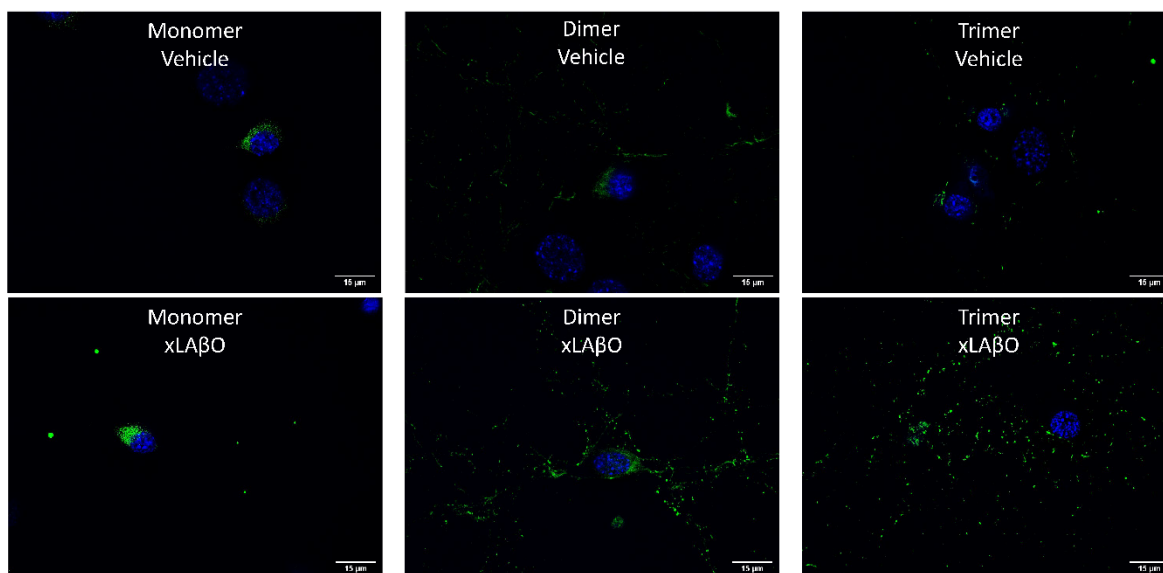


Figure 4.3 Nusc1 megamolecules detect cell-bound A β O (images). Representative images of mature, hippocampal neurons to which was applied 500 nM xLA β O or PBS vehicle and which were immunofluorescently labeled with Nusc1 monomer, dimer, or trimer (green) and DAPI (blue) are shown. Brightness and contrast are adjusted evenly for each set of two images labelled with the same megamolecule (Monomer 10-25, Dimer, 20-100, Trimer 100-255).

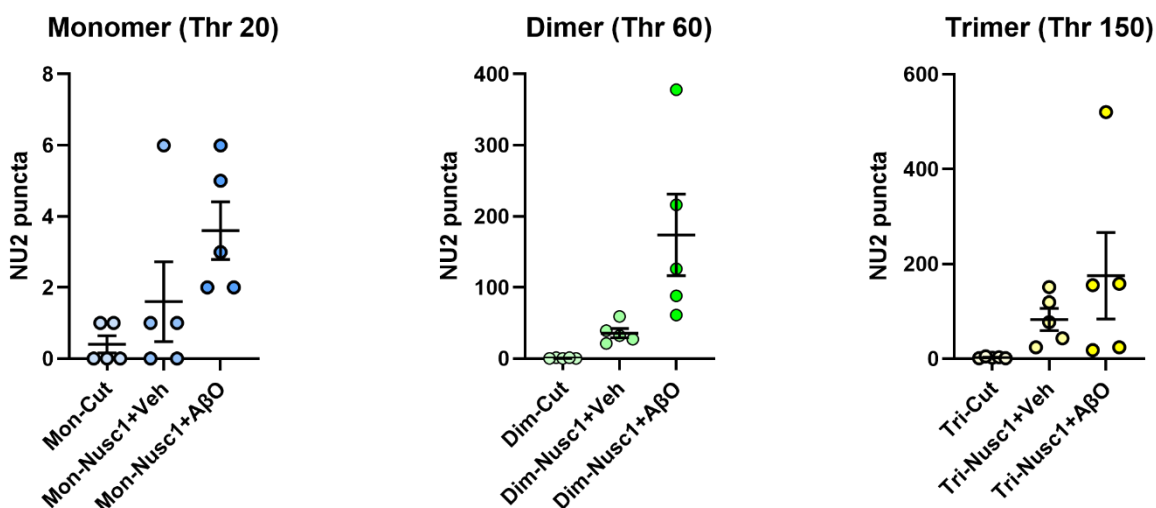


Figure 4.4 Nusc1 megamolecules detect cell-bound A β O (quantification). Analysis of megamolecule-detected puncta count in mature, hippocampal neurons to which was applied 500 nM xLA β O or PBS vehicle and which were immunofluorescently labeled with Nusc1 monomer, dimer, or trimer are shown. Cutinase-only scaffolds were also included as controls. Number of Nusc1-labeled puncta in each image were quantified in ImageJ at a threshold of 20, 60, or 150 for increasing sizes of megamolecules. N = 5 images per condition are plotted as individual data points. Mean and standard error are also plotted. NU2 puncta over vehicle were 2.0 ± 1.4 for monomer, 140 ± 58 for dimer, 92 ± 94 for trimer.

However, the use of Nusc1 megamolecules for immunofluorescent labeling was challenging overall because the lack of a constant region meant the absence of the typical signal amplification obtained from the binding of numerous secondary antibodies to each primary antibody. Across the megamolecules tested, increasing valency from monomer to dimer and trimer was predicted to enhance binding potency. It was observed that both specific and nonspecific detection of A β O by megamolecules increased with increasing n-mer size (Figures 4.5 and 4.6). At the concentrations tested, the best signal over background for A β O detection was obtained with dimer (Figure 4.4).

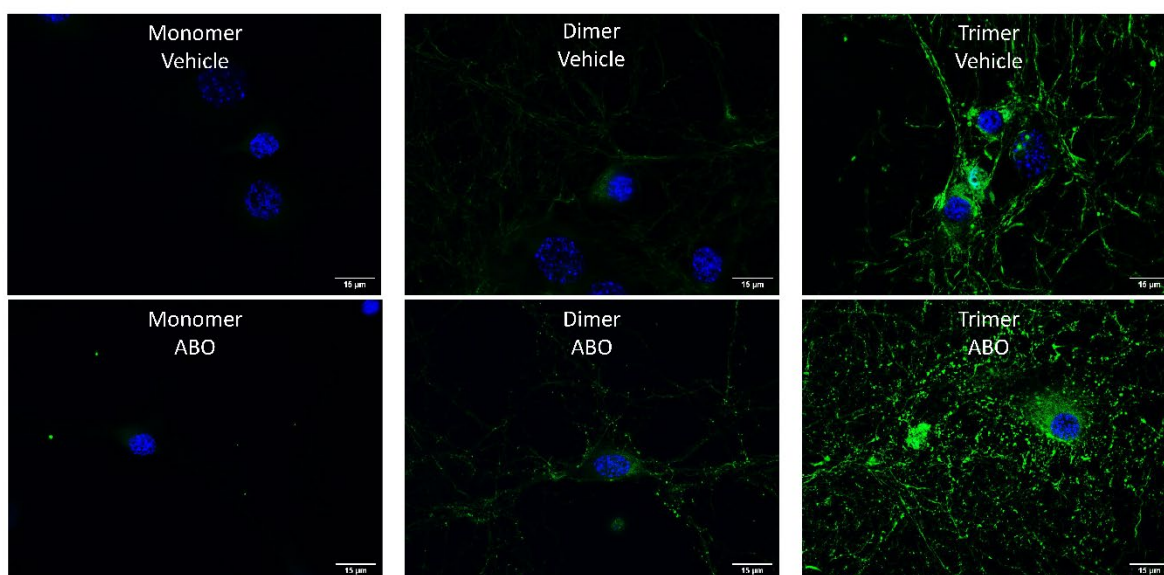


Figure 4.5 Both specific and nonspecific binding of Nusc1 megamolecules increase with n-mer size (images). Representative images of mature, hippocampal neurons to which was applied 500 nM xLA β O or PBS vehicle and which were immunofluorescently labeled with Nusc1 monomer, dimer, or trimer (green) and DAPI (blue) are shown. Brightness and contrast were unadjusted for all images, then brightness and contrast then were increased equally for all images in Powerpoint.

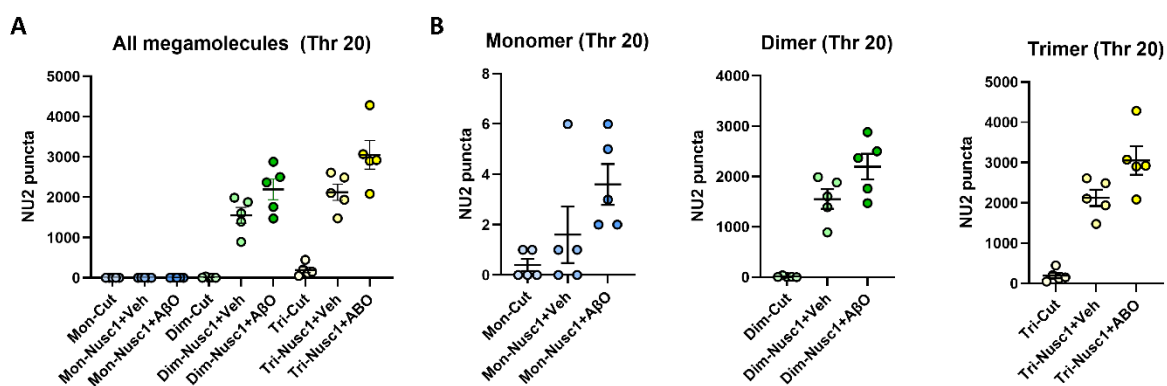


Figure 4.6 Both specific and nonspecific binding of Nusc1 megamolecules increases with n-mer size (quantification). Analysis of megamolecule-detected puncta count in mature, hippocampal neurons to which was applied 500 nM xLA β O or PBS vehicle and which were immunofluorescently labeled with Nusc1 monomer, dimer, or trimer are shown. Cutinase-only scaffolds were also included as controls. Number of Nusc1-labeled puncta in each image were quantified in ImageJ at a threshold of 20. N = 5 images per condition. In Panel (A), all datasets are included together along the same scale. Panel (B) shows individually-scaled images. When thresholds were identical, number of NU2 puncta was 1.6 for Mon-Nusc1+Veh, 3.6 for Mon-Nusc1+A β O, 440 for Dim-Nusc1+Veh, 570 for Dim-Nusc1+A β O, 2100 for Tri-Nusc1+Veh, and 3100 for Tri-Nusc1+A β O.

4.2.2 Neutralization with higher concentrations of megamolecules block A β O binding for monomer and dimer

Since all megamolecules can bind to cell-bound A β O, we next measured whether megamolecules were capable of neutralizing A β O to prevent them from binding to cells. To do this, we incubated megamolecules (0.4 μ M) with xLA β O (0.2 μ M) for 1 h prior to application onto cells. Then, we probed for neuron-bound A β O by immunofluorescence with antibodies against A β O (NU2) and neuronal dendrites (MAP2). At this concentration, both monomer and dimer megamolecules of Nusc1 blocked the binding of A β O to neurons (Figure 4.7). A scaffold containing just a dimer of cutinase had no effect on A β O binding, indicating that A β O neutralization by the Nusc1 dimer was specific. However, neutralization of A β O binding by the

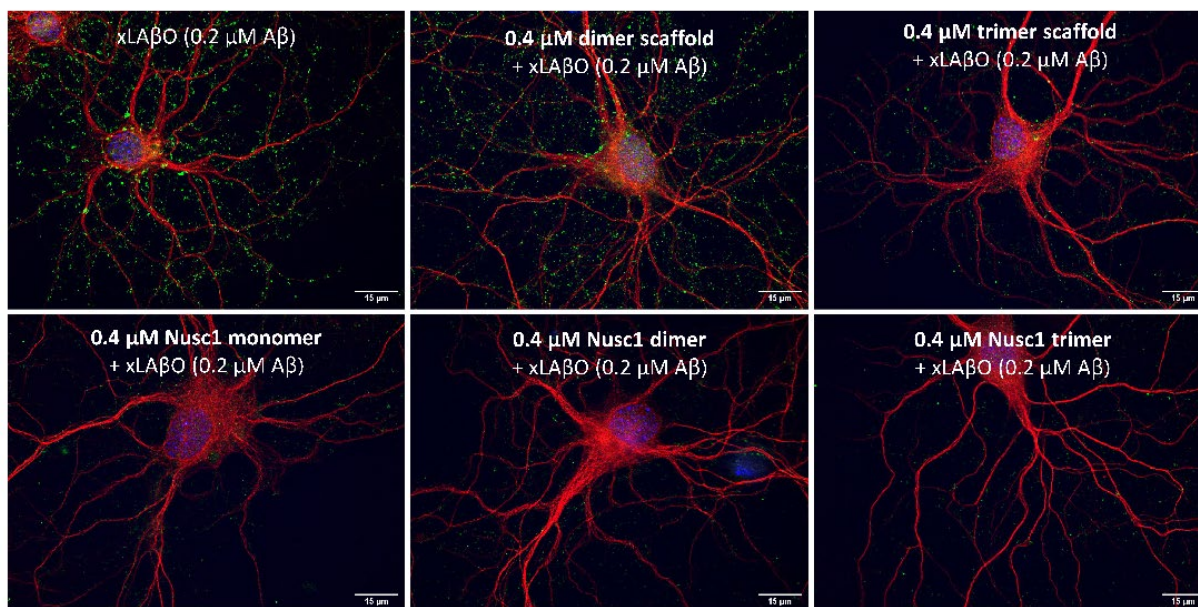


Figure 4.7 High concentration Nusc1 monomer and dimer prevent A β O binding; Nusc1 trimer prevents A β O binding but scaffold reduces binding as well. Representative images of mature hippocampal neurons to which were added 0.2 μ M xLA β O in the presence of 0.4 μ M Nusc1 megamolecules, megamolecule cutinase scaffolds, or PBS vehicle. Immunofluorescent labeling was used to label A β O (NU2, green), dendrites (MAP2, red), and nuclei (DAPI, blue). Brightness and contrast were adjusted evenly for all images.

Nusc1 trimer was not; the trimer cutinase scaffold also blocked A β O binding nonspecifically. This result matches the previously observed nonspecific binding of the Nusc1 trimer to cellular structures, and suggests a stickiness of the trimer cutinase structure, which may be susceptible to nonspecific interactions.

4.2.3 Differential neutralization by Nusc1 across concentrations

To determine a range of concentrations over which the dose-responses of A β O neutralization by Nusc1 megamolecules could be measured, A β O neutralization by the original scFv Nusc1 was first measured over a range of concentrations (0.05 μ M-1 μ M). The A β O concentration was maintained constant at 0.5 μ M. At 1 μ M, Nusc1 effectively neutralized A β O binding (Figure 4.8). At 0.17-0.5 μ M, Nusc1 visibly reduced A β O binding. At 0.05 μ M, Nusc1 had a low or minimal effect on A β O binding. Over this range of 0.05 to 1 μ M, Nusc1 neutralized A β O binding in a dose-dependent manner (Figure 4.9, $IC_{50} = 0.1 \mu$ M, $R^2 = 0.73$).

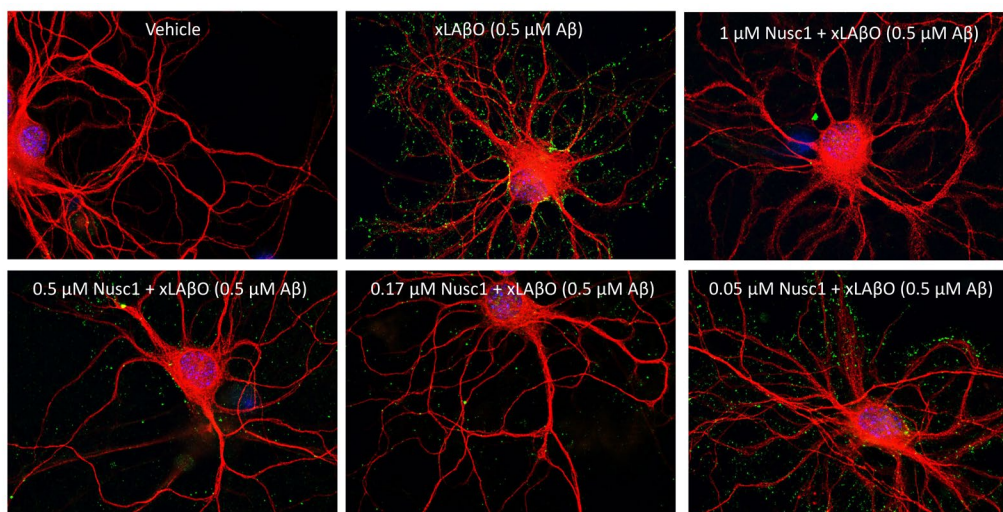


Figure 4.8 Neutralization by the original Nusc1 scFv was effective at the highest concentration, less effective with dilutions (images). Representative images of mature hippocampal neurons to which were added 0.5 μ M xLA β O in the presence of 0.05-1 μ M Nusc1 scFv or PBS vehicle. A β O (NU2, green), dendrites (MAP2, red), and nuclei (DAPI, blue) were labeled. Brightness and contrast were adjusted equally for all images.

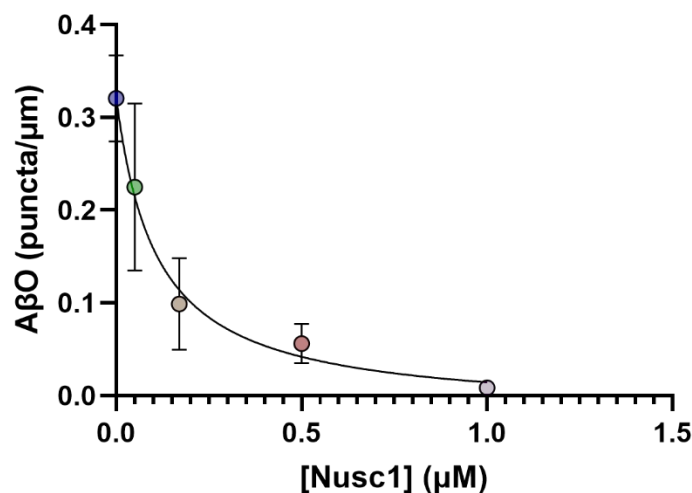


Figure 4.9 Neutralization by the original Nusc1 scFv was effective at the highest concentration, less effective with dilutions (quantification). AβO puncta per micron length along dendrites was quantified from n=10 images per condition in ImageJ. Dose-response was quantified using a 3-parameter nonlinear regression to a sigmoidal curve with a Hill slope in GraphPad Prism. IC₅₀ was calculated at 0.1 μM, R² = 0.73.

4.2.4 Differential neutralization by Nusc1 megamolecules across concentrations

Because Nusc1 exhibited a dose-dependent neutralization of AβO binding over 0.05-1 μM, the efficacy of Nusc1 megamolecules was tested over 0.05-0.5 μM. The AβO concentration was again maintained constant at 0.5 μM. The Nusc1 monomer yielded a clear dose-response over the measured range (Figure 4.10, IC₅₀ ~ 0.07 μM, R² = 0.70). At 0.05 μM, the Nusc1 monomer did not block AβO binding, and at 0.5 μM, the Nusc1 monomer almost completely neutralized AβOs. The Nusc1 dimer neutralized AβOs much more effectively, almost completely blocking AβO binding across the entire measured range, including at a 10x lower concentration than that required for neutralization by monomer (Figure 4.11).

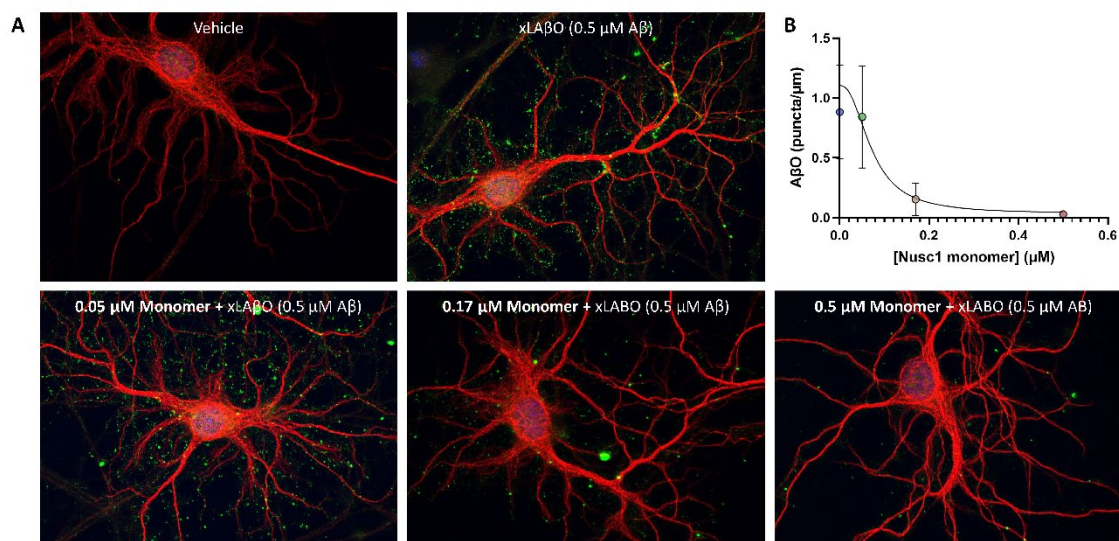


Figure 4.10 Nusc1 monomer reduced A β O binding in a dose-dependent manner. (A) Representative images of mature hippocampal neurons to which were added 0.5 μ M xLA β O which had been preincubated with 0.05-0.5 μ M Nusc1 monomer or an equal volume of PBS vehicle. Immunofluorescent labeling was used to label A β O (NU2, green), dendrites (MAP2, red), and nuclei (DAPI, blue). Brightness and contrast were adjusted evenly for all images. (B) Quantification of A β O puncta per μ m length of dendrites from $n = 5$ images in each condition. Dose-response was quantified using a 5-parameter asymmetric nonlinear regression to a sigmoidal curve in GraphPad Prism. IC₅₀ was approximately estimated at 0.07 μ M, $R^2 = 0.70$.

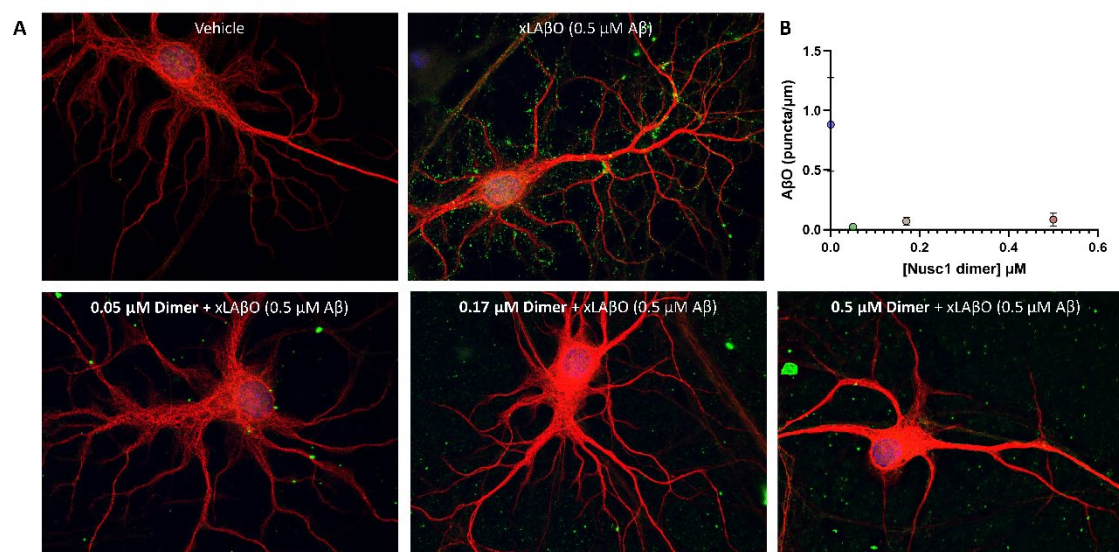


Figure 4.11 Nusc1 dimer reduced A β O binding across the measured range. (A) Representative images of mature hippocampal neurons to which were added 0.5 μ M xLA β O which had been preincubated with 0.05-0.5 μ M Nusc1 dimer or an equal volume of PBS vehicle. Immunofluorescent labeling was used to label A β O (NU2, green), dendrites (MAP2, red), and nuclei (DAPI, blue). Brightness and contrast were adjusted evenly for all images. (B) Quantification of A β O puncta per μ m length of dendrites from $n = 5$ images in each condition.

Additionally, to identify a range at which specific inhibition by the Nuscl trimer could be measured, we also tested nonspecific neutralization by the Nuscl trimer cutinase scaffold across the range of 0.05-0.17 μM . At these concentrations, nonspecific neutralization reduced dose-dependently, but was not eliminated (Figure 4.12). Interpolation of these data in GraphPad Prism using a four-parameter dose-response curve predicted that nonspecific neutralization would be minimal at a concentration of 0.003 μM , although this has not yet been tested experimentally.

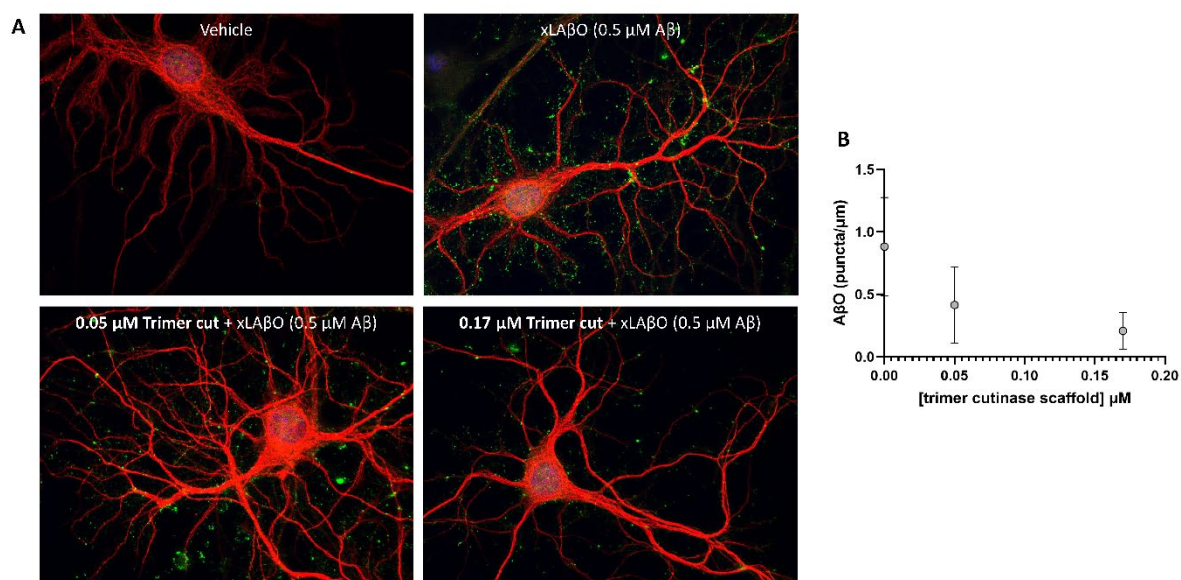


Figure 4.12 Trimer cutinase scaffold reduced A β O binding. (A) Representative images of mature hippocampal neurons to which were added 0.5 μM xLA β O which had been preincubated with 0.05-0.5 μM trimer cutinase scaffold or an equal volume of PBS vehicle. Immunofluorescent labeling was used to label A β O (NU2, green), dendrites (MAP2, red), and nuclei (DAPI, blue). Brightness and contrast were adjusted evenly for all images. (B) Quantification of A β O puncta per μm length of dendrites from $n = 5$ images in each condition.

4.3 Discussion

4.3.1 Summary of results

In this work, monospecific multivalent Nuscl megamolecules, including monomer, dimer, and trimer, were verified to bind to A β O_s in cell culture. Higher valency Nuscl megamolecules exhibited increases in both specific and nonspecific binding. At the concentrations tested, the Nuscl dimer detected A β O_s with the highest specificity. The differential ability of Nuscl megamolecules to neutralize A β O_s, thereby preventing A β O_s from binding to cultured neurons, was quantified. In this assay, the increasing valency increased neutralization but also nonspecific interaction. In both cases, at the concentrations tested, the Nuscl dimer demonstrated a robust ability to bind A β O_s sensitively with minimal nonspecific interactions.

4.3.2 Nuscl monomer effectively detects and neutralizes A β O_s

The Nuscl monomer comprised a fusion protein of Nuscl with cutinase. The monomer specifically detected cell-bound A β O_s, and dose-dependently neutralized A β O binding to neurons. However, the monomer exhibited the weakest detection and neutralization of the three megamolecules over 0.05-0.5 μ M monomer. Interestingly, although the Nuscl monomer was tested in a separate experiment, it appeared neutralize A β O binding more effectively than the original Nuscl scFv. The original scFv only partially neutralized A β O binding at 0.5 μ M, while the Nuscl monomer completely neutralized A β O binding at the same concentration. Accordingly, the estimated IC₅₀ of the Nuscl monomer was 0.07 μ M, while that of the scFv alone was 0.1 μ M. This finding suggests that fusion of a cutinase to Nuscl may provide thermodynamic stabilization that improves functional efficacy of the monomer. However, the

Nusc1 monomer contains an active cutinase due to the absence of an attached linker; as such, it is possible that the enzymatic activity of the cutinase could be responsible for the enhanced effect of the Nusc1 monomer. Regardless, these results support the conclusion that the Nusc1 monomer could be used to effectively neutralize neuron-binding A β O for therapeutic use and would be an effective building block for a multi-functional megamolecule.

4.3.3 Nusc1 dimer exhibits multi-fold enhancement of A β O neutralization

To form the Nusc1 dimer, two fusion proteins of Nusc1 with cutinase were linked with a symmetrical pNPP linker. The Nusc1 dimer detected cell-bound A β O with higher sensitivity than the Nusc1 monomer and also neutralized A β O binding more effectively. Previous literature by Alam et al. showed that trimerization of an anti-HER3 scFv using the Spycatcher platform resulted in a 12-fold enhancement of the dissociation constant⁴⁸⁸, and results obtained by Cuesta et al. showed that trimerization of anti-NIP scFv fused to collagen trimerization domains produced at least a 100-fold increase in functional affinity compared to the monovalent species⁴⁸⁷. Our results also support the conclusion that multimerization results in multiple-fold increases in binding, as the Nusc1 dimer maintained full neutralization of A β O binding at 10-fold lower concentration than monomer. These results support the conclusion that the Nusc1 dimer could be used therapeutically to block A β O binding more completely than monomer. Additionally, the minimal nonspecific binding of the dimer-cutinase scaffold supports the potential future use of a dimer scaffold to combine the Nusc1 monomer with other scFvs for additional tau clearance or CNS-targeting. Overall, the Nusc1 dimer was shown to provide more sensitive detection and neutralization of A β O than monomer, with minimal nonspecific interaction.

4.3.4 *Nusc1 trimer scaffold interacts non-specifically with substrates*

The Nusc1 trimer included three fusion proteins of Nusc1 with cutinase, combined with a trifold pNPP linker. The Nusc1 trimer non-specifically stuck to cells in immunofluorescence experiments. Given that a non-specific interaction of the trimer-cutinase scaffold with A β O_s was also observed in neutralization experiments, non-specific binding of the Nusc1 trimer can likely be attributed to the structure of the trimer-cutinase scaffold. However, the specific threshold for neutralization of A β O binding by the Nusc1 trimer has not yet been quantified, although it is predicted to be higher than that of the Nusc1 dimer given the increased valency. As such, the exact specificity of the Nusc1 trimer for A β O_s relative to other Nusc1 megamolecules cannot be concluded from these experiments.

4.3.5 *Future work*

In the future, additional experiments will help to identify precise parameters for use of Nusc1 megamolecules. Lower concentrations of Nusc1 megamolecules could be tested to establish dose-response ranges for A β O neutralization by Nusc1 dimer and trimer. A concentration of 0.003 μ M would be a useful starting point to characterize specificity of the trimer in comparison to monomer and dimer. Given that target engagement and neutralization of A β O_s by Nusc1 megamolecules have been demonstrated in cell cultures, effectiveness of these molecules to neutralize A β O_s could also be tested *in vivo*. These tests could also be used to probe whether increased size of megamolecules results in reduced brain penetration, which could be counteracted by installation of brain-targeting moieties, or reduced clearance, which would be therapeutically beneficial.

4.3.6 Significance

One key benefit of the megamolecule platform is the ability for precise, modular assembly of molecules with different functionality²⁹¹⁻²⁹³. Currently, one bispecific tandem scFv, blinatumomab, is FDA-approved for cancer immunotherapy⁴⁹². However, the design of such bispecific tandem scFvs requires extensive structural optimization, impeding high-throughput screening of multiple modalities. Megamolecules containing Nuscl-cutinase could be linked to other building blocks by a heterobifunctional linker to a SnapTag fusion protein or a heterotrifunctional linker to SnapTag and HaloTag. In this way, the megamolecule platform could easily be used to screen modular combinations of Nuscl with other antibody fragments for multi-modal activity. For example, antibody fragments against brain-uptake receptors such as insulin-like growth factor 1 receptor, transferrin receptor, or vascular cell adhesion molecule 1 could be added to Nuscl containing megamolecules to enhance brain uptake^{490,493}. Targeting to a specific brain region of interest, such as hippocampus, might also be achieved by introduction of an antibody fragment against a receptor enriched in hippocampus, such as the Kv4.2 channel⁴⁹⁴. Further, incorporation of anti-A β O fragments with different structural specificities, including camelid nanobodies or other scFvs⁴⁹⁵, could be used to tune megamolecule activity to target varying ranges of A β O species, and installation of an anti-phosphorylated tau fragment antibody, anti-inflammatory agent, antioxidant, insulin, or other potential AD therapeutic agent, could also be used for a multi-modal therapeutic approach²⁷¹. As such, this work provides a foundation to establish feasibility of using megamolecules containing Nuscl, which could provide a powerful tool to prevent A β O-triggered neurodegeneration in AD.

4.4 Methods

4.4.1 Megamolecule synthesis

Nusc1 megamolecules were synthesized by our collaborators in the Mrksich lab, Dr. Justin Modica and Alexandra Barajas, building on previously published methods^{291,292,496}. Briefly, Nusc1-cutinase fusion proteins were expressed in TOP10 *E. coli* cells and purified by immobilized metal affinity chromatography to isolate the His-tagged material, followed by fast protein liquid chromatography to isolate the light chain, and finally size-exclusion chromatography. Purified fusion proteins were then combined with the appropriate homo-bifunctional or homo-trifunctional poly-ethylene glycol linkers with pNPP groups at each end overnight at RT. The final megamolecules were purified by size-exclusion chromatography.

4.4.2 Hippocampal neuronal cell culture

One pair of combined E18 Sprague-Dawley rat hippocampus, cortex, and sub-ventricular zone tissue was obtained fresh from Transnetyx (SDEHCV) and cultured according to the manufacturer's protocol, based on the procedures from Brewer et al.^{360,361}. Cells were diluted to 0.11 million/mL and plated at 0.15 mL/coverlip directly onto sterile poly-D-lysine coated 12 mm circular coverslips (Fisher Scientific 07-000-190), which were prearranged 4/dish in 35 mm culture dishes. This yielded a density of approximately 15,000 cells/cm². Cells were fed 4 days after plating by half-media exchange with NbActiv1 (Transnetyx NB1-500), and subsequently every 2-3 days by half-media exchange with NbActiv1.

4.4.3 Synthesis of crosslinked A β O_s (xLA β O_s)

xLA β O_s were prepared according to the method of Cline et al. using A β (Peptides International PAM-4349), 1,5-difluoro-2,4-dinitrobenzene (Thermo Scientific 21525), and dithiothreitol (Sigma-Aldrich D-0632). xLA β O_s were buffer-exchanged six times into PBS to remove excess reagents and enrich A β O_s¹³⁸.

4.4.4 Megamolecule immunofluorescence

Nusc1 megamolecule immunofluorescence labeling was optimized using Nusc1 dimer by testing the conditions outlined in Figure 4.13. In all cases, A β O_s were applied to mature hippocampal cells for 1 h, then the cells were washed with sterile PBS. Most cells were fixed with formaldehyde, which was subsequently removed by three washes with PBS. Then the coverslips were blocked and labeled with megamolecules as a primary antibody and a variety of secondary antibodies. Finally, the coverslips were mounted on glass slides and imaged. Overall signal amplification was limited by the use of a fluorophore conjugated anti-His tag. Future optimization might benefit from labeling first with a mouse anti-His tag and subsequently with an anti-mouse secondary to enhance signal. Nonetheless, a clear signal over background for A β O detection of megamolecules was obtained using the following optimized immunofluorescence conditions.

Optimized immunofluorescence conditions, used in Figures 4.3-4.6, were as follows. 500 nM xLA β O_s or PBS vehicle was applied to mature hippocampal neurons (20-25 *div*) for 1 h, then the cells were washed with sterile PBS. The cells were subsequently fixed with formaldehyde, first by 1:1 addition of 3.7% formaldehyde (Sigma-Aldrich F8775-500) for 10 min, and then by replacement with 3.7% formaldehyde for 10 min. Formaldehyde was removed

by three washes with PBS. The coverslips were then blocked for two intervals of 10 min and one interval of 40 min, RT. The blocking buffer contained 3% bovine serum albumin (Sigma-Aldrich A7906-500G) in PBS. Megamolecules were applied overnight at concentrations of 0.2 μM monomer, 0.1 μM dimer, or 0.07 μM trimer in blocking buffer at 4 $^{\circ}\text{C}$, with orbital shaking. The coverslips were washed twice with PBS for 5-10 min each.

Primary	Secondary	Fixation?	Block	Result	
0.66 μM dimer	1:1000 aHis488	Fixed	5% FBS, 1h	Nonspecific labeling for vehicle and ABO, but not for scaffold or secondary only	
0.66 μM dimer	1:1000 aHis488	Live	5% FBS, 1h	Nonspecific (internalization or clumping) for vehicle and ABO, but not for scaffold or secondary only	
0.66 μM dimer	1:500 FITC-L	Fixed	2% BSA, 1h	Nonspecific binding for vehicle and ABO (others not tested)	
0.66 μM dimer	1:500 FITC-L	Live	2% BSA, 1h	Nonspecific (internalization or clumping) for vehicle and ABO, but not for scaffold or secondary only	
0.3 μM dimer	1:500 FITC-L	Fixed	3% BSA, 2x10 min, 1x40 min	Nonspecific binding for F12 vehicle and F12 ABO as well as PBS vehicle and xLABO	
0.3 μM dimer	1:500 FITC-L	Fixed + fixed again after primary	3% BSA, 2x10 min, 1x40 min	Nonspecific binding for PBS vehicle and xLABO (others not tested)	
0.1 μM dimer	1:500 FITC-L	Fixed + fixed again after primary	3% BSA, 2x10 min, 1x40 min	Nonspecific binding for F12 vehicle and F12 ABO as well as PBS vehicle and xLABO	
0.1 μM dimer	1:500 FITC-L	Fixed + fixed again after secondary	3% BSA, 2x10 min, 1x40 min	Nonspecific binding for PBS vehicle and xLABO (others not tested)	
0.3 μM dimer	1:1000 or 1:500 aHis488	Fixed	3% BSA, 2x10 min, 1x40 min	Very low s/n for F12 vehicle vs F12 ABO at 1:1000, Moderate s/n at 1:500 aHis488	
0.3 μM dimer	1:1000 or 1:500 aHis488	Fixed + fixed again after primary	3% BSA, 2x10 min, 1x40 min	Very low s/n for F12 vehicle vs F12 ABO	
0.1 μM dimer	1:500 aHis488	Fixed + fixed again after secondary	3% BSA, 2x10 min, 1x40 min	Fairly low s/n for PBS vehicle vs xLABO (others not tested)	
0.1 μM dimer	1:500 aHis488	Fixed + fixed again after primary	3% BSA, 2x10 min, 1x40 min	Moderate s/n for PBS vehicle vs xLABO (worked well for F12 ABOs)	

Figure 4.13 Nuscl megamolecule immunofluorescence conditions. Nuscl megamolecule immunofluorescence labeling was optimized using Nuscl dimer to test the specified conditions. In all cases, A β O_s were applied to mature hippocampal cells for 1 h, then cells were washed with sterile PBS. Most cells were fixed with formaldehyde, which was subsequently removed by three washes with PBS. Then coverslips were blocked and labeled with dimer as a primary antibody and a variety of secondary antibodies. In some cases, fixation steps were performed after addition of primary or secondary. Finally, coverslips were mounted on glass slides and imaged. Abbreviations: aHis488 (Alexa Fluor 488 anti-His tag), FITC-L (FITC-tagged protein L), BSA (bovine serum albumin).

The remaining bound primary antibody was then fixed by replacement of PBS with 3.7% formaldehyde for 10 min, which was then removed by three washes with PBS. The secondary antibody, Alexa Fluor 488 anti-His Tag (1:1000, BioLegend 652509) in a solution of 3%

blocking buffer was added for 3 h at RT in the dark. The coverslips were washed twice for 10 min each, then mounted on slides in Prolong Diamond Antifade mountant with DAPI (Thermo Fisher Scientific P36862) and allowed to dry at RT, protected from light. Images were collected using a Leica DM6B fluorescent microscope using the 63x objective. Using the Leica LAS-X software, 3D deconvolution was applied for 3 iterations, and subsequently maximum projections were obtained for each image.

Image analysis was conducted using ImageJ, by measurement of the total fluorescent integrated density or the count of ROIs above an equal threshold for all images. Data analysis was conducted using GraphPad Prism.

4.4.5 *A β O neutralization assays*

For all neutralization assays, xLA β O_s were first preincubated with megamolecules, Nusc1, cutinase scaffolds, or PBS vehicle for 1 h at 37 °C. For the initial experiment in Figure 4.7, 0.4 μ M of each megamolecule, cutinase scaffold, or an equal volume of PBS vehicle was preincubated with 0.2 μ M xLA β O. For the Nusc1 scFv experiment in Figure 4.8, 0.05-1 μ M Nusc1 or an equal volume of PBS vehicle was preincubated with 0.5 μ M xLA β O_s. For the multi-dose megamolecule experiments in Figures 4.10-4.12, 0.05-0.5 μ M of each megamolecule or an equal volume of PBS vehicle was preincubated with 0.5 μ M xLA β O_s.

These solutions were then applied to mature hippocampal neurons on glass coverslips (20-24 *div*) for 1 h at 37 °C. The coverslips were washed with sterile PBS and fixed first by 1:1 addition of 3.7% formaldehyde (Sigma-Aldrich F8775-500) for 10 min and then by full volume replacement with 3.7% formaldehyde for an additional 10 min. Formaldehyde was removed by three PBS washes, and coverslips were blocked for 1 h at RT. The blocking buffer consisted of

5% normal goat serum and 0.1% Triton X-100 (Sigma-Aldrich T9284-500ML) in PBS. The primary antibodies, NU2 (1:1500-1:2000, in-house) and MAP2 (1:10,000, EnCor Biotechnology CPCA-MAP2), were then applied in blocking buffer at 4 °C overnight with orbital shaking. The coverslips were washed three times with PBS. The secondary antibodies, goat anti-mouse Alexa Fluor 488 (1:2000, Fisher Scientific A11029) and goat anti-chicken Alexa Fluor 568 (1:2000, Thermo Fisher Scientific A11036), were added in a solution of 10% blocking buffer in PBS for 3 h at RT in the dark. The coverslips were washed three times with PBS and mounted on a Prolong Diamond Antifade mountant with DAPI (Thermo Fisher Scientific P36862).

Images were collected using a Leica DM6B fluorescent microscope using the 63x objective. Using the Leica LAS-X software, 3D deconvolution was applied for 3 iterations, and, subsequently, maximum projections were obtained for each image.

A β O binding analysis was conducted on immunofluorescent images in which MAP2 was used as an indicator of dendrites. ImageJ was used for analysis. Briefly, tiff images were assigned random numbers to avoid bias during analysis, and then cell bodies were manually traced and deleted from each image to eliminate signal from nonspecific antibody accumulation in the cell body. To calculate total dendrite length in each image, a Gaussian blur was applied to the MAP2 signal, the signal above an equal threshold for each image was skeletonized, and the total length of the skeleton was measured. To calculate the total A β O puncta along processes, again a Gaussian blur was applied to the dendrite signal, and the signal above an equal threshold was selected. Then, the signal was dilated to encompass the area around the dendrites by 15 dilations. The area around the dendrites was used as a selection, and within the selection area, ImageJ particle analysis and summary was used to count the NU2 puncta above an equal

threshold for each image. Thresholds were chosen based on one or two positive and negative control images. The total number of NU2 puncta was divided by the total dendrite length to calculate the A β O puncta/micron. Data analysis was conducted in GraphPad Prism using nonlinear regression.

References

1. Nichols, E. et al. Estimation of the global prevalence of dementia in 2019 and forecasted prevalence in 2050: an analysis for the Global Burden of Disease Study 2019. *Lancet Public Health* **7**, e105-e125 (2022).
2. 2022 Alzheimer's disease facts and figures. *Alzheimers Dement* **18**, 700-789 (2022).
3. Busted, L.M., Nielsen, D.S. & Birkelund, R. "Sometimes it feels like thinking in syrup" - the experience of losing sense of self in those with young onset dementia. *Int J Qual Stud Health Well-being* **15**, 1734277 (2020).
4. Athanasiadou, E. et al. Care of Patients with Alzheimer's Disease. *Adv Exp Med Biol* **1339**, 9-20 (2021).
5. Mozersky, J. & Davis, D.S. Living with Alzheimer Disease and Other Types of Dementia: Stories from Caregivers. *Narrat Inq Bioeth* **10**, 89-93 (2020).
6. Aguirre-Acevedo, D.C. et al. Cognitive Decline in a Colombian Kindred With Autosomal Dominant Alzheimer Disease: A Retrospective Cohort Study. *JAMA Neurol* **73**, 431-8 (2016).
7. Cairns, N.J. et al. Neuropathologic assessment of participants in two multi-center longitudinal observational studies: The Alzheimer Disease Neuroimaging Initiative (ADNI) and the Dominantly Inherited Alzheimer Network (DIAN). *Neuropathology* **35**, 390-400 (2015).
8. Barthélemy, N.R. et al. A soluble phosphorylated tau signature links tau, amyloid and the evolution of stages of dominantly inherited Alzheimer's disease. *Nat Med* **26**, 398-407 (2020).
9. Quiroz, Y.T. et al. Plasma neurofilament light chain in the presenilin 1 E280A autosomal dominant Alzheimer's disease kindred: a cross-sectional and longitudinal cohort study. *Lancet Neurol* **19**, 513-521 (2020).
10. Villemagne, V.L. et al. Amyloid β deposition, neurodegeneration, and cognitive decline in sporadic Alzheimer's disease: a prospective cohort study. *Lancet Neurol* **12**, 357-67 (2013).
11. Gordon, B.A. et al. Spatial patterns of neuroimaging biomarker change in individuals from families with autosomal dominant Alzheimer's disease: a longitudinal study. *Lancet Neurol* **17**, 241-250 (2018).
12. Bateman, R.J. et al. Clinical and biomarker changes in dominantly inherited Alzheimer's disease. *N Engl J Med* **367**, 795-804 (2012).
13. Flicker, C., Ferris, S.H. & Reisberg, B. Mild cognitive impairment in the elderly: predictors of dementia. *Neurology* **41**, 1006-9 (1991).
14. Petersen, R.C. et al. Mild cognitive impairment: clinical characterization and outcome. *Arch Neurol* **56**, 303-8 (1999).
15. Wilson, R.S., Leurgans, S.E., Boyle, P.A. & Bennett, D.A. Cognitive decline in prodromal Alzheimer disease and mild cognitive impairment. *Arch Neurol* **68**, 351-6 (2011).
16. Taragano, F.E., Allegri, R.F. & Lyketsos, C. Mild behavioral impairment: A prodromal stage of dementia. *Dement Neuropsychol* **2**, 256-260 (2008).
17. Vermunt, L. et al. Duration of preclinical, prodromal, and dementia stages of Alzheimer's disease in relation to age, sex, and APOE genotype. *Alzheimers Dement* **15**, 888-898 (2019).
18. Eramudugolla, R. et al. Evaluation of a research diagnostic algorithm for DSM-5 neurocognitive disorders in a population-based cohort of older adults. *Alzheimers Res Ther* **9**, 15 (2017).
19. Jack, C.R., Jr. et al. NIA-AA Research Framework: Toward a biological definition of Alzheimer's disease. *Alzheimers Dement* **14**, 535-562 (2018).
20. Mayeda, E.R. et al. Survival after dementia diagnosis in five racial/ethnic groups. *Alzheimers Dement* **13**, 761-769 (2017).

21. Rajan, K.B. et al. Population estimate of people with clinical Alzheimer's disease and mild cognitive impairment in the United States (2020-2060). *Alzheimers Dement* **17**, 1966-1975 (2021).
22. Gatz, M. et al. Role of genes and environments for explaining Alzheimer disease. *Arch Gen Psychiatry* **63**, 168-74 (2006).
23. Scheuner, D. et al. Secreted amyloid beta-protein similar to that in the senile plaques of Alzheimer's disease is increased in vivo by the presenilin 1 and 2 and APP mutations linked to familial Alzheimer's disease. *Nat Med* **2**, 864-70 (1996).
24. De Strooper, B. et al. Deficiency of presenilin-1 inhibits the normal cleavage of amyloid precursor protein. *Nature* **391**, 387-90 (1998).
25. Wolfe, M.S. et al. Two transmembrane aspartates in presenilin-1 required for presenilin endoproteolysis and gamma-secretase activity. *Nature* **398**, 513-7 (1999).
26. Szaruga, M. et al. Qualitative changes in human γ -secretase underlie familial Alzheimer's disease. *J Exp Med* **212**, 2003-13 (2015).
27. Prasher, V.P. et al. Molecular mapping of Alzheimer-type dementia in Down's syndrome. *Ann Neurol* **43**, 380-3 (1998).
28. Rovelet-Lecrux, A. et al. APP locus duplication causes autosomal dominant early-onset Alzheimer disease with cerebral amyloid angiopathy. *Nat Genet* **38**, 24-6 (2006).
29. Jonsson, T. et al. A mutation in APP protects against Alzheimer's disease and age-related cognitive decline. *Nature* **488**, 96-9 (2012).
30. Corder, E.H. et al. Gene dose of apolipoprotein E type 4 allele and the risk of Alzheimer's disease in late onset families. *Science* **261**, 921-3 (1993).
31. Strittmatter, W.J. et al. Apolipoprotein E: high-avidity binding to beta-amyloid and increased frequency of type 4 allele in late-onset familial Alzheimer disease. *Proc Natl Acad Sci U S A* **90**, 1977-81 (1993).
32. Michaelson, D.M. APOE ϵ 4: The most prevalent yet understudied risk factor for Alzheimer's disease. *Alzheimers Dement* **10**, 861-868 (2014).
33. van der Lee, S.J. et al. The effect of APOE and other common genetic variants on the onset of Alzheimer's disease and dementia: a community-based cohort study. *Lancet Neurol* **17**, 434-444 (2018).
34. Jansen, I.E. et al. Genome-wide meta-analysis identifies new loci and functional pathways influencing Alzheimer's disease risk. *Nat Genet* **51**, 404-413 (2019).
35. Bellenguez, C. et al. New insights into the genetic etiology of Alzheimer's disease and related dementias. *Nat Genet* **54**, 412-436 (2022).
36. Escott-Price, V., Myers, A.J., Huentelman, M. & Hardy, J. Polygenic risk score analysis of pathologically confirmed Alzheimer disease. *Ann Neurol* **82**, 311-314 (2017).
37. Ngandu, T. et al. A 2 year multidomain intervention of diet, exercise, cognitive training, and vascular risk monitoring versus control to prevent cognitive decline in at-risk elderly people (FINGER): a randomised controlled trial. *Lancet* **385**, 2255-63 (2015).
38. Sando, S.B. et al. Risk-reducing effect of education in Alzheimer's disease. *Int J Geriatr Psychiatry* **23**, 1156-62 (2008).
39. McDowell, I., Xi, G., Lindsay, J. & Tierney, M. Mapping the connections between education and dementia. *J Clin Exp Neuropsychol* **29**, 127-41 (2007).
40. Saczynski, J.S. et al. The effect of social engagement on incident dementia: the Honolulu-Asia Aging Study. *Am J Epidemiol* **163**, 433-40 (2006).
41. Fann, J.R. et al. Long-term risk of dementia among people with traumatic brain injury in Denmark: a population-based observational cohort study. *Lancet Psychiatry* **5**, 424-431 (2018).

42. Barnes, D.E. et al. Association of Mild Traumatic Brain Injury With and Without Loss of Consciousness With Dementia in US Military Veterans. *JAMA Neurol* **75**, 1055-1061 (2018).
43. Turner, R.C., Lucke-Wold, B.P., Robson, M.J., Lee, J.M. & Bailes, J.E. Alzheimer's disease and chronic traumatic encephalopathy: Distinct but possibly overlapping disease entities. *Brain Inj* **30**, 1279-1292 (2016).
44. Alzheimer, A. Uber einen eigenartigen schweren Erkrankungsprozess der Hirninde. *Neurologisches Centralblatt* **25**, 1134 (1906).
45. Hyman, B.T. & Trojanowski, J.Q. Consensus recommendations for the postmortem diagnosis of Alzheimer disease from the National Institute on Aging and the Reagan Institute Working Group on diagnostic criteria for the neuropathological assessment of Alzheimer disease. *J Neuropathol Exp Neurol* **56**, 1095-7 (1997).
46. Sato, C. et al. Tau Kinetics in Neurons and the Human Central Nervous System. *Neuron* **97**, 1284-1298.e7 (2018).
47. Hanseeuw, B.J. et al. Association of Amyloid and Tau With Cognition in Preclinical Alzheimer Disease: A Longitudinal Study. *JAMA Neurol* **76**, 915-924 (2019).
48. Terry, R.D., Gonatas, N.K. & Weiss, M. Ultrastructural studies in Alzheimer's presenile dementia. *Am J Pathol* **44**, 269-97 (1964).
49. Wang, H.F. et al. Clinical and biomarker trajectories in sporadic Alzheimer's disease: A longitudinal study. *Alzheimers Dement (Amst)* **12**, e12095 (2020).
50. Braak, H. & Braak, E. Frequency of stages of Alzheimer-related lesions in different age categories. *Neurobiol Aging* **18**, 351-357 (1997).
51. Terry, R.D. et al. Physical basis of cognitive alterations in Alzheimer's disease: synapse loss is the major correlate of cognitive impairment. *Ann Neurol* **30**, 572-80 (1991).
52. Villemagne, V.L. et al. Longitudinal assessment of A β and cognition in aging and Alzheimer disease. *Ann Neurol* **69**, 181-192 (2011).
53. Selkoe, D.J. & Hardy, J. The amyloid hypothesis of Alzheimer's disease at 25 years. *EMBO Mol Med* **8**, 595-608 (2016).
54. Cline, E.N., Bicca, M.A., Viola, K.L. & Klein, W.L. The Amyloid- β Oligomer Hypothesis: Beginning of the Third Decade. *J Alzheimers Dis* **64**, S567-s610 (2018).
55. Maggio, J.E. et al. Reversible in vitro growth of Alzheimer disease beta-amyloid plaques by deposition of labeled amyloid peptide. *Proc Natl Acad Sci U S A* **89**, 5462-6 (1992).
56. Koffie, R.M. et al. Oligomeric amyloid beta associates with postsynaptic densities and correlates with excitatory synapse loss near senile plaques. *Proc Natl Acad Sci U S A* **106**, 4012-7 (2009).
57. Ahmad, M.H., Fatima, M. & Mondal, A.C. Influence of microglia and astrocyte activation in the neuroinflammatory pathogenesis of Alzheimer's disease: Rational insights for the therapeutic approaches. *J Clin Neurosci* **59**, 6-11 (2019).
58. Arranz, A.M. & De Strooper, B. The role of astroglia in Alzheimer's disease: pathophysiology and clinical implications. *Lancet Neurol* **18**, 406-414 (2019).
59. Butterfield, D.A. & Halliwell, B. Oxidative stress, dysfunctional glucose metabolism and Alzheimer disease. *Nat Rev Neurosci* **20**, 148-160 (2019).
60. de la Monte, S.M. & Wands, J.R. Alzheimer's disease is type 3 diabetes-evidence reviewed. *J Diabetes Sci Technol* **2**, 1101-13 (2008).
61. Miyakawa, T. Vascular pathology in Alzheimer's disease. *Psychogeriatrics* **10**, 39-44 (2010).
62. Kalaria, R.N., Akinyemi, R. & Ihara, M. Does vascular pathology contribute to Alzheimer changes? *J Neurol Sci* **322**, 141-147 (2012).
63. Poirel, O. et al. Moderate decline in select synaptic markers in the prefrontal cortex (BA9) of patients with Alzheimer's disease at various cognitive stages. *Sci Rep* **8**, 938 (2018).

64. Du, A.T. et al. Different regional patterns of cortical thinning in Alzheimer's disease and frontotemporal dementia. *Brain* **130**, 1159-66 (2007).
65. Glynn-Servedio, B.E. & Ranola, T.S. AChE Inhibitors and NMDA Receptor Antagonists in Advanced Alzheimer's Disease. *Consult Pharm* **32**, 511-518 (2017).
66. Marucci, G. et al. Efficacy of acetylcholinesterase inhibitors in Alzheimer's disease. *Neuropharmacology* **190**, 108352 (2021).
67. Copenhaver, P.F. & Kögel, D. Role of APP Interactions with Heterotrimeric G Proteins: Physiological Functions and Pathological Consequences. *Front Mol Neurosci* **10**, 3 (2017).
68. Hefter, D. & Draguhn, A. APP as a Protective Factor in Acute Neuronal Insults. *Front Mol Neurosci* **10**, 22 (2017).
69. Haass, C., Kaether, C., Thinakaran, G. & Sisodia, S. Trafficking and proteolytic processing of APP. *Cold Spring Harb Perspect Med* **2**, a006270 (2012).
70. Müller, T., Meyer, H.E., Egensperger, R. & Marcus, K. The amyloid precursor protein intracellular domain (AICD) as modulator of gene expression, apoptosis, and cytoskeletal dynamics-relevance for Alzheimer's disease. *Prog Neurobiol* **85**, 393-406 (2008).
71. Rice, H.C. et al. Secreted amyloid- β precursor protein functions as a GABA(B)R1a ligand to modulate synaptic transmission. *Science* **363**(2019).
72. Choy, R.W.-Y., Cheng, Z. & Schekman, R. Amyloid precursor protein (APP) traffics from the cell surface via endosomes for amyloid β (A β) production in the trans-Golgi network. *Proc Natl Acad Sci U S A* **109**, E2077-E2082 (2012).
73. Yu, Y., Jans, D.C., Winblad, B., Tjernberg, L.O. & Schedin-Weiss, S. Neuronal A β 42 is enriched in small vesicles at the presynaptic side of synapses. *Life Sci Alliance* **1**, e201800028 (2018).
74. Lin, T., Tjernberg, L.O. & Schedin-Weiss, S. Neuronal Trafficking of the Amyloid Precursor Protein—What Do We Really Know? in *Biomedicines* Vol. 9 (2021).
75. Jiang, S. et al. Trafficking regulation of proteins in Alzheimer's disease. *Mol Neurodegener* **9**, 6 (2014).
76. Sandebring, A., Welander, H., Winblad, B., Graff, C. & Tjernberg, L.O. The Pathogenic A β 43 Is Enriched in Familial and Sporadic Alzheimer Disease. *PLOS ONE* **8**, e55847 (2013).
77. Welander, H. et al. A β 43 is more frequent than A β 40 in amyloid plaque cores from Alzheimer disease brains. *J Neurochem* **110**, 697-706 (2009).
78. Lee, M.-H. et al. Somatic APP gene recombination in Alzheimer's disease and normal neurons. *Nature* **563**, 639-645 (2018).
79. Bemporad, F., Cecchi, C. & Chiti, F. Capturing A β 42 aggregation in the cell. *J Biol Chem* **294**, 1488-1489 (2019).
80. Vandersteen, A. et al. A comparative analysis of the aggregation behavior of amyloid- β peptide variants. *FEBS Lett* **586**, 4088-4093 (2012).
81. Kimberly, W.T. et al. Gamma-secretase is a membrane protein complex comprised of presenilin, nicastrin, Aph-1, and Pen-2. *Proc Natl Acad Sci U S A* **100**, 6382-7 (2003).
82. Bai, X.-c. et al. An atomic structure of human γ -secretase. *Nature* **525**, 212-217 (2015).
83. Kumar, D.K. et al. Amyloid- β peptide protects against microbial infection in mouse and worm models of Alzheimer's disease. *Sci Transl Med* **8**, 340ra72 (2016).
84. Beydoun, M.A. et al. Clinical and Bacterial Markers of Periodontitis and Their Association with Incident All-Cause and Alzheimer's Disease Dementia in a Large National Survey. *J Alzheimers Dis* **75**, 157-172 (2020).
85. Puzzo, D. et al. Picomolar amyloid-beta positively modulates synaptic plasticity and memory in hippocampus. *J Neurosci* **28**, 14537-45 (2008).

86. De Strooper, B. Proteases and Proteolysis in Alzheimer Disease: A Multifactorial View on the Disease Process. *Physiol Rev* **90**, 465-494 (2010).
87. Ciechanover, A. & Kwon, Y.T. Degradation of misfolded proteins in neurodegenerative diseases: therapeutic targets and strategies. *Exp Mol Med* **47**, e147-e147 (2015).
88. Hansson, O. et al. Prediction of Alzheimer's Disease Using the CSF A β 42/A β 40 Ratio in Patients with Mild Cognitive Impairment. *Dement Geriatr Cogn Disord* **23**, 316-320 (2007).
89. Mawuenyega, K.G. et al. Decreased clearance of CNS beta-amyloid in Alzheimer's disease. *Science* **330**, 1774 (2010).
90. Lue, L.F. et al. Soluble amyloid beta peptide concentration as a predictor of synaptic change in Alzheimer's disease. *Am J Pathol* **155**, 853-62 (1999).
91. Lambert, M.P. et al. Diffusible, nonfibrillar ligands derived from Abeta1-42 are potent central nervous system neurotoxins. *Proc Natl Acad Sci U S A* **95**, 6448-6453 (1998).
92. Gyure, K.A., Durham, R., Stewart, W.F., Smialek, J.E. & Troncoso, J.C. Intraneuronal abeta-amyloid precedes development of amyloid plaques in Down syndrome. *Arch Pathol Lab Med* **125**, 489-92 (2001).
93. Hartmann, T. et al. Distinct sites of intracellular production for Alzheimer's disease A β 40/42 amyloid peptides. *Nat Med* **3**, 1016-1020 (1997).
94. Hook, V.Y. Unique neuronal functions of cathepsin L and cathepsin B in secretory vesicles: biosynthesis of peptides in neurotransmission and neurodegenerative disease. *Biol Chem* **387**, 1429-39 (2006).
95. Chromy, B.A. et al. Self-assembly of Abeta(1-42) into globular neurotoxins. *Biochemistry* **42**, 12749-60 (2003).
96. Chang, L., Bakhos, L., Wang, Z., Venton, D.L. & Klein, W.L. Femtomole immunodetection of synthetic and endogenous amyloid- β oligomers and its application to Alzheimer's disease drug candidate screening. *J Mol Neurosci* **20**, 305-313 (2003).
97. Benilova, I., Karran, E. & De Strooper, B. The toxic A β oligomer and Alzheimer's disease: an emperor in need of clothes. *Nat Neurosci* **15**, 349-357 (2012).
98. Sakono, M. & Zako, T. Amyloid oligomers: formation and toxicity of Abeta oligomers. *FEBS J* **277**, 1348-58 (2010).
99. Miti, T., Mulaj, M., Schmit, J.D. & Muschol, M. Stable, Metastable, and Kinetically Trapped Amyloid Aggregate Phases. *Biomacromolecules* **16**, 326-335 (2015).
100. Kummer, M.P. & Heneka, M.T. Truncated and modified amyloid-beta species. *Alzheimers Res Ther* **6**, 28 (2014).
101. Gouras, G.K. et al. Intraneuronal Abeta42 accumulation in human brain. *Am J Pathol* **156**, 15-20 (2000).
102. LaFerla, F.M., Green, K.N. & Oddo, S. Intracellular amyloid- β in Alzheimer's disease. *Nat Rev Neurosci* **8**, 499-509 (2007).
103. Hu, X. et al. Amyloid seeds formed by cellular uptake, concentration, and aggregation of the amyloid-beta peptide. *Proc Natl Acad Sci U S A* **106**, 20324-9 (2009).
104. Wood, S.J., Maleeff, B., Hart, T. & Wetzel, R. Physical, morphological and functional differences between pH 5.8 and 7.4 aggregates of the Alzheimer's amyloid peptide Abeta. *J Mol Biol* **256**, 870-7 (1996).
105. Takahashi, R.H. et al. Oligomerization of Alzheimer's beta-amyloid within processes and synapses of cultured neurons and brain. *J Neurosci* **24**, 3592-9 (2004).
106. Schützmann, M.P. et al. Endo-lysosomal A β concentration and pH trigger formation of A β oligomers that potently induce Tau missorting. *Nat Commun* **12**, 4634 (2021).

107. Esbjörner, E.K. et al. Direct observations of amyloid β self-assembly in live cells provide insights into differences in the kinetics of A β (1-40) and A β (1-42) aggregation. *Chem Biol* **21**, 732-42 (2014).
108. Kanekiyo, T. & Bu, G. The low-density lipoprotein receptor-related protein 1 and amyloid- β clearance in Alzheimer's disease. *Front Aging Neurosci* **6**(2014).
109. Deane, R. et al. RAGE mediates amyloid-beta peptide transport across the blood-brain barrier and accumulation in brain. *Nat Med* **9**, 907-13 (2003).
110. Takuma, K. et al. RAGE-mediated signaling contributes to intraneuronal transport of amyloid- β and neuronal dysfunction. *Proc Natl Acad Sci U S A* **106**, 20021-20026 (2009).
111. Yamamoto, N. et al. A ganglioside-induced toxic soluble Abeta assembly. Its enhanced formation from Abeta bearing the Arctic mutation. *J Biol Chem* **282**, 2646-55 (2007).
112. Almeida, C.G., Takahashi, R.H. & Gouras, G.K. Beta-amyloid accumulation impairs multivesicular body sorting by inhibiting the ubiquitin-proteasome system. *J Neurosci* **26**, 4277-88 (2006).
113. Takahashi, R.H. et al. Intraneuronal Alzheimer abeta42 accumulates in multivesicular bodies and is associated with synaptic pathology. *Am J Pathol* **161**, 1869-79 (2002).
114. Ochiishi, T. et al. New Alzheimer's disease model mouse specialized for analyzing the function and toxicity of intraneuronal Amyloid β oligomers. *Sci Rep* **9**, 17368 (2019).
115. Umeda, T. et al. Intraneuronal amyloid β oligomers cause cell death via endoplasmic reticulum stress, endosomal/lysosomal leakage, and mitochondrial dysfunction in vivo. *J Neurosci Res* **89**, 1031-42 (2011).
116. Tseng, B.P., Green, K.N., Chan, J.L., Blurton-Jones, M. & LaFerla, F.M. Abeta inhibits the proteasome and enhances amyloid and tau accumulation. *Neurobiol Aging* **29**, 1607-18 (2008).
117. Manczak, M. et al. Mitochondria are a direct site of A beta accumulation in Alzheimer's disease neurons: implications for free radical generation and oxidative damage in disease progression. *Hum Mol Genet* **15**, 1437-49 (2006).
118. Chen, J.X. & Yan, S.D. Amyloid-beta-induced mitochondrial dysfunction. *J Alzheimers Dis* **12**, 177-84 (2007).
119. Yang, A.J., Chandswangbhuvana, D., Margol, L. & Glabe, C.G. Loss of endosomal/lysosomal membrane impermeability is an early event in amyloid Abeta1-42 pathogenesis. *J Neurosci Res* **52**, 691-8 (1998).
120. Nath, S. et al. Spreading of neurodegenerative pathology via neuron-to-neuron transmission of β -amyloid. *J Neurosci* **32**, 8767-77 (2012).
121. Sardar Sinha, M. et al. Alzheimer's disease pathology propagation by exosomes containing toxic amyloid-beta oligomers. *Acta Neuropathol* **136**, 41-56 (2018).
122. Bode, D.C., Freeley, M., Nield, J., Palma, M. & Viles, J.H. Amyloid- β oligomers have a profound detergent-like effect on lipid membrane bilayers, imaged by atomic force and electron microscopy. *J Biol Chem* **294**, 7566-7572 (2019).
123. Ahmed, M. et al. Structural conversion of neurotoxic amyloid-beta(1-42) oligomers to fibrils. *Nat Struct Mol Biol* **17**, 561-7 (2010).
124. Chimon, S. et al. Evidence of fibril-like β -sheet structures in a neurotoxic amyloid intermediate of Alzheimer's β -amyloid. *Nat Struct Mol Biol* **14**, 1157-64 (2007).
125. Stroud, J.C., Liu, C., Teng, P.K. & Eisenberg, D. Toxic fibrillar oligomers of amyloid- β have cross- β structure. *Proc Natl Acad Sci U S A* **109**, 7717-7722 (2012).
126. Paravastu, A.K., Leapman, R.D., Yau, W.-M. & Tycko, R. Molecular structural basis for polymorphism in Alzheimer's β -amyloid fibrils. *Proc Natl Acad Sci U S A* **105**, 18349-18354 (2008).
127. Huang, D. et al. Antiparallel β -Sheet Structure within the C-Terminal Region of 42-Residue Alzheimer's Amyloid- β Peptides When They Form 150-kDa Oligomers. *J Mol Biol* **427**, 2319-28 (2015).

128. Tay, W.M., Huang, D., Rosenberry, T.L. & Paravastu, A.K. The Alzheimer's amyloid- β (1-42) peptide forms off-pathway oligomers and fibrils that are distinguished structurally by intermolecular organization. *J Mol Biol* **425**, 2494-508 (2013).
129. Gao, Y. et al. Out-of-Register Parallel β -Sheets and Antiparallel β -Sheets Coexist in 150-kDa Oligomers Formed by Amyloid- β (1-42). *J Mol Biol* **432**, 4388-4407 (2020).
130. Barghorn, S. et al. Globular amyloid β -peptide1-42 oligomer – a homogenous and stable neuropathological protein in Alzheimer's disease. *J Neurochem* **95**, 834-847 (2005).
131. Yu, L. et al. Structural characterization of a soluble amyloid β -peptide oligomer. *Biochemistry* **48**, 1870-1877 (2009).
132. Sandberg, A. et al. Stabilization of neurotoxic Alzheimer amyloid- β oligomers by protein engineering. *Proc Natl Acad Sci U S A* **107**, 15595-15600 (2010).
133. Doi, T. et al. Solid-state NMR analysis of the β -strand orientation of the protofibrils of amyloid β -protein. *Biochem Biophys Res Commun* **428**, 458-462 (2012).
134. Kaye, R. et al. Annular protofibrils are a structurally and functionally distinct type of amyloid oligomer. *J Biol Chem* **284**, 4230-7 (2009).
135. Lasagna-Reeves, C.A., Glabe, C.G. & Kaye, R. Amyloid- β annular protofibrils evade fibrillar fate in Alzheimer disease brain. *J Biol Chem* **286**, 22122-30 (2011).
136. Durell, S.R., Kaye, R. & Guy, H.R. The amyloid concentric β -barrel hypothesis: Models of amyloid beta 42 oligomers and annular protofibrils. *Proteins* **90**, 1190-1209 (2022).
137. Mustata, G.-M. et al. Insights into the mechanism of Alzheimer's β -amyloid aggregation as a function of concentration by using atomic force microscopy. *Appl Phys Lett* **100**, 133704 (2012).
138. Cline, E.N. et al. A novel crosslinking protocol stabilizes amyloid β oligomers capable of inducing Alzheimer's-associated pathologies. *J Neurochem* **148**, 822-836 (2019).
139. Nirmalraj, P.N. et al. Complete aggregation pathway of amyloid β (1-40) and (1-42) resolved on an atomically clean interface. *Sci Adv* **6**, eaaz6014 (2020).
140. Noguchi, A. et al. Isolation and characterization of patient-derived, toxic, high mass amyloid beta-protein (A β) assembly from Alzheimer disease brains. *J Biol Chem* **284**, 32895-905 (2009).
141. Parthasarathy, S. et al. Structural Insight into an Alzheimer's Brain-Derived Spherical Assembly of Amyloid β by Solid-State NMR. *J Am Chem Soc* **137**, 6480-6483 (2015).
142. Xiao, Y. et al. NMR-based site-resolved profiling of β -amyloid misfolding reveals structural transitions from pathologically relevant spherical oligomer to fibril. *J Biol Chem* **295**, 458-467 (2020).
143. Kass, B. et al. A β oligomer concentration in mouse and human brain and its drug-induced reduction ex vivo. *Cell Rep Med* **3**, 100630 (2022).
144. Kreutzer, A.G. & Nowick, J.S. Elucidating the Structures of Amyloid Oligomers with Macrocyclic β -Hairpin Peptides: Insights into Alzheimer's Disease and Other Amyloid Diseases. *Acc Chem Res* **51**, 706-718 (2018).
145. Ciudad, S. et al. A β (1-42) tetramer and octamer structures reveal edge conductivity pores as a mechanism for membrane damage. *Nat Commun* **11**, 3014 (2020).
146. Wu, J. et al. Cryo-electron Microscopy Imaging of Alzheimer's Amyloid-beta 42 Oligomer Displayed on a Functionally and Structurally Relevant Scaffold. *Angew Chem Int Ed* **60**, 18680-18687 (2021).
147. Ricciarelli, R. & Fedele, E. cAMP, cGMP and Amyloid β : Three Ideal Partners for Memory Formation. *Trends Neurosci* **41**, 255-266 (2018).
148. Wu, J., Anwyl, R. & Rowan, M.J. β -amyloid-(1-40) increases long-term potentiation in rat hippocampus in vitro. *Eur J Pharmacol* **284**, R1-R3 (1995).

149. Abramov, E. et al. Amyloid- β as a positive endogenous regulator of release probability at hippocampal synapses. *Nat Neurosci* **12**, 1567-1576 (2009).
150. Zhou, B., Lu, J.G., Siddu, A., Wernig, M. & Südhof, T.C. Synaptogenic effect of APP-Swedish mutation in familial Alzheimer's disease. *Sci Transl Med* **14**, eabn9380.
151. Bartley, S.C. et al. An Essential Role for Alzheimer's-Linked Amyloid Beta Oligomers in Neurodevelopment: Transient Expression of Multiple Proteoforms during Retina Histogenesis. *Int J Mol Sci* **23**(2022).
152. Lambert, M.P. et al. Monoclonal antibodies that target pathological assemblies of A β . *J Neurochem* **100**, 23-35 (2007).
153. Sehlin, D. et al. Large aggregates are the major soluble A β species in AD brain fractionated with density gradient ultracentrifugation. *PLoS One* **7**, e32014 (2012).
154. Gong, Y. et al. Alzheimer's disease-affected brain: Presence of oligomeric A β ligands (ADDLs) suggests a molecular basis for reversible memory loss. *Proc Natl Acad Sci U S A* **100**, 10417-10422 (2003).
155. Esparza, T.J. et al. Amyloid- β oligomerization in Alzheimer dementia versus high-pathology controls. *Ann Neurol* **73**, 104-19 (2013).
156. Bilousova, T. et al. Synaptic amyloid- β oligomers precede p-Tau and differentiate high pathology control cases. *Am J Pathol* **186**, 185-98 (2016).
157. Mc Donald, J.M. et al. The presence of sodium dodecyl sulphate-stable A β dimers is strongly associated with Alzheimer-type dementia. *Brain* **133**, 1328-41 (2010).
158. Pham, E. et al. Progressive accumulation of amyloid-beta oligomers in Alzheimer's disease and in amyloid precursor protein transgenic mice is accompanied by selective alterations in synaptic scaffold proteins. *FEBS J* **277**, 3051-67 (2010).
159. Georganopoulou, D.G. et al. Nanoparticle-based detection in cerebral spinal fluid of a soluble pathogenic biomarker for Alzheimer's disease. *Proc Natl Acad Sci U S A* **102**, 2273-2276 (2005).
160. Wang, M.J. et al. Oligomeric forms of amyloid- β protein in plasma as a potential blood-based biomarker for Alzheimer's disease. *Alzheimer's Res Ther* **9**, 98 (2017).
161. Pyun, J.M. et al. Plasma Amyloid- β Oligomerization Tendency Predicts Amyloid PET Positivity. *Clin Interv Aging* **16**, 749-755 (2021).
162. Babapour Mofrad, R. et al. Plasma amyloid- β oligomerization assay as a pre-screening test for amyloid status. *Alzheimers Res Ther* **13**, 133 (2021).
163. Sandhu, G.K. et al. Correlation Between Plasma Oligomeric Amyloid- β and Performance on the Language Neutral Visual Cognitive Assessment Test in a Southeast Asian Population. *J Alzheimers Dis* (2022).
164. Yoo, S.-J. et al. Longitudinal profiling of oligomeric A β in human nasal discharge reflecting cognitive decline in probable Alzheimer's disease. *Sci Rep* **10**, 11234 (2020).
165. Tomiyama, T. et al. A new amyloid beta variant favoring oligomerization in Alzheimer's-type dementia. *Ann Neurol* **63**, 377-87 (2008).
166. Nishitsuji, K. et al. The E693Delta mutation in amyloid precursor protein increases intracellular accumulation of amyloid beta oligomers and causes endoplasmic reticulum stress-induced apoptosis in cultured cells. *Am J Pathol* **174**, 957-69 (2009).
167. Shimada, H. et al. Clinical course of patients with familial early-onset Alzheimer's disease potentially lacking senile plaques bearing the E693Delta mutation in amyloid precursor protein. *Dement Geriatr Cogn Disord* **32**, 45-54 (2011).
168. Inayathullah, M. & Teplow, D.B. Structural dynamics of the Δ E22 (Osaka) familial Alzheimer's disease-linked amyloid β -protein. *Amyloid* **18**, 98-107 (2011).

169. Kutoku, Y. et al. A second pedigree with amyloid-less familial Alzheimer's disease harboring an identical mutation in the amyloid precursor protein gene (E693delta). *Intern Med* **54**, 205-8 (2015).
170. Tomiyama, T. & Shimada, H. APP Osaka Mutation in Familial Alzheimer's Disease-Its Discovery, Phenotypes, and Mechanism of Recessive Inheritance. *Int J Mol Sci* **21**(2020).
171. Nilsberth, C. et al. The 'Arctic' APP mutation (E693G) causes Alzheimer's disease by enhanced Abeta protofibril formation. *Nat Neurosci* **4**, 887-93 (2001).
172. Schöll, M. et al. Low PiB PET retention in presence of pathologic CSF biomarkers in Arctic APP mutation carriers. *Neurology* **79**, 229-36 (2012).
173. Kamino, K. et al. Linkage and mutational analysis of familial Alzheimer disease kindreds for the APP gene region. *Am J Hum Genet* **51**, 998-1014 (1992).
174. Meyer-Luehmann, M. et al. Exogenous induction of cerebral beta-amyloidogenesis is governed by agent and host. *Science* **313**, 1781-4 (2006).
175. Epelbaum, S. et al. Acute amnesic encephalopathy in amyloid- β oligomer-injected mice is due to their widespread diffusion in vivo. *Neurobiol Aging* **36**, 2043-2052 (2015).
176. Eisele, Y.S. et al. Peripherally applied Abeta-containing inoculates induce cerebral beta-amyloidosis. *Science* **330**, 980-2 (2010).
177. Baerends, E. et al. Modeling the early stages of Alzheimer's disease by administering intracerebroventricular injections of human native A β oligomers to rats. *Acta Neuropathol Commun* **10**, 113 (2022).
178. Balducci, C. et al. Synthetic amyloid-beta oligomers impair long-term memory independently of cellular prion protein. *Proc Natl Acad Sci U S A* **107**, 2295-300 (2010).
179. Faucher, P., Mons, N., Micheau, J., Louis, C. & Beracochea, D.J. Hippocampal Injections of Oligomeric Amyloid β -peptide (1-42) Induce Selective Working Memory Deficits and Long-lasting Alterations of ERK Signaling Pathway. *Front Aging Neurosci* **7**, 245-245 (2016).
180. Nicole, O. et al. Soluble amyloid beta oligomers block the learning-induced increase in hippocampal sharp wave-ripple rate and impair spatial memory formation. *Sci Rep* **6**, 22728 (2016).
181. Forny-Germano, L. et al. Alzheimer's disease-like pathology induced by amyloid-beta oligomers in nonhuman primates. *J Neurosci* **34**, 13629-43 (2014).
182. Beckman, D. et al. Oligomeric Abeta in the monkey brain impacts synaptic integrity and induces accelerated cortical aging. *Proc Natl Acad Sci U S A* (2019).
183. Yue, F. et al. Synthetic amyloid- β oligomers drive early pathological progression of Alzheimer's disease in nonhuman primates. *iScience* **24**, 103207 (2021).
184. Wakeman, D.R. et al. Intrathecal amyloid-beta oligomer administration increases tau phosphorylation in the medial temporal lobe in the African green monkey: A nonhuman primate model of Alzheimer's disease. *Neuropathol Appl Neurobiol* **48**, e12800 (2022).
185. Schemmert, S. et al. A β Oligomer Elimination Restores Cognition in Transgenic Alzheimer's Mice with Full-blown Pathology. *Mol Neurobiol* **56**, 2211-2223 (2019).
186. Shi, M., Chu, F., Zhu, F. & Zhu, J. Impact of Anti-amyloid- β Monoclonal Antibodies on the Pathology and Clinical Profile of Alzheimer's Disease: A Focus on Aducanumab and Lecanemab. *Front Aging Neurosci* **14**, 870517 (2022).
187. Panza, F., Lozupone, M., Logroscino, G. & Imbimbo, B.P. A critical appraisal of amyloid-beta-targeting therapies for Alzheimer disease. *Nat Rev Neurol* **15**, 73-88 (2019).
188. Tolar, M., Hey, J., Power, A. & Abushakra, S. Neurotoxic Soluble Amyloid Oligomers Drive Alzheimer's Pathogenesis and Represent a Clinically Validated Target for Slowing Disease Progression. in *Int J Mol Sci* Vol. 22 (2021).

189. Sevigny, J. et al. The antibody aducanumab reduces A β plaques in Alzheimer's disease. *Nature* **537**, 50-6 (2016).
190. Budd Haeberlein, S. et al. Two Randomized Phase 3 Studies of Aducanumab in Early Alzheimer's Disease. *J Prev Alzheimers Dis* **9**, 197-210 (2022).
191. Swanson, C.J. et al. A randomized, double-blind, phase 2b proof-of-concept clinical trial in early Alzheimer's disease with lecanemab, an anti-A β protofibril antibody. *Alzheimers Res Ther* **13**, 80 (2021).
192. van Dyck, C.H. et al. Lecanemab in Early Alzheimer's Disease. *N Engl J Med* (2022).
193. Walsh, D.M. et al. Naturally secreted oligomers of amyloid beta protein potently inhibit hippocampal long-term potentiation in vivo. *Nature* **416**, 535-9 (2002).
194. Tsui, H.C., Pope, W.B., Kim, C.S. & Klein, W.L. Transient expression of adhesion molecules during chick retinal development. *J Neurobiol* **23**, 720-38 (1992).
195. Wang, H.W. et al. Soluble oligomers of beta amyloid (1-42) inhibit long-term potentiation but not long-term depression in rat dentate gyrus. *Brain Res* **924**, 133-40 (2002).
196. Lacor, P.N. et al. Abeta oligomer-induced aberrations in synapse composition, shape, and density provide a molecular basis for loss of connectivity in Alzheimer's disease. *J Neurosci* **27**, 796-807 (2007).
197. De Felice, F.G. et al. Alzheimer's disease-type neuronal tau hyperphosphorylation induced by A beta oligomers. *Neurobiol Aging* **29**, 1334-47 (2008).
198. Hu, J., Akama, K.T., Krafft, G.A., Chromy, B.A. & Van Eldik, L.J. Amyloid-beta peptide activates cultured astrocytes: morphological alterations, cytokine induction and nitric oxide release. *Brain Res* **785**, 195-206 (1998).
199. Kim, H.J. et al. Selective neuronal degeneration induced by soluble oligomeric amyloid beta protein. *FASEB J* **17**, 118-20 (2003).
200. Poling, A. et al. Oligomers of the amyloid-beta protein disrupt working memory: confirmation with two behavioral procedures. *Behav Brain Res* **193**, 230-4 (2008).
201. Viola, K.L. et al. The therapeutic and diagnostic potential of amyloid β oligomers selective antibodies to treat Alzheimer's disease. *Front Neurosci* **15**(2022).
202. Kaye, R. et al. Common structure of soluble amyloid oligomers implies common mechanism of pathogenesis. *Science* **300**, 486-9 (2003).
203. Oddo, S. et al. Temporal profile of amyloid-beta (A β) oligomerization in an in vivo model of Alzheimer disease. A link between A β and tau pathology. *J Biol Chem* **281**, 1599-604 (2006).
204. Lacor, P.N. et al. Synaptic targeting by Alzheimer's-related amyloid beta oligomers. *J Neurosci* **24**, 10191-200 (2004).
205. Krafft, G.A., Jerecic, J., Siemers, E. & Cline, E.N. ACU193: An immunotherapeutic poised to test the amyloid β oligomer hypothesis of Alzheimer's disease. *Front Neurosci* **16**, 848215 (2022).
206. Arispe, N., Pollard, H.B. & Rojas, E. Giant multilevel cation channels formed by Alzheimer disease amyloid beta-protein [A beta P-(1-40)] in bilayer membranes. *Proc Natl Acad Sci U S A* **90**, 10573-7 (1993).
207. Arispe, N., Rojas, E. & Pollard, H.B. Alzheimer disease amyloid beta protein forms calcium channels in bilayer membranes: blockade by tromethamine and aluminum. *Proc Natl Acad Sci U S A* **90**, 567-71 (1993).
208. Kawahara, M., Kuroda, Y., Arispe, N. & Rojas, E. Alzheimer's beta-amyloid, human islet amylin, and prion protein fragment evoke intracellular free calcium elevations by a common mechanism in a hypothalamic GnRH neuronal cell line. *J Biol Chem* **275**, 14077-83 (2000).
209. Demuro, A., Smith, M. & Parker, I. Single-channel Ca(2+) imaging implicates A β 1-42 amyloid pores in Alzheimer's disease pathology. *J Cell Biol* **195**, 515-24 (2011).

210. Demuro, A. et al. Calcium dysregulation and membrane disruption as a ubiquitous neurotoxic mechanism of soluble amyloid oligomers. *J Biol Chem* **280**, 17294-300 (2005).
211. Saura, C.A., Deprada, A., Capilla-López, M.D. & Parra-Damas, A. Revealing cell vulnerability in Alzheimer's disease by single-cell transcriptomics. *Semin Cell Dev Biol* (2022).
212. Leng, K. et al. Molecular characterization of selectively vulnerable neurons in Alzheimer's disease. *Nat Neurosci* **24**, 276-287 (2021).
213. Renner, M. et al. Deleterious effects of amyloid beta oligomers acting as an extracellular scaffold for mGluR5. *Neuron* **66**, 739-54 (2010).
214. Decker, H. et al. N-methyl-D-aspartate receptors are required for synaptic targeting of Alzheimer's toxic amyloid- β peptide oligomers. *J Neurochem* **115**, 1520-9 (2010).
215. Kudo, W. et al. Cellular prion protein is essential for oligomeric amyloid- β -induced neuronal cell death. *Hum Mol Genet* **21**, 1138-1144 (2012).
216. De Felice, F.G. et al. A β oligomers induce neuronal oxidative stress through an N-methyl-D-aspartate receptor-dependent mechanism that is blocked by the Alzheimer drug memantine. *J Biol Chem* **282**, 11590-601 (2007).
217. Newcomer, J.W., Farber, N.B. & Olney, J.W. NMDA receptor function, memory, and brain aging. *Dialogues Clin Neurosci* **2**, 219-32 (2000).
218. Arbel-Ornath, M. et al. Soluble oligomeric amyloid- β induces calcium dyshomeostasis that precedes synapse loss in the living mouse brain. *Mol Neurodegener* **12**, 27 (2017).
219. Shankar, G.M. et al. Natural oligomers of the Alzheimer amyloid-beta protein induce reversible synapse loss by modulating an NMDA-type glutamate receptor-dependent signaling pathway. *J Neurosci* **27**, 2866-75 (2007).
220. Yamin, G. NMDA receptor-dependent signaling pathways that underlie amyloid beta-protein disruption of LTP in the hippocampus. *J Neurosci Res* **87**, 1729-36 (2009).
221. Taniguchi, K. et al. Amyloid- β oligomers interact with NMDA receptors containing GluN2B subunits and metabotropic glutamate receptor 1 in primary cortical neurons: Relevance to the synapse pathology of Alzheimer's disease. *Neurosci Res* **180**, 90-98 (2022).
222. Rammes, G., Hasenjäger, A., Sroka-Saidi, K., Deussing, J.M. & Parsons, C.G. Therapeutic significance of NR2B-containing NMDA receptors and mGluR5 metabotropic glutamate receptors in mediating the synaptotoxic effects of β -amyloid oligomers on long-term potentiation (LTP) in murine hippocampal slices. *Neuropharmacology* **60**, 982-990 (2011).
223. Brody, A.H. & Strittmatter, S.M. Synaptotoxic Signaling by Amyloid Beta Oligomers in Alzheimer's Disease Through Prion Protein and mGluR5. *Adv Pharmacol* **82**, 293-323 (2018).
224. Laurén, J., Gimbel, D.A., Nygaard, H.B., Gilbert, J.W. & Strittmatter, S.M. Cellular prion protein mediates impairment of synaptic plasticity by amyloid-beta oligomers. *Nature* **457**, 1128-32 (2009).
225. Wulf, M.-A., Senatore, A. & Aguzzi, A. The biological function of the cellular prion protein: an update. *BMC Biology* **15**, 34 (2017).
226. Um, J.W. et al. Alzheimer amyloid- β oligomer bound to postsynaptic prion protein activates Fyn to impair neurons. *Nat Neurosci* **15**, 1227-1235 (2012).
227. Jeong, J.K. & Park, S.Y. Neuroprotective effect of cellular prion protein (PrPC) is related with activation of alpha7 nicotinic acetylcholine receptor (α 7nAChR)-mediated autophagy flux. *Oncotarget* **6**, 24660-74 (2015).
228. Haas, L.T. & Strittmatter, S.M. Oligomers of Amyloid β Prevent Physiological Activation of the Cellular Prion Protein-Metabotropic Glutamate Receptor 5 Complex by Glutamate in Alzheimer Disease. *J Biol Chem* **291**, 17112-21 (2016).

229. Carulla, P. et al. Neuroprotective role of PrPC against kainate-induced epileptic seizures and cell death depends on the modulation of JNK3 activation by GluR6/7-PSD-95 binding. *Mol Biol Cell* **22**, 3041-54 (2011).
230. Zhang, Y. et al. Cellular prion protein as a receptor of toxic amyloid- β 42 oligomers is important for Alzheimer's disease. *Front Cell Neurosci* **13**, 339 (2019).
231. Hamilton, A., Zamponi, G.W. & Ferguson, S.S.G. Glutamate receptors function as scaffolds for the regulation of β -amyloid and cellular prion protein signaling complexes. *Mol Brain* **8**, 18 (2015).
232. Rushworth, J.V., Griffiths, H.H., Watt, N.T. & Hooper, N.M. Prion protein-mediated toxicity of amyloid- β oligomers requires lipid rafts and the transmembrane LRP1. *J Biol Chem* **288**, 8935-51 (2013).
233. Ohnishi, T. et al. Na, K-ATPase α 3 is a death target of Alzheimer patient amyloid- β assembly. *Proc Natl Acad Sci U S A* **112**, E4465-74 (2015).
234. Komura, H. et al. Alzheimer A β Assemblies Accumulate in Excitatory Neurons upon Proteasome Inhibition and Kill Nearby NAK α 3 Neurons by Secretion. *iScience* **13**, 452-477 (2019).
235. Petrushanko, I.Y. et al. Na,K-ATPase acts as a beta-amyloid receptor triggering Src kinase activation. *Cells* **11**(2022).
236. Sasahara, T., Satomura, K., Tada, M., Kakita, A. & Hoshi, M. Alzheimer's A β assembly binds sodium pump and blocks endothelial NOS activity via ROS-PKC pathway in brain vascular endothelial cells. *iScience* **24**, 102936 (2021).
237. DiChiara, T. et al. Alzheimer's toxic amyloid beta oligomers: unwelcome visitors to the Na/K ATPase alpha3 docking station. *Yale J Biol Med* **90**, 45-61 (2017).
238. Townsend, M., Mehta, T. & Selkoe, D.J. Soluble Abeta inhibits specific signal transduction cascades common to the insulin receptor pathway. *J Biol Chem* **282**, 33305-33312 (2007).
239. Zhao, W.Q. et al. Amyloid beta oligomers induce impairment of neuronal insulin receptors. *FASEB J* **22**, 246-60 (2008).
240. De Felice, F.G. et al. Protection of synapses against Alzheimer's-linked toxins: insulin signaling prevents the pathogenic binding of Abeta oligomers. *Proc Natl Acad Sci U S A* **106**, 1971-6 (2009).
241. Zhao, W.-Q. et al. Insulin receptor dysfunction impairs cellular clearance of neurotoxic oligomeric A β . *J Biol Chem* **284**, 18742-18753 (2009).
242. Batista, A.F. et al. The diabetes drug liraglutide reverses cognitive impairment in mice and attenuates insulin receptor and synaptic pathology in a non-human primate model of Alzheimer's disease. *J Pathol* **245**, 85-100 (2018).
243. Magdesian, M.H. et al. Amyloid-beta binds to the extracellular cysteine-rich domain of Frizzled and inhibits Wnt/beta-catenin signaling. *J Biol Chem* **283**, 9359-68 (2008).
244. Dann, C.E. et al. Insights into Wnt binding and signalling from the structures of two Frizzled cysteine-rich domains. *Nature* **412**, 86-90 (2001).
245. Gordon, M.D. & Nusse, R. Wnt signaling: multiple pathways, multiple receptors, and multiple transcription factors. *J Biol Chem* **281**, 22429-33 (2006).
246. Yaar, M. et al. Binding of beta-amyloid to the p75 neurotrophin receptor induces apoptosis. A possible mechanism for Alzheimer's disease. *J Clin Invest* **100**, 2333-40 (1997).
247. Tsukamoto, E. et al. Characterization of the toxic mechanism triggered by Alzheimer's amyloid-beta peptides via p75 neurotrophin receptor in neuronal hybrid cells. *J Neurosci Res* **73**, 627-36 (2003).
248. Costantini, C. et al. Characterization of the signaling pathway downstream p75 neurotrophin receptor involved in beta-amyloid peptide-dependent cell death. *J Mol Neurosci* **25**, 141-56 (2005).

249. Patnaik, A., Zagrebelsky, M., Korte, M. & Holz, A. Signaling via the p75 neurotrophin receptor facilitates amyloid- β -induced dendritic spine pathology. *Sci Rep* **10**, 13322 (2020).
250. Yang, T., Tran, K.C., Zeng, A.Y., Massa, S.M. & Longo, F.M. Small molecule modulation of the p75 neurotrophin receptor inhibits multiple amyloid beta-induced tau pathologies. *Sci Rep* **10**, 20322 (2020).
251. Zhao, W.Q. et al. Inhibition of calcineurin-mediated endocytosis and alpha-amino-3-hydroxy-5-methyl-4-isoxazolepropionic acid (AMPA) receptors prevents amyloid beta oligomer-induced synaptic disruption. *J Biol Chem* **285**, 7619-32 (2010).
252. Zhao, D., Watson, J.B. & Xie, C.W. Amyloid beta prevents activation of calcium/calmodulin-dependent protein kinase II and AMPA receptor phosphorylation during hippocampal long-term potentiation. *J Neurophysiol* **92**, 2853-8 (2004).
253. Nagele, R.G., D'Andrea, M.R., Anderson, W.J. & Wang, H.Y. Intracellular accumulation of beta-amyloid(1-42) in neurons is facilitated by the alpha 7 nicotinic acetylcholine receptor in Alzheimer's disease. *Neuroscience* **110**, 199-211 (2002).
254. Wang, H.Y. et al. Beta-Amyloid(1-42) binds to alpha7 nicotinic acetylcholine receptor with high affinity: Implications for Alzheimer's disease pathology. *J Biol Chem* **275**, 5626-32 (2000).
255. Oddo, S. et al. Chronic nicotine administration exacerbates tau pathology in a transgenic model of Alzheimer's disease. *Proc Natl Acad Sci U S A* **102**, 3046-51 (2005).
256. Hernandez, C.M., Kaye, R., Zheng, H., Sweatt, J.D. & Dineley, K.T. Loss of alpha7 nicotinic receptors enhances beta-amyloid oligomer accumulation, exacerbating early-stage cognitive decline and septohippocampal pathology in a mouse model of Alzheimer's disease. *J Neurosci* **30**, 2442-53 (2010).
257. Yang, A.J., Chandswangbhuvana, D., Shu, T., Henschen, A. & Glabe, C.G. Intracellular accumulation of insoluble, newly synthesized A β _n-42 in amyloid precursor protein-transfected cells that have been treated with A β ₁₋₄₂*. *J Biol Chem* **274**, 20650-20656 (1999).
258. Burdick, D., Kosmoski, J., Knauer, M.F. & Glabe, C.G. Preferential adsorption, internalization and resistance to degradation of the major isoform of the Alzheimer's amyloid peptide, A beta 1-42, in differentiated PC12 cells. *Brain Res* **746**, 275-84 (1997).
259. Bahr, B.A. et al. Amyloid beta protein is internalized selectively by hippocampal field CA1 and causes neurons to accumulate amyloidogenic carboxyterminal fragments of the amyloid precursor protein. *J Comp Neurol* **397**, 139-47 (1998).
260. Yu, C., Nwabuisi-Heath, E., Laxton, K. & LaDu, M.J. Endocytic pathways mediating oligomeric A β ₄₂ neurotoxicity. *Mol Neurodegener* **5**, 19 (2010).
261. D'Andrea, M.R., Nagele, R.G., Wang, H.Y., Peterson, P.A. & Lee, D.H. Evidence that neurones accumulating amyloid can undergo lysis to form amyloid plaques in Alzheimer's disease. *Histopathology* **38**, 120-34 (2001).
262. Glabe, C. Intracellular mechanisms of amyloid accumulation and pathogenesis in Alzheimer's disease. *J Mol Neurosci* **17**, 137-45 (2001).
263. Weller, J. & Budson, A. Current understanding of Alzheimer's disease diagnosis and treatment. *F1000Res* **7**(2018).
264. Mukhopadhyay, S. & Banerjee, D. A primer on the evolution of aducanumab: the first antibody approved for treatment of Alzheimer's disease. *J Alzheimers Dis* **83**, 1537-1552 (2021).
265. Kocis, P. et al. Elucidating the abeta42 anti-aggregation mechanism of action of tramiprosate in Alzheimer's disease: integrating molecular analytical methods, pharmacokinetic and clinical data. *CNS Drugs* **31**, 495-509 (2017).
266. Sabbagh, M.N. Clinical effects of oral tramiprosate in APOE4/4 homozygous patients with mild Alzheimer's disease suggest disease modification. *J Prev Alzheimers Dis* **4**, 136-137 (2017).

267. Park, S.Y. et al. Cilostazol modulates autophagic degradation of β -amyloid peptide via SIRT1-coupled LKB1/AMPK α signaling in neuronal cells. *PLoS One* **11**, e0160620 (2016).
268. Ono, K. & Tsuji, M. Pharmacological potential of cilostazol for Alzheimer's disease. *Front Pharmacol* **10**, 559 (2019).
269. Taguchi, A. et al. Cilostazol improves cognitive function in patients with mild cognitive impairment: a retrospective analysis. *Psychogeriatrics* **13**, 164-9 (2013).
270. Tolar, M., Abushakra, S., Hey, J.A., Porsteinsson, A. & Sabbagh, M. Aducanumab, gantenerumab, BAN2401, and ALZ-801—the first wave of amyloid-targeting drugs for Alzheimer's disease with potential for near term approval. *Alz Res Ther* **12**, 95 (2020).
271. Cummings, J. et al. Alzheimer's disease drug development pipeline: 2022. *Alzheimers Dement (NY)* **8**, e12295 (2022).
272. Woloshin, S. & Kesselheim, A.S. What to know about the Alzheimer drug aducanumab (Aduhelm). *JAMA Internal Medicine* **182**, 892-892 (2022).
273. Mintun, M.A. et al. Donanemab in early Alzheimer's disease. *N Engl J Med* **384**, 1691-1704 (2021).
274. Bayer, T.A. Pyroglutamate A β cascade as drug target in Alzheimer's disease. *Mol Psychiatry* **27**, 1880-1885 (2022).
275. Bohrmann, B. et al. Gantenerumab: a novel human anti-A β antibody demonstrates sustained cerebral amyloid- β binding and elicits cell-mediated removal of human amyloid- β . *J Alzheimers Dis* **28**, 49-69 (2012).
276. Wang, C.Y. et al. UB-311, a novel UBITH[®] amyloid β peptide vaccine for mild Alzheimer's disease. *Alzheimers Dement (N Y)* **3**, 262-272 (2017).
277. Rishton, G.M. et al. Discovery of investigational drug CT1812, an antagonist of the sigma-2 receptor complex for Alzheimer's disease. *ACS Med Chem Lett* **12**, 1389-1395 (2021).
278. Abstract: 15th Conference Clinical Trials Alzheimer's Disease, November 29- December 2, 2022, San Francisco, USA: Symposia - Oral Communications - Late Breaking News. *J Prev Alzheimers Dis* **9**, S8-s50 (2022).
279. Hori, Y. et al. A Food and Drug Administration-approved asthma therapeutic agent impacts amyloid β in the brain in a transgenic model of Alzheimer disease. *J Biol Chem* **290**, 1966-78 (2015).
280. Ngo, S.T., Truong, D.T., Tam, N.M. & Nguyen, M.T. EGCG inhibits the oligomerization of amyloid beta (16-22) hexamer: Theoretical studies. *J Mol Graph Model* **76**, 1-10 (2017).
281. Ryan, T.M. et al. Stabilization of nontoxic A β -oligomers: insights into the mechanism of action of hydroxyquinolines in Alzheimer's disease. *J Neurosci* **35**, 2871-84 (2015).
282. Kutzsche, J. et al. Safety and pharmacokinetics of the orally available antiprionic compound PRI-002: A single and multiple ascending dose phase I study. *Alzheimers Dement (N Y)* **6**, e12001 (2020).
283. Vijverberg, E.G.B. et al. Rationale and study design of a randomized, placebo-controlled, double-blind phase 2b trial to evaluate efficacy, safety, and tolerability of an oral glutaminyl cyclase inhibitor varoglutamstat (PQ912) in study participants with MCI and mild AD—VIVIAD. *Alzheimers Res Ther* **13**, 142 (2021).
284. Figueiredo, C.P. et al. Memantine rescues transient cognitive impairment caused by high-molecular-weight abeta oligomers but not the persistent impairment induced by low-molecular-weight oligomers. *J Neurosci* **33**, 9626-34 (2013).
285. Zhang, Y.-J., Xu, Y.-F., Liu, Y.-H., Yin, J. & Wang, J.-Z. Nitric oxide induces tau hyperphosphorylation via glycogen synthase kinase-3 β activation. *FEBS Lett* **579**, 6230-6236 (2005).
286. Zahid, S., Khan, R., Oellerich, M., Ahmed, N. & Asif, A.R. Differential S-nitrosylation of proteins in Alzheimer's disease. *Neuroscience* **256**, 126-36 (2014).

287. Qu, J. et al. S-Nitrosylation activates Cdk5 and contributes to synaptic spine loss induced by β -amyloid peptide. *Proc Natl Acad Sci U S A* **108**, 14330-14335 (2011).
288. Uehara, T. et al. S-Nitrosylated protein-disulphide isomerase links protein misfolding to neurodegeneration. *Nature* **441**, 513-517 (2006).
289. Lee, M.-C. et al. Zinc ion rapidly induces toxic, off-pathway amyloid- β oligomers distinct from amyloid- β derived diffusible ligands in Alzheimer's disease. *Sci Reports* **8**, 4772 (2018).
290. Bossy-Wetzel, E. et al. Crosstalk between nitric oxide and zinc pathways to neuronal cell death involving mitochondrial dysfunction and p38-activated K⁺ channels. *Neuron* **41**, 351-365 (2004).
291. Modica, J.A., Skarpathiotis, S. & Mrksich, M. Modular assembly of protein building blocks to create precisely defined megamolecules. *Chembiochem* **13**, 2331-4 (2012).
292. Modica, J.A., Iderzorig, T. & Mrksich, M. Design and synthesis of megamolecule mimics of a therapeutic antibody. *J Am Chem Soc* **142**, 13657-13661 (2020).
293. Kimmel, B.R., Modica, J.A., Parker, K., Dravid, V. & Mrksich, M. Solid-phase synthesis of megamolecules. *J Am Chem Soc* **142**, 4534-4538 (2020).
294. Frackowiak, J., Zoltowska, A. & Wisniewski, H.M. Non-fibrillar beta-amyloid protein is associated with smooth muscle cells of vessel walls in Alzheimer disease. *J Neuropathol Exp Neurol* **53**, 637-45 (1994).
295. Kim, Y. et al. Comparative analyses of plasma amyloid-B; levels in heterogeneous and monomerized states by interdigitated microelectrode sensor system. *Sci Adv* **5**, eaav1388 (2019).
296. Tomiyama, T. et al. A mouse model of amyloid β oligomers: their contribution to synaptic alteration, abnormal tau phosphorylation, glial activation, and neuronal loss in vivo. *J Neurosci* **30**, 4845 (2010).
297. Gandy, S. et al. Days to criterion as an indicator of toxicity associated with human Alzheimer amyloid-beta oligomers. *Ann Neurol* **68**, 220-30 (2010).
298. Xiao, C. et al. Brain transit and ameliorative effects of intranasally delivered anti-amyloid- β oligomer antibody in 5XFAD mice. *J Alzheimers Dis* **35**, 777-88 (2013).
299. Zhao, M. et al. Pan-amyloid oligomer specific scFv antibody attenuates memory deficits and brain amyloid burden in mice with Alzheimer's disease. *Curr Alzheimer Res* **11**, 69-78 (2014).
300. Ross, C.A. & Poirier, M.A. Protein aggregation and neurodegenerative disease. *Nat Med* **10 Suppl**, S10-7 (2004).
301. Gadad, B.S., Britton, G.B. & Rao, K.S. Targeting oligomers in neurodegenerative disorders: lessons from α -synuclein, tau, and amyloid- β peptide. *J Alzheimers Dis* **24 Suppl 2**, 223-32 (2011).
302. Prudencio, M., Hart, P.J., Borchelt, D.R. & Andersen, P.M. Variation in aggregation propensities among ALS-associated variants of SOD1: correlation to human disease. *Hum Mol Genet* **18**, 3217-26 (2009).
303. Benkler, C. et al. Aggregated SOD1 causes selective death of cultured human motor neurons. *Sci Rep* **8**, 16393 (2018).
304. Johnson, B.S. et al. TDP-43 is intrinsically aggregation-prone, and amyotrophic lateral sclerosis-linked mutations accelerate aggregation and increase toxicity. *J Biol Chem* **284**, 20329-39 (2009).
305. Ravits, J.M. & La Spada, A.R. ALS motor phenotype heterogeneity, focality, and spread: deconstructing motor neuron degeneration. *Neurology* **73**, 805-811 (2009).
306. Zhang, W. et al. Cyclohexane 1,3-diones and their inhibition of mutant SOD1-dependent protein aggregation and toxicity in PC12 cells. *Bioorg Med Chem* **20**, 1029-1045 (2012).
307. Genç, B. et al. Improving mitochondria and ER stability helps eliminate upper motor neuron degeneration that occurs due to mSOD1 toxicity and TDP-43 pathology. *Clin Transl Med* **11**, e336 (2021).

308. LeVine III, H. Alzheimer's β -peptide oligomer formation at physiologic concentrations. *Anal Biochem* **335**, 81-90 (2004).
309. Zhang, Y. et al. Chiral cyclohexane 1,3-diones as inhibitors of mutant SOD1-dependent protein aggregation for the treatment of ALS. *ACS Med Chem Lett* **3**, 584-587 (2012).
310. Lambert, M.P. et al. Vaccination with soluble Abeta oligomers generates toxicity-neutralizing antibodies. *J Neurochem* **79**, 595-605 (2001).
311. Velasco, P.T. et al. Synapse-binding subpopulations of A β oligomers sensitive to peptide assembly blockers and scFv antibodies. *ACS Chem Neurosci* **3**, 972-981 (2012).
312. Wang, X. et al. An acute functional screen identifies an effective antibody targeting amyloid- β oligomers based on calcium imaging. *Sci Rep* **8**, 4634 (2018).
313. Hernandez-Guillamon, M. et al. Sequential Amyloid- β Degradation by the Matrix Metalloproteases MMP-2 and MMP-9. *J Biol Chem* **290**, 15078-15091 (2015).
314. Marshall, K.E., Vadukul, D.M., Staras, K. & Serpell, L.C. Misfolded amyloid- β -42 impairs the endosomal-lysosomal pathway. *Cell Mol Life Sci* **77**, 5031-5043 (2020).
315. Wesén, E., Jeffries, G.D.M., Matson Dzebo, M. & Esbjörner, E.K. Endocytic uptake of monomeric amyloid- β peptides is clathrin- and dynamin-independent and results in selective accumulation of A β (1-42) compared to A β (1-40). *Sci Rep* **7**, 2021 (2017).
316. Lopez Salon, M., Pasquini, L., Besio Moreno, M., Pasquini, J.M. & Soto, E. Relationship between beta-amyloid degradation and the 26S proteasome in neural cells. *Exp Neurol* **180**, 131-43 (2003).
317. Schmitz, A., Schneider, A., Kummer, M.P. & Herzog, V. Endoplasmic reticulum-localized amyloid beta-peptide is degraded in the cytosol by two distinct degradation pathways. *Traffic* **5**, 89-101 (2004).
318. Dasuri, K. et al. Selective vulnerability of neurons to acute toxicity after proteasome inhibitor treatment: implications for oxidative stress and insolubility of newly synthesized proteins. *Free Radic Biol Med* **49**, 1290-1297 (2010).
319. Spilman, P. et al. Inhibition of mTOR by rapamycin abolishes cognitive deficits and reduces amyloid-beta levels in a mouse model of Alzheimer's disease. *PLoS One* **5**, e9979 (2010).
320. Kim, H.N., Seo, B.R., Kim, H. & Koh, J.Y. Cilostazol restores autophagy flux in bafilomycin A1-treated, cultured cortical astrocytes through lysosomal reacidification: roles of PKA, zinc and metallothionein 3. *Sci Rep* **10**, 9175 (2020).
321. Yoshiyama, Y., Arai, K., Oki, T. & Hattori, T. Expression of invariant chain and pro-cathepsin L in Alzheimer's brain. *Neurosci Lett* **290**, 125-8 (2000).
322. Islam, M.I. et al. Regulatory role of cathepsin L in induction of nuclear laminopathy in Alzheimer's disease. *Aging Cell* **21**, e13531 (2022).
323. Boland, B. & Campbell, V. Abeta-mediated activation of the apoptotic cascade in cultured cortical neurones: a role for cathepsin-L. *Neurobiol Aging* **25**, 83-91 (2004).
324. Cataldo, A.M. & Nixon, R.A. Enzymatically active lysosomal proteases are associated with amyloid deposits in Alzheimer brain. *Proc Natl Acad Sci U S A* **87**, 3861-5 (1990).
325. Cataldo, A.M., Barnett, J.L., Pieroni, C. & Nixon, R.A. Increased neuronal endocytosis and protease delivery to early endosomes in sporadic Alzheimer's disease: neuropathologic evidence for a mechanism of increased beta-amyloidogenesis. *J Neurosci* **17**, 6142-51 (1997).
326. Hook, V. et al. Inhibition of cathepsin B reduces beta-amyloid production in regulated secretory vesicles of neuronal chromaffin cells: evidence for cathepsin B as a candidate beta-secretase of Alzheimer's disease. *Biol Chem* **386**, 931-40 (2005).
327. Mueller-Stainer, S. et al. Anti-amyloidogenic and neuroprotective functions of cathepsin B: implications for Alzheimer's disease. *Neuron* **51**, 703-14 (2006).

328. Embury, C.M. et al. Cathepsin B improves β -amyloidosis and learning and memory in models of Alzheimer's disease. *J Neuroimmune Pharmacol* **12**, 340-352 (2017).
329. Hwang, J. et al. The role of lysosomes in a broad disease-modifying approach evaluated across transgenic mouse models of Alzheimer's disease and Parkinson's disease and models of mild cognitive impairment. *Int J Mol Sci* **20**(2019).
330. Hook, V.Y., Kindy, M. & Hook, G. Inhibitors of cathepsin B improve memory and reduce beta-amyloid in transgenic Alzheimer disease mice expressing the wild-type, but not the Swedish mutant, beta-secretase site of the amyloid precursor protein. *J Biol Chem* **283**, 7745-53 (2008).
331. Hook, G., Yu, J., Toneff, T., Kindy, M. & Hook, V. Brain pyroglutamate amyloid- β is produced by cathepsin B and is reduced by the cysteine protease inhibitor E64d, representing a potential Alzheimer's disease therapeutic. *J Alzheimers Dis* **41**, 129-149 (2014).
332. Oakley, H. et al. Intraneuronal beta-amyloid aggregates, neurodegeneration, and neuron loss in transgenic mice with five familial Alzheimer's disease mutations: potential factors in amyloid plaque formation. *J Neurosci* **26**, 10129-40 (2006).
333. Forner, S. et al. Systematic phenotyping and characterization of the 5xFAD mouse model of Alzheimer's disease. *Sci Data* **8**, 270 (2021).
334. Fang, Y.-S. et al. Full-length TDP-43 forms toxic amyloid oligomers that are present in frontotemporal lobar dementia-TDP patients. *Nat Commun* **5**, 4824 (2014).
335. Proctor, E.A. et al. Nonnative SOD1 trimer is toxic to motor neurons in a model of amyotrophic lateral sclerosis. *Proc Natl Acad Sci U S A* **113**, 614-9 (2016).
336. Nonaka, T. et al. Prion-like properties of pathological TDP-43 aggregates from diseased brains. *Cell Rep* **4**, 124-34 (2013).
337. Münch, C., O'Brien, J. & Bertolotti, A. Prion-like propagation of mutant superoxide dismutase-1 misfolding in neuronal cells. *Proc Natl Acad Sci U S A* **108**, 3548-3553 (2011).
338. Cataldo, A.M. et al. Endocytic pathway abnormalities precede amyloid beta deposition in sporadic Alzheimer's disease and Down syndrome: differential effects of APOE genotype and presenilin mutations. *Am J Pathol* **157**, 277-286 (2000).
339. Van Acker, Z.P., Bretou, M. & Annaert, W. Endo-lysosomal dysregulations and late-onset Alzheimer's disease: impact of genetic risk factors. *Mol Neurodegener* **14**, 20 (2019).
340. Soura, V. et al. Visualization of co-localization in A β 42-administered neuroblastoma cells reveals lysosome damage and autophagosome accumulation related to cell death. *Biochem J* **441**, 579-90 (2012).
341. Grbovic, O.M. et al. Rab5-stimulated up-regulation of the endocytic pathway increases intracellular beta-cleaved amyloid precursor protein carboxyl-terminal fragment levels and Abeta production. *J Biol Chem* **278**, 31261-8 (2003).
342. Bertram, L., McQueen, M.B., Mullin, K., Blacker, D. & Tanzi, R.E. Systematic meta-analyses of Alzheimer disease genetic association studies: the AlzGene database. *Nat Genet* **39**, 17-23 (2007).
343. Rogaeva, E. et al. The neuronal sortilin-related receptor SORL1 is genetically associated with Alzheimer disease. *Nat Genet* **39**, 168-77 (2007).
344. Harold, D. et al. Genome-wide association study identifies variants at CLU and PICALM associated with Alzheimer's disease. *Nat Genet* **41**, 1088-93 (2009).
345. Hollingworth, P. et al. Common variants at ABCA7, MS4A6A/MS4A4E, EPHA1, CD33 and CD2AP are associated with Alzheimer's disease. *Nat Genet* **43**, 429-35 (2011).
346. Naj, A.C. et al. Common variants at MS4A4/MS4A6E, CD2AP, CD33 and EPHA1 are associated with late-onset Alzheimer's disease. *Nat Genet* **43**, 436-41 (2011).
347. Wang, C., Sun, B., Zhou, Y., Grubb, A. & Gan, L. Cathepsin B degrades amyloid- β in mice expressing wild-type human amyloid precursor protein. *J Biol Chem* **287**, 39834-41 (2012).

348. Wandinger-Ness, A. & Zerial, M. Rab proteins and the compartmentalization of the endosomal system. *Cold Spring Harb Perspect Biol* **6**, a022616 (2014).
349. Zhang, J., Jiang, Z. & Shi, A. Rab GTPases: The principal players in crafting the regulatory landscape of endosomal trafficking. *Comput Struct Biotechnol J* **20**, 4464-4472 (2022).
350. Gowrishankar, S., Wu, Y. & Ferguson, S.M. Impaired JIP3-dependent axonal lysosome transport promotes amyloid plaque pathology. *J Cell Biol* **216**, 3291-3305 (2017).
351. Jordens, I. et al. The Rab7 effector protein RILP controls lysosomal transport by inducing the recruitment of dynein-dynactin motors. *Curr Biol* **11**, 1680-5 (2001).
352. Ghosh, P., Dahms, N.M. & Kornfeld, S. Mannose 6-phosphate receptors: new twists in the tale. *Nat Rev Mol Cell Biol* **4**, 202-213 (2003).
353. Saido, T. & Leissring, M.A. Proteolytic degradation of amyloid β -protein. *Cold Spring Harb Perspect Med* **2**, a006379 (2012).
354. Pacheco-Quinto, J. et al. Intracellular metalloprotease activity controls intraneuronal A β aggregation and limits secretion of A β via exosomes. *FASEB J* **33**, 3758-3771 (2019).
355. Nackenoff, A.G. et al. PLD3 is a neuronal lysosomal phospholipase D associated with β -amyloid plaques and cognitive function in Alzheimer's disease. *PLoS Genet* **17**, e1009406 (2021).
356. Schneider, A., Schulz-Schaeffer, W., Hartmann, T., Schulz, J.B. & Simons, M. Cholesterol depletion reduces aggregation of amyloid-beta peptide in hippocampal neurons. *Neurobiol Dis* **23**, 573-7 (2006).
357. Oberstein, T.J. et al. The role of cathepsin B in the degradation of A β and in the production of A β peptides starting with ala2 in cultured astrocytes. *Front Mol Neurosci* **13**, 615740 (2020).
358. Pitt, J. et al. Neuroprotective astrocyte-derived insulin/insulin-like growth factor 1 stimulates endocytic processing and extracellular release of neuron-bound A β oligomers. *Mol Biol Cell* **28**, 2623-2636 (2017).
359. Kapasi, A., DeCarli, C. & Schneider, J.A. Impact of multiple pathologies on the threshold for clinically overt dementia. *Acta Neuropathol* **134**, 171-186 (2017).
360. Brewer, G.J., Torricelli, J.R., Evege, E.K. & Price, P.J. Optimized survival of hippocampal neurons in B27-supplemented Neurobasal, a new serum-free medium combination. *J Neurosci Res* **35**, 567-76 (1993).
361. Brewer, G.J. & Price, P.J. Viable cultured neurons in ambient carbon dioxide and hibernation storage for a month. *Neuroreport* **7**, 1509-12 (1996).
362. Sigma-Aldrich. Enzymatic Assay of Cathepsin B. Vol. 2022 (Sigma-Aldrich).
363. Barrett, A.J. Fluorimetric assays for cathepsin B and cathepsin H with methylcoumarylamide substrates. *Biochem J* **187**, 909-12 (1980).
364. Barrett, A.J. & Kirschke, H. Cathepsin B, Cathepsin H, and cathepsin L. *Methods Enzymol* **80 Pt C**, 535-61 (1981).
365. Mason, R.W., Green, G.D. & Barrett, A.J. Human liver cathepsin L. *Biochem J* **226**, 233-41 (1985).
366. Save, E., Poucet, B., Foreman, N. & Buhot, M.C. Object exploration and reactions to spatial and nonspatial changes in hooded rats following damage to parietal cortex or hippocampal formation. *Behav Neurosci* **106**, 447-56 (1992).
367. Bicca, M.A. et al. B₂ receptor blockage prevents A β -induced cognitive impairment by neuroinflammation inhibition. *Behav Brain Res* **278**, 482-91 (2015).
368. Hyman, B.T. et al. National Institute on Aging-Alzheimer's Association guidelines for the neuropathologic assessment of Alzheimer's disease. *Alzheimers Dement* **8**, 1-13 (2012).
369. Jack, C.R., Jr. et al. Serial PIB and MRI in normal, mild cognitive impairment and Alzheimer's disease: implications for sequence of pathological events in Alzheimer's disease. *Brain* **132**, 1355-65 (2009).

370. Smith, M.A., Richey Harris, P.L., Sayre, L.M., Beckman, J.S. & Perry, G. Widespread peroxynitrite-mediated damage in Alzheimer's disease. *J Neurosci* **17**, 2653-7 (1997).
371. Chen, G.-f. et al. Amyloid beta: structure, biology and structure-based therapeutic development. *Acta Pharmacol Sin* **38**, 1205-1235 (2017).
372. Viola, K.L. & Klein, W.L. Amyloid beta oligomers in Alzheimer's disease pathogenesis, treatment, and diagnosis. *Acta Neuropathol* **129**, 183-206 (2015).
373. Sackmann, C. & Hallbeck, M. Oligomeric amyloid- β induces early and widespread changes to the proteome in human iPSC-derived neurons. *Sci Rep* **10**, 6538 (2020).
374. Ramesh, M., Gopinath, P. & Govindaraju, T. Role of post-translational modifications in Alzheimer's disease. *Chembiochem* **21**, 1052-1079 (2020).
375. Zempel, H., Thies, E., Mandelkow, E. & Mandelkow, E.M. Abeta oligomers cause localized Ca(2+) elevation, missorting of endogenous Tau into dendrites, Tau phosphorylation, and destruction of microtubules and spines. *J Neurosci* **30**, 11938-50 (2010).
376. Jho, Y.S., Zhulina, E.B., Kim, M.W. & Pincus, P.A. Monte carlo simulations of tau proteins: effect of phosphorylation. *Biophys J* **99**, 2387-97 (2010).
377. Li, C. & Götz, J. Somatodendritic accumulation of Tau in Alzheimer's disease is promoted by Fyn-mediated local protein translation. *EMBO J* **36**, 3120-3138 (2017).
378. Despres, C. et al. Identification of the Tau phosphorylation pattern that drives its aggregation. *Proc Natl Acad Sci U S A* **114**, 9080-9085 (2017).
379. Hu, W. et al. Hyperphosphorylation determines both the spread and the morphology of tau pathology. *Alzheimers Dement* **12**, 1066-1077 (2016).
380. Bloom, G.S. Amyloid-beta and tau: the trigger and bullet in Alzheimer disease pathogenesis. *JAMA Neurol* **71**, 505-8 (2014).
381. Krüger, L. & Mandelkow, E.M. Tau neurotoxicity and rescue in animal models of human Tauopathies. *Curr Opin Neurobiol* **36**, 52-58 (2016).
382. Kopeikina, K., Hyman, B. & Spires-Jones, T. Soluble forms of tau are toxic in Alzheimer's disease. *Transl Neurosci* **3**, 223-233 (2012).
383. Texidó, L., Martín-Satué, M., Alberdi, E., Solsona, C. & Matute, C. Amyloid β peptide oligomers directly activate NMDA receptors. *Cell Calcium* **49**, 184-190 (2011).
384. Rönicke, R. et al. Early neuronal dysfunction by amyloid β oligomers depends on activation of NR2B-containing NMDA receptors. *Neurobiol Aging* **32**, 2219-2228 (2011).
385. Chakroborty, S., Kim, J., Schneider, C., West, A.R. & Stutzmann, G.E. Nitric oxide signaling is recruited as a compensatory mechanism for sustaining synaptic plasticity in Alzheimer's disease mice. *J Neurosci* **35**, 6893-902 (2015).
386. Ge, M. et al. Role of calcium homeostasis in Alzheimer's disease. *Neuropsychiatr Dis Treat* **18**, 487-498 (2022).
387. Tochio, H. et al. Formation of nNOS/PSD-95 PDZ dimer requires a preformed beta-finger structure from the nNOS PDZ domain. *J Mol Biol* **303**, 359-70 (2000).
388. Arbonés, M.L. et al. Characteristics of nitric oxide synthase type I of rat cerebellar astrocytes. *Glia* **18**, 224-32 (1996).
389. Brenman, J.E. et al. Interaction of nitric oxide synthase with the postsynaptic density protein PSD-95 and alpha1-syntrophin mediated by PDZ domains. *Cell* **84**, 757-67 (1996).
390. Niethammer, M., Kim, E. & Sheng, M. Interaction between the C terminus of NMDA receptor subunits and multiple members of the PSD-95 family of membrane-associated guanylate kinases. *J Neurosci* **16**, 2157-63 (1996).
391. Brown, G.C. & Bal-Price, A. Inflammatory neurodegeneration mediated by nitric oxide, glutamate, and mitochondria. *Mol Neurobiol* **27**, 325-55 (2003).

392. Weissman, B.A., Jones, C.L., Liu, Q. & Gross, S.S. Activation and inactivation of neuronal nitric oxide synthase: characterization of Ca²⁺-dependent [125I]Calmodulin binding. *Eur J Pharmacol* **435**, 9-18 (2002).
393. Garthwaite, J., Charles, S.L. & Chess-Williams, R. Endothelium-derived relaxing factor release on activation of NMDA receptors suggests role as intercellular messenger in the brain. *Nature* **336**, 385-8 (1988).
394. Garthwaite, J. & Boulton, C.L. Nitric oxide signaling in the central nervous system. *Annu Rev Physiol* **57**, 683-706 (1995).
395. Lu, Y.-F., Kandel, E.R. & Hawkins, R.D. Nitric oxide signaling contributes to late-phase LTP and CREB phosphorylation in the hippocampus. *J Neurosci* **19**, 10250 (1999).
396. Ohki, K. et al. Nitric oxide induces c-fos gene expression via cyclic AMP response element binding protein (CREB) phosphorylation in rat retinal pigment epithelium. *Brain Res* **696**, 140-4 (1995).
397. Förstermann, U. & Sessa, W.C. Nitric oxide synthases: regulation and function. *Eur Heart J* **33**, 829-37, 837a-837d (2012).
398. Sunico, C.R., González-Forero, D., Domínguez, G., García-Verdugo, J.M. & Moreno-López, B. Nitric oxide induces pathological synapse loss by a protein kinase G-, Rho kinase-dependent mechanism preceded by myosin light chain phosphorylation. *J Neurosci* **30**, 973-84 (2010).
399. Cao, J. et al. The PSD95–nNOS interface : a target for inhibition of excitotoxic p38 stress-activated protein kinase activation and cell death. *J Cell Biol* **168**, 117-126 (2005).
400. Aarts, M. et al. Treatment of ischemic brain damage by perturbing NMDA receptor- PSD-95 protein interactions. *Science* **298**, 846-50 (2002).
401. Li, W. et al. Synergistic neuroprotection by bis(7)-tacrine via concurrent blockade of N-methyl-D-aspartate receptors and neuronal nitric-oxide synthase. *Mol Pharmacol* **71**, 1258-67 (2007).
402. Thorns, V., Hansen, L. & Masliah, E. nNOS expressing neurons in the entorhinal cortex and hippocampus are affected in patients with Alzheimer's disease. *Exp Neurol* **150**, 14-20 (1998).
403. Norris, P.J., Faull, R.L.M. & Emson, P.C. Neuronal nitric oxide synthase (nNOS) mRNA expression and NADPH-diaphorase staining in the frontal cortex, visual cortex and hippocampus of control and Alzheimer's disease brains. *Mol Brain Res* **41**, 36-49 (1996).
404. Nakamura, T. et al. Aberrant protein S-nitrosylation in neurodegenerative diseases. *Neuron* **78**, 596-614 (2013).
405. Zhao, Q.-F., Yu, J.-T. & Tan, L. S-Nitrosylation in Alzheimer's disease. *Mol Neurobiol* **51**, 268-280 (2015).
406. Dyer, R.R., Ford, K.I. & Robinson, R.A.S. Chapter Twenty-One - The roles of S-nitrosylation and S-glutathionylation in Alzheimer's disease. in *Methods Enzymol*, Vol. 626 (ed. Garcia, B.A.) 499-538 (Academic Press, 2019).
407. Hensley, K. et al. Electrochemical analysis of protein nitrotyrosine and dityrosine in the Alzheimer brain indicates region-specific accumulation. *J Neurosci* **18**, 8126 (1998).
408. Lüth, H.-J., Münch, G. & Arendt, T. Aberrant expression of NOS isoforms in Alzheimer's disease is structurally related to nitrotyrosine formation. *Brain Res* **953**, 135-143 (2002).
409. Zhang, Y. et al. nNOS-CAPON interaction mediates amyloid- β -induced neurotoxicity, especially in the early stages. *Aging Cell* **17**, e12754 (2018).
410. Hashimoto, S. et al. Tau binding protein CAPON induces tau aggregation and neurodegeneration. *Nat Commun* **10**, 2394 (2019).
411. Mukherjee, P., Cinelli, M.A., Kang, S. & Silverman, R.B. Development of nitric oxide synthase inhibitors for neurodegeneration and neuropathic pain. *Chem Soc Rev* **43**, 6814-38 (2014).

412. Cinelli, M.A., Li, H., Chreifi, G., Poulos, T.L. & Silverman, R.B. Nitrile in the hole: discovery of a small auxiliary pocket in neuronal nitric oxide synthase leading to the development of potent and selective 2-aminoquinoline inhibitors. *J Med Chem* **60**, 3958-3978 (2017).
413. Cinelli, M.A. et al. Phenyl ether- and aniline-containing 2-aminoquinolines as potent and selective inhibitors of neuronal nitric oxide synthase. *J Med Chem* **58**, 8694-8712 (2015).
414. Wang, H.-Y. et al. Potent and selective human neuronal nitric oxide synthase inhibition by optimization of the 2-aminopyridine-based scaffold with a pyridine linker. *J Med Chem* **59**, 4913-4925 (2016).
415. Do, H.T. et al. Improvement of cell permeability of human neuronal nitric oxide synthase inhibitors using potent and selective 2-aminopyridine-based scaffolds with a fluorobenzene linker. *J Med Chem* **60**, 9360-9375 (2017).
416. Hitchcock, S.A. & Pennington, L.D. Structure-brain exposure relationships. *J Med Chem* **49**, 7559-83 (2006).
417. Xue, F. et al. Potent and selective neuronal nitric oxide synthase inhibitors with improved cellular permeability. *Bioorg Med Chem Lett* **20**, 554-7 (2010).
418. Jansen, A.H., Batenburg, K.L., Pecho-Vrieseling, E. & Reits, E.A. Visualization of prion-like transfer in Huntington's disease models. *Biochim Biophys Acta Mol Basis Dis* **1863**, 793-800 (2017).
419. Rautio, J. et al. Prodrugs: design and clinical applications. *Nat Rev Drug Discov* **7**, 255-270 (2008).
420. Prokai, L., Prokai-Tatrai, K. & Bodor, N. Targeting drugs to the brain by redox chemical delivery systems. *Med Res Rev* **20**, 367-416 (2000).
421. Krise, J.P. & Oliyai, R. Prodrugs of Amines. in *Prodrugs: Challenges and Rewards Part 1* (eds. Stella, V.J. et al.) 801-831 (Springer New York, New York, NY, 2007).
422. Di, L., Kerns, E.H., Fan, K., McConnell, O.J. & Carter, G.T. High throughput artificial membrane permeability assay for blood-brain barrier. *Eur J Med Chem* **38**, 223-32 (2003).
423. Avdeef, A. Absorption and drug development. *J Med Chem* **47**, 1868-1868 (2004).
424. Wager, T.T. et al. Defining desirable central nervous system drug space through the alignment of molecular properties, in vitro ADME, and safety attributes. *ACS Chem Neurosci* **1**, 420-34 (2010).
425. Wager, T.T., Hou, X., Verhoest, P.R. & Villalobos, A. Moving beyond rules: the development of a central nervous system multiparameter optimization (CNS MPO) approach to enable alignment of druglike properties. *ACS Chem Neurosci* **1**, 435-49 (2010).
426. Nott, A., Robinson, J. & Riccio, A. DAF-FM detection of nitric oxide in embryonic cortical neurons. *Protoc Exch* (2008).
427. Kolarow, R. et al. BDNF-induced nitric oxide signals in cultured rat hippocampal neurons: time course, mechanism of generation, and effect on neurotrophin secretion. *Front Cell Neurosci* **8**, 323 (2014).
428. Keelan, J., Vergun, O. & Duchon, M.R. Excitotoxic mitochondrial depolarisation requires both calcium and nitric oxide in rat hippocampal neurons. *J Physiol* **520 Pt 3**, 797-813 (1999).
429. Rothe, F., Canzler, U. & Wolf, G. Subcellular localization of the neuronal isoform of nitric oxide synthase in the rat brain: A critical evaluation. *Neuroscience* **83**, 259-269 (1998).
430. DeKosky, S.T. & Scheff, S.W. Synapse loss in frontal cortex biopsies in Alzheimer's disease: Correlation with cognitive severity. *Ann Neurol* **27**, 457-464 (1990).
431. Scheff, S.W., Price, D.A., Schmitt, F.A. & Mufson, E.J. Hippocampal synaptic loss in early Alzheimer's disease and mild cognitive impairment. *Neurobiol Aging* **27**, 1372-1384 (2006).
432. Kashyap, G. et al. Synapse loss and progress of Alzheimer's disease -A network model. *Sci Rep* **9**, 6555 (2019).
433. Town, T. et al. p35/Cdk5 pathway mediates soluble amyloid- β peptide-induced tau phosphorylation in vitro. *J Neurosci Res* **69**, 362-372 (2002).

434. Hashiguchi, M., Saito, T., Hisanaga, S. & Hashiguchi, T. Truncation of CDK5 activator p35 induces intensive phosphorylation of Ser202/Thr205 of human tau. *J Biol Chem* **277**, 44525-30 (2002).
435. Kimura, T., Ishiguro, K. & Hisanaga, S.-i. Physiological and pathological phosphorylation of tau by Cdk5. *Front Mol Neurosci* **7**(2014).
436. Noble, W. et al. Cdk5 is a key factor in tau aggregation and tangle formation in vivo. *Neuron* **38**, 555-565 (2003).
437. Saito, T. et al. Cdk5 increases MARK4 activity and augments pathological tau accumulation and toxicity through tau phosphorylation at Ser262. *Hum Mol Genet* **28**, 3062-3071 (2019).
438. Shanley, M.R. et al. LRRK2 Facilitates tau Phosphorylation through Strong Interaction with tau and cdk5. *Biochemistry* **54**, 5198-208 (2015).
439. Yao, G. et al. NO up-regulates migraine-related CGRP via activation of an Akt/GSK-3 β /NF- κ B signaling cascade in trigeminal ganglion neurons. *Aging (Albany NY)* **12**, 6370-6384 (2020).
440. Pei, J.J. et al. Distribution of active glycogen synthase kinase 3beta (GSK-3beta) in brains staged for Alzheimer disease neurofibrillary changes. *J Neuropathol Exp Neurol* **58**, 1010-9 (1999).
441. Alvarez, G. et al. Lithium protects cultured neurons against beta-amyloid-induced neurodegeneration. *FEBS Lett* **453**, 260-4 (1999).
442. Takashima, A. et al. Activation of tau protein kinase I/glycogen synthase kinase-3beta by amyloid beta peptide (25-35) enhances phosphorylation of tau in hippocampal neurons. *Neurosci Res* **31**, 317-23 (1998).
443. Weingarten, M.D., Lockwood, A.H., Hwo, S.Y. & Kirschner, M.W. A protein factor essential for microtubule assembly. *Proc Natl Acad Sci U S A* **72**, 1858-62 (1975).
444. Witman, G.B., Cleveland, D.W., Weingarten, M.D. & Kirschner, M.W. Tubulin requires tau for growth onto microtubule initiating sites. *Proc Natl Acad Sci U S A* **73**, 4070-4 (1976).
445. Trojanowski, J.Q., Schuck, T., Schmidt, M.L. & Lee, V.M. Distribution of tau proteins in the normal human central and peripheral nervous system. *J Histochem Cytochem* **37**, 209-15 (1989).
446. Ando, K. et al. Stabilization of microtubule-unbound tau via tau phosphorylation at Ser262/356 by Par-1/MARK contributes to augmentation of AD-related phosphorylation and A β 42-induced tau toxicity. *PLoS Genet* **12**, e1005917 (2016).
447. Braun, N.J., Yao, K.R., Alford, P.W. & Liao, D. Mechanical injuries of neurons induce tau mislocalization to dendritic spines and tau-dependent synaptic dysfunction. *Proc Natl Acad Sci U S A* **117**, 29069-29079 (2020).
448. Hoover, B.R. et al. Tau mislocalization to dendritic spines mediates synaptic dysfunction independently of neurodegeneration. *Neuron* **68**, 1067-81 (2010).
449. Ittner, L.M. et al. Dendritic function of tau mediates amyloid-beta toxicity in Alzheimer's disease mouse models. *Cell* **142**, 387-97 (2010).
450. Nakazawa, T. et al. Characterization of Fyn-mediated tyrosine phosphorylation sites on GluR epsilon 2 (NR2B) subunit of the N-methyl-D-aspartate receptor. *J Biol Chem* **276**, 693-9 (2001).
451. Rong, Y., Lu, X., Bernard, A., Khrestchatisky, M. & Baudry, M. Tyrosine phosphorylation of ionotropic glutamate receptors by Fyn or Src differentially modulates their susceptibility to calpain and enhances their binding to spectrin and PSD-95. *J Neurochem* **79**, 382-90 (2001).
452. Gorsky, M.K., Burnouf, S., Dols, J., Mandelkow, E. & Partridge, L. Acetylation mimic of lysine 280 exacerbates human Tau neurotoxicity in vivo. *Sci Rep* **6**, 22685 (2016).
453. Cohen, T.J. et al. The acetylation of tau inhibits its function and promotes pathological tau aggregation. *Nat Commun* **2**, 252 (2011).
454. Irwin, D.J. et al. Acetylated tau, a novel pathological signature in Alzheimer's disease and other tauopathies. *Brain* **135**, 807-18 (2012).

455. Tracy, T.E. et al. Acetylated tau obstructs KIBRA-mediated signaling in synaptic plasticity and promotes tauopathy-related memory loss. *Neuron* **90**, 245-60 (2016).
456. Min, S.W. et al. Acetylation of tau inhibits its degradation and contributes to tauopathy. *Neuron* **67**, 953-66 (2010).
457. Cook, C., Stankowski, J.N., Carlomagno, Y., Stetler, C. & Petrucelli, L. Acetylation: a new key to unlock tau's role in neurodegeneration. *Alz Res Ther* **6**, 29 (2014).
458. Sen, T., Saha, P. & Sen, N. Nitrosylation of GAPDH augments pathological tau acetylation upon exposure to amyloid-beta. *Sci Signal* **11**(2018).
459. Jaffrey, S.R., Snowman, A.M., Eliasson, M.J., Cohen, N.A. & Snyder, S.H. CAPON: a protein associated with neuronal nitric oxide synthase that regulates its interactions with PSD95. *Neuron* **20**, 115-24 (1998).
460. Li, L.-L. et al. The nNOS-p38MAPK pathway is mediated by NOS1AP during neuronal death. *J Neurosci* **33**, 8185 (2013).
461. Hashimoto, M. et al. Analysis of microdissected neurons by 18O mass spectrometry reveals altered protein expression in Alzheimer's disease. *J Cell Mol Med* **16**, 1686-700 (2012).
462. Li, N. et al. mTOR-dependent synapse formation underlies the rapid antidepressant effects of NMDA antagonists. *Science* **329**, 959-64 (2010).
463. Li, H., Aksenova, M., Bertrand, S.J., Mactutus, C.F. & Booze, R. Quantification of filamentous actin (F-actin) puncta in rat cortical neurons. *JoVE*, e53697-e53697 (2016).
464. Wei, H. et al. The therapeutic effect of memantine through the stimulation of synapse formation and dendritic spine maturation in autism and fragile X syndrome. *PLoS One* **7**, e36981 (2012).
465. Ruddy, R.M., Chen, Y., Milenkovic, M. & Ramsey, A.J. Differential effects of NMDA receptor antagonism on spine density. *Synapse* **69**, 52-56 (2015).
466. Ultanir, S.K. et al. Regulation of spine morphology and spine density by NMDA receptor signaling in vivo. *Proc Natl Acad Sci U S A* **104**, 19553-19558 (2007).
467. Deshpande, A., Kawai, H., Metherate, R., Glabe, C.G. & Busciglio, J. A role for synaptic zinc in activity-dependent A β oligomer formation and accumulation at excitatory synapses. *J Neurosci* **29**, 4004-4015 (2009).
468. Fani, G. et al. A β oligomers dysregulate calcium homeostasis by mechanosensitive activation of AMPA and NMDA receptors. *ACS Chem Neurosci* **12**, 766-781 (2021).
469. Kent, S.A., Spires-Jones, T.L. & Durrant, C.S. The physiological roles of tau and A β : implications for Alzheimer's disease pathology and therapeutics. *Acta Neuropathol* **140**, 417-447 (2020).
470. Ristori, E., Donnini, S. & Ziche, M. New insights into blood-brain barrier maintenance: the homeostatic role of β -amyloid precursor protein in cerebral vasculature. *Front Physiol* **11**, 1056 (2020).
471. Zago, W. et al. Vascular alterations in PDAPP mice after anti-A β immunotherapy: Implications for amyloid-related imaging abnormalities. *Alzheimers Dement* **9**, S105-S115 (2013).
472. Sperling, R.A. et al. Amyloid-related imaging abnormalities in amyloid-modifying therapeutic trials: Recommendations from the Alzheimer's Association Research Roundtable Workgroup. *Alzheimers Dement* **7**, 367-385 (2011).
473. Bates, A. & Power, C.A. David vs. Goliath: the structure, function, and clinical prospects of antibody fragments. *Antibodies (Basel)* **8**(2019).
474. Faresjö, R. et al. Brain pharmacokinetics of two BBB penetrating bispecific antibodies of different size. *Fluids Barriers CNS* **18**, 26 (2021).
475. Kouhi, A. et al. Brain disposition of antibody-based therapeutics: dogma, approaches and perspectives. *Int J Mol Sci* **22**(2021).

476. Fuller, J.P., Stavenhagen, J.B. & Teeling, J.L. New roles for Fc receptors in neurodegeneration-the impact on immunotherapy for Alzheimer's Disease. *Front Neurosci* **8**, 235 (2014).
477. Khatib, S.E. & Salla, M. The mosaic puzzle of the therapeutic monoclonal antibodies and antibody fragments - A modular transition from full-length immunoglobulins to antibody mimetics. *LRR* **18**, 100335 (2022).
478. Saunders, K.O. Conceptual approaches to modulating antibody effector functions and circulation half-life. *Front Immunol* **10**(2019).
479. Bird, R.E. et al. Single-chain antigen-binding proteins. *Science* **242**, 423-6 (1988).
480. Huang, L., Su, X. & Federoff, H.J. Single-chain fragment variable passive immunotherapies for neurodegenerative diseases. in *Int J Mol Sci* Vol. 14 19109-19127 (2013).
481. Sebollela, A. et al. A human scFv antibody that targets and neutralizes high molecular weight pathogenic amyloid- β oligomers. *J Neurochem* **142**, 934-947 (2017).
482. Selles, M.C. et al. AAV-mediated neuronal expression of a scFv antibody selective for A β oligomers protects synapses and rescues memory in Alzheimer models. *Mol Ther* (2022).
483. Esquerda-Canals, G., Martí-Clúa, J. & Villegas, S. Pharmacokinetic parameters and mechanism of action of an efficient anti-A β single chain antibody fragment. *PLoS One* **14**, e0217793 (2019).
484. Kipriyanov, S.M. Generation of bispecific and tandem diabodies. *Methods Mol Biol* **562**, 177-93 (2009).
485. Hornig, N. & Färber-Schwarz, A. Production of bispecific antibodies: diabodies and tandem scFv. *Methods Mol Biol* **907**, 713-27 (2012).
486. Alvarez-Cienfuegos, A. et al. Intramolecular trimerization, a novel strategy for making multispecific antibodies with controlled orientation of the antigen binding domains. *Sci Rep* **6**, 28643 (2016).
487. Cuesta, A.M. et al. Improved stability of multivalent antibodies containing the human collagen XV trimerization domain. *MAbs* **4**, 226-32 (2012).
488. Alam, M.K. et al. A novel synthetic trivalent single chain variable fragment (tri-scFv) construction platform based on the SpyTag/SpyCatcher protein ligase system. *BMC Biotechnol* **18**, 55 (2018).
489. Arimori, T. et al. Fv-clasp: an artificially designed small antibody fragment with improved production compatibility, stability, and crystallizability. *Structure* **25**, 1611-1622.e4 (2017).
490. Soleimanizadeh, A., Dinter, H. & Schindowski, K. Central nervous system delivery of antibodies and their single-domain antibodies and variable fragment derivatives with focus on intranasal nose to brain administration. *Antibodies (Basel)* **10**(2021).
491. Cline, E.N. et al. A novel crosslinking protocol stabilizes amyloid beta oligomers capable of inducing Alzheimer's-associated pathologies. *J Neurochem* **148**, 822-836 (2019).
492. Zhou, S., Liu, M., Ren, F., Meng, X. & Yu, J. The landscape of bispecific T cell engager in cancer treatment. *Biomark Res* **9**, 38 (2021).
493. Johnsen, K.B. et al. Targeting transferrin receptors at the blood-brain barrier improves the uptake of immunoliposomes and subsequent cargo transport into the brain parenchyma. *Sci Rep* **7**, 10396 (2017).
494. Lugo, J.N., Brewster, A.L., Spencer, C.M. & Anderson, A.E. Kv4.2 knockout mice have hippocampal-dependent learning and memory deficits. *Learn Mem* **19**, 182-9 (2012).
495. Habiba, U. et al. Detection of retinal and blood A β oligomers with nanobodies. *Alzheimers Dement (Amst)* **13**, e12193 (2021).
496. Zhou, S. et al. Synthesis, characterization, and simulation of four-armed megamolecules. *Biomacromolecules* **22**, 2363-2372 (2021).